5-2018

Pregnancy Induced Alterations of Reproductive Tract Collagen and Elastin in a Murine Model

Basant K. Dhital
The Graduate Center, City University of New York

Pregnancy induced alterations of reproductive tract collagen and elastin in a murine model

by

Basant Kumar Dhital

A dissertation submitted to the Graduate Faculty in Physics in partial fulfillment of the requirements for the degree of Doctor of Philosophy, The City University of New York-The Graduate Center.

2018

This manuscript has been read and accepted for the Graduate Faculty in Physics in satisfaction of the dissertation requirements for the degree of Doctor of Philosophy.

(required signature)

_____ _____

Date Chair of Examining Committee

(required signature)

_____ _____

Date Executive Officer

Keith T. Downing

_____

Emmanuel J. Chang

_____

Ruth E. Stark

_____

Nicolas Biais

_____

Supervisory Committee

THE CITY UNIVERSITY OF NEW YORK

Abstract

Pregnancy induced alterations of reproductive tract collagen and elastin in a murine model

by

Basant Kumar Dhital

Advisor: Gregory S. Boutis

This thesis reports on structural and dynamical modifications of reproductive tract elastin and collagen as a function of parity. Pelvic floor dysfunction, including pelvic organ prolapse (POP) is a major concern affecting female health worldwide, leading to surgeries costing billions of dollars annually. Collagen, elastic fibers, and proteoglycans are major extracellular matrix (ECM) components found in connective tissues. Vaginal child birth, advancing age, and disruption or dysfunction of connective tissue are major risk factors of POP. In the female reproductive tract, the assembly of elastic fibers is crucial for the pelvic floor support. Any disturbance in the synthesis, assembly, and degradation of elastic fibers in the reproductive tract during parturition or aging may result in pelvic floor dysfunction. Various experimental methods were implemented to probe the structural and dynamical changes of these proteins, as a function of the number of pregnancies, including ^{13}C nuclear magnetic

resonance (NMR), ^{2}H NMR, spectrophotometry, MALDI mass spectrometry, and histology. Results of this study provide the gynecological community with further understanding relating to how elastin and collagen of the reproductive tract are altered as a function of the number of births, and may contribute to the loss of tissue elasticity and the onset of pelvic floor dysfunction.

The concentration of elastin in the reproductive tract is approximately 1.5% by weight making quantification challenging. This thesis has provided an important step in understanding how pregnancy and/or parturition may lead to alterations of reproductive tract elastin. In the elastin study, experimental data unveils remarkably different ^{13}C spectra for virgin rat cohorts may be due to higher concentration of MMP-2 and MMP-9, which degrade elastin, compared to elastin from the multiparous rat cohorts. Single pregnancy cohorts exhibit spectra similar to the virgin rat, whereas elastin from cohorts that have undergone three pregnancies resembled that from the multiparous rat cohorts. By applying solid state NMR relaxation measurements the dynamics of major backbone and side chain carbon nuclei in the major amino acids, (e.g., glycine, valine, proline, etc.) were found to vary significantly in virgin cohorts in comparison to multiparous cohorts. Furthermore, the concentration of desmosine was found to be highest in the multiparous cohorts and similar to that found in other mammalian elastins. While the microscopic structure of elastin in multiparous cohorts appears strikingly similar to elastin in other mammalian tissues, the elastic fibers are fragmented and highly tortuous. Our current model suggests that the elastic fiber fragmentation, which occurs over length scales of approximately 10-50 micrometers (the length of an elastic fiber), together with collagen content may play a crucial role in

tissue scaffolding than alterations in microscopic structure (e.g. desmosine crosslinks) .

Collagen, another major component of extracellular matrix protein in the reproductive tract, also undergoes significant remodeling and alterations during pregnancy. Interestingly, the structure of collagen was found to be intact despite tremendous remodeling and alterations during pregnancy. However, collagen content was observed to be highest in the virgin cohorts compared to multiparous cohorts, by histological methods. ^{2}H NMR relaxation methods were used to characterize the dynamics and distribution of water in both collagen and elastin as well as only elastin of various cohorts. The redistribution of water due to pregnancy and/or parturition results in additional water reservoir in postpartum and multiparous cohorts in collagen and elastin samples. However, in only elastin from multiparous and virgin cohorts, dynamics of water were observed to vary significantly across cohorts due to fiber fragmentation, and microscopic alterations driven by MMP concentration.

Apart from reproductive tract collagen and elastin, this thesis has provided detailed measurements relating to the effects of ultraviolet (UV) irradiation on elastic fibers. UV-A (365 nm) exposure of elastic fibers was shown to result in distinct cracks and disruption in regular array of elastic fibers. Additionally, the concentration of desmosine in elastin is reduced in comparison to the nonirradiated elastic fibers after UV irradiation. This portion of the thesis has introduced a method for readily measuring the concentration of desmosine in tissues and other bodily fluids by MALDI mass spectrometry.

Acknowledgements

First and foremost, I would like to thank my research advisor, Professor Gregory S. Boutis, for his continuous support and guidance throughout the entire PhD project. I felt fortunate to have him as a thesis advisor. His valuable criticism, comments, and advice helped me to develop my knowledge in performing scientific research and accomplish my goals.

Second, I would like to thank my collaborator Dr. Keith T. Downing for providing samples for this project. His ideas and suggestions regarding this project were invaluable. I would also like to acknowledge and thank Professor Emmanuel J. Chang for allowing me to work in his lab. His guidance and ideas regarding desmosine measurements were very exciting and useful. Special thanks to my thesis committee members, Professor Ruth E. Stark and Professor Nicolas Biais for their valuable guidance and suggestions.

Third, I would like to thank my lab mates and colleagues. Farhana Gul-E-Noor, a great friend and scientist, who was a first reader of my all manuscripts and taught experimental tricks. Steven W. Morgan and Anthony Papaioannou, great friends and scientists who helped me to understand basic physics of NMR and taught me different computer programs (Latex, Matlab, etc.). I would also like to thank my friends at the Graduate Center of CUNY, Dipendra Dahal, Nikesh Maharjan, Pradip Niraula, Sunita Humagain, Umesh Khanaiya,

and Pratik Rathod for help and useful discussions during all these years.

Last but not least, I would like to thank my dear parents, my wife and other family members for their endless love, support, and understanding.

For my parents Chetkant Dhital and Lilabati Dhital,

my wife, Aruna Ranabhat,

for their love, support, and understanding.

For my cute little trouble maker Aarush Dhital.

Contents

List of Figures

List of Tables

Chapter 1

Introduction

Pelvic floor disorder, a condition including pelvic organ prolapse (POP) and urinary incontinence, is a major concern affecting female health worldwide. Vaginal child birth, advancing age, and increasing body mass are major risk factors of pelvic organ prolapse. In addition, vaginal delivery, aging, and disruption or dysfunction of connective tissues contribute to a lesser extent [1, 2]. Aging and multiparity (through spontaneous vaginal birth) results in weakening of the connective tissues associated with the pelvic floor, are other risk factors associated with pelvic floor dysfunction [2, 3]. Collagen, elastic fibers, and proteoglycans are major extracellular matrix (ECM) components found in connective tissues [4]. During pregnancy, the remodeling of the vaginal wall and other pelvic floor connective tissues occurs throughout fetal development and involution [4]. This remodeling alters the composition and concentration of the extracellular matrix; there is a rapid increase in the weight of the uterus as well as the size due to the deposition of collagen and elastin. In the case of rats, studies have shown that the increase in the weight of the uterus is six to eight fold compared to non-pregnant uteri [5, 6], 11 fold in humans [7], and 14 fold in ewe. [8]. Collagen, elastin,

and smooth muscle play an important role in the remodeling and adapting the uterine tissue during pregnancy and involution.

The National Center for Health Statistics lists genital prolapse as one of the three most common reasons for hysterectomy in women during the year 2000 —more than 338,000 procedures for prolapse are performed annually in the United States. The majority of published studies are from clinical studies, especially from registries of surgical procedures that are specific for prolapse. However, identifying POP by surgical intervention is likely to identify only the most severe degrees of prolapse [9]. Parity was shown to be the strongest risk factor for pelvic organ prolapse as study performed by the Oxford Family Planning Association. In this work, Hendrix et al. showed that POP increased with increasing parity in postmenopausal women from the ages of 50 to 79 [10].

In an experiment by Drewes et al., who were studying the regulation of elastic fiber synthesis and assembly in the vaginal wall of mice during pregnancy and after vaginal delivery, elastase was injected into the posterior vaginal wall of eight postpartum mice on the day of delivery. By 72 hours, prolapse of the posterior vagina was observed in six of the eight elastase-treated mice but none in the controls [11]. They also observed in the immediate postpartum, a burst in the protein expression of FBLN 5, a secreted ECM protein, and tropoelastin proteins. Elastic fiber integrity as well as the synthesis and degradation equilibrium, was shown to be imperative to the structural integrity of the uterus, and if imbalanced, POP may develop. Additionally, various studies have shown that the activity of matrix metalloproteinases, a group of endopeptidases that regulate changes in the ECM of uterus during pregnancy increases [12, 13]. Therefore, it is important to understand the

activity and structure of elastin, collagen, and associated enzymes that might provide insight into the risk factors of POP.

Elastin, one of the main structural components of connective tissue, confers elasticity and resiliency [14, 15]. This large, cross-linked protein is found in the ECM of skin, lung, arterial blood vessel, uterus, and elastic ligament where elasticity is crucial for repeated stretch and subsequent recoil [16, 17, 18, 19]. Elastin is 12 times more extensible, approximately 1000 times less stiff than collagen [20]. Although the mechanical characteristics are different, elastin also plays a load bearing role together with collagen [21, 14]. Initial deposition of elastin and its assembly is important as this insoluble polymer, once laid down during perinatal development, does not show any significant turnover under normal circumstances [22, 23, 19]. However, the female uterus is an exception that undergoes acute changes to adapt the fetus during the course of pregnancy and involution. These alterations include the growth of the tissue, ECM deposition (that contain structural proteins such as collagen and elastin), and remodeling [24, 25, 26, 27]. Elastic tissues play an important physiological role and provide dynamic mechanical function to the uterus [28]. Several studies showed that collagen and elastin content of the ECM increases during pregnancy from its non-pregnant controls and varies in different animals [7, 6, 5, 29, 27]. Additionally, several groups have observed different morphology or structural organization of the elastic tissue in the uterus, compared to that of aorta, skin, and lungs [28, 30, 31].

Elastin is a complex, cross-linked macromolecule that is assembled from its soluble precursor, tropoelastin. Elastin is insoluble in water, and most solvents, and consists of hydrophobic and cross-linking domains. The hydrophobic domain is believed to play a pivotal role in the

elastomeric properties of elastin. This domain is often rich in valine, proline, and glycine and is comprised of domains that consists of units such as VPGVG, whose structure has been well studied and characterized [32]. The cross-linking domain is comprised of desmosine and isodesmosine, which anchor the tropolelastin molecules together [33, 34, 35, 17, 36]. Though elastin is insoluble and hydrophobic in nature, this polymer requires water to confer mobility which gives rise to its elastomeric characteristics [37, 21, 38, 39, 40, 35, 41].

Several models have been proposed to understand the mechanisms of elasticity in elastin. The elasticity of elastin is believed to be driven by an entropic force mediated by conformational and/or dynamical changes [42]. The elasticity in elastin has been investigated by considering short repeating peptides $(VPGVG)_n$ comprising tropoelastin have been studied [43]. Urry and coworkers studied this repeating peptide extensively and proposed the librational entropy mechanism for the elasticity of elastin [44]. In this model elastin consists of consecutive type II β-turns that make up an 'idealized β-spiral' and assuming fixed ends, the conformation of the macromolecule allows for librational motion. Upon mechanical deformation the libration of the peptide results in a change in entropy giving rise to an entropic force that mediates the elastic character. An alternate model described as the sliding β-turn model consisting of mobile conformations was suggested by Tamburro et al. [45]. In this model, the conformation of the polypeptide changes under deformation and results in reduction of entropy which gives rise to elasticity. Hong and coworkers measured isotropic and anisotropic ^{13}C and ^{15}N NMR chemical shifts of the elastin mimetic polypeptide $(VPGVG)_3$. In their study, Pro-2 C_α, C_β and ^{15}N isotropic shifts, and the Gly C_α isotropic and anisotropic chemical shifts indicated that type II β turn is dominnant at the Pro-Gly position in the

mimetic VPGVG sequence [35].

Limited structural information of this protein is available as it is amorphous and insoluble, which limits the utility of rudimentary X-ray and solution Nuclear Magnetic Resonance (NMR) approaches [46, 47, 48, 49]. Different analytical techniques, such as Fourier transform infrared spectroscopy (FTIR), circular dichroism, and as well as different microscopic techniques have also been employed to study the structure of elastin [50, 51, 52, 53, 54]. Solid-state NMR, one of the methods used in this study, has been used to obtain into the structure and dynamics of this highly cross-linked protein [55, 34, 21, 56, 57, 58]. ^{13}C SS-NMR has been applied to study the bovine nuchal ligament elastin structure by Papaioannu et al. [36]. In the aliphatic region, the highest intensity peaks at 18.0 and 19.0 ppm were assigned to alanine C_β and valine C_γ, respectively. The signal at 22.0 ppm may also correspond to alanine C_β pointing to β-strand secondary structure conformation. The isoleucine C_γ and C_δ were observed at 11.0 and 16.0 ppm, respectively. Leucine C_δ and proline C_γ were observed at approximately 23.5 and 25.6 ppm. The peak at 31.0 ppm and 37.0 ppm were assigned to proline C_γ or valine C_β and isoleucine C_β, respectively. Glycine C_α was observed at 43.4 ppm in α-helical conformation. The peaks at 48.0, and 51.0 ppm were assigned to alanine C_α with β-strand and random coil secondary structures while peak at 53.0 ppm was assigned to alanine C_α with α-helical conformation. The valine C_α signal appeared at 60.4 ppm. The backbone carbonyl was observed at 172.1 ppm while the broad peak at 129.0 ppm as assigned to aromatic carbons of tyrosine. Additional discussion relating to the structure of elastin based on ^{13}C NMR is discussed in chapter 4.

Previous work on reproductive tract tissue stiffness has shown that the tissue stiffness

was found to decrease in multiparous as well as 2 days postpartum rats (spontaneous or simulated) in comparison to the virgin rats. However, in 2 weeks postpartum rats (where the elastic fibers are in the course of recovery) the tissue stiffness returns back to virgin rats stiffness [59]. Several studies on prolapsed tissues has also shown that the architecture of elastic fibers may directly impact the macroscopic properties of tissues. Liu et al., observed substantial accumulation of elastin monomers with decreased cross-links in case of LOXL1 deficient mice [60]. Additionally, different groups have observed fragmented and tortuous elastic fibers with reduced elastin content in women with POP [2, 61]. Goepel et al. observed irregular fragmented distributions of elastic fibers in studies of female stress urinary incontinence [62]. All these observations highlight the important scaffolding role of elastic fibers in the reproductive tract and any disturbance in the equilibrium lead to pelvic floor dysfunction.

Collagen is a ubiquitous protein found in all multicellular organisms and is the most abundant component of extracellular matrix of many tissues in humans [63, 64]. It is a major constituent of tendons, ligaments, organic matrix in bone and dentin, and present in the extracellular matrix of skin, arteries, and cartilage. Collagen is produced as long, thin molecules which align themselves into highly ordered one dimensional fibrous arrays that are cross-linked to provide vertebrate tissues with high tensile strength [6, 65]. Collagen has high mechanical strength but poor elasticity [7]; it is 1091 times stiffer but 12 times less extensible than elastin [20]. Its tensile strength is 0.12 GPa which is 60 times stronger than that of elastin [20]. At present, an accepted notion is that the role of collagen fibers in the tissue is to provide a scaffold for elastic fibers [7]. Collagen is rich in glycine (33 $\pm$ 1.3)%,

proline (11.8 ± 0.9)%, alanine (10.8 ± 0.9)%, hydroxyproline (9.1 ± 1.3)%, and glutamic acid (7.4 ± 10)%, which constitute approximately 72% of the protein [66].

In collagen, three parallel polypeptide strands in left handed helical conformations coil around each other to form a right handed collagen triple helix. Each of the three α-chains which makes a helix contains about 1000 amino acids. Each triple helix, termed tropocollagen, aggregates in a complex and hierarchical manner to form fibers and networks. Each triple helical structure consists of a repeating sequence $(Gly - X - Y)_n$, with X and Y frequently being proline or hydroxyproline residues, respectively. The tight packing of polypeptide strands in collagen requires every third residue to be glycine. The interstrand hydrogen bonds between the NH-group of glycine and backbone CO of neighboring residues are the major stabilizing motifs of collagen. Other factors such as hydration, van der Waals interactions, periodicity of glycine, relatively higher amounts of amino acids that induce conformational limitations, hydroxyl groups of hydroxyproline, etc. play a vital role in the stability of the triple helix [67, 63].

There is a rapid formation of collagen in the uterus during pregnancy and following parturition, collagen content reduces to its value prior to the pregnancy. Collagen formation is smallest on the placental side and maximal in the region of greatest uterine extension [7]. Harkness et al. showed that during the first ten days of pregnancy, collagen content increases faster than the changes in weight, and thereafter there is an observed decrease in the rate of increase in rat uteri. Soon after parturition, weight, and collagen content of the uterus falls precipitously and reaches a value below non-pregnant controls [5]. The increase in collagen content during pregnancy is 4 fold per fetus [68, 69] in rats, whereas in humans there is an

6.8 fold increase [26]. In rats, this increase has been shown to depend on various factors such as the number of fetuses, age, and weight of the animal [70, 69, 5, 71]. After parturition the degradation of collagen is very rapid and is complete within three to four days in rats [69], whereas in humans, it completes within three weeks [26].

Numerous studies have shown that there is a marked distention followed by a rapid return to the pre-pregnant state of the vaginal wall and pelvic floor during pregnancy and parturition. Various epidemiological studies show that many women fail to recover back to the pre-pregnant state with vaginal distention trauma, which may be a major cause associated for the development of pelvic floor dysfunction [12]. The cause of pelvic floor dysfunction is influenced by circumstances such as multiparty, obstetric trauma, chronic increased intra-abdominal pressure, aging, and estrogen deficiency. The risk of developing POP increases by 4 to 11 times with vaginal delivery [72]. It has been suggested that the primary cause of POP may arise from the inherent weakness in the supporting connective tissues of the pelvic structure. The decreased fibroblast and increased collagen content may be key factors associated with pelvic support disorder [73].

In this thesis, an experimental investigation to follow the effects of parity on the structure and dynamics of collagen and elastin derived from reproductive tract of Sprague-Dawley rats using several experimental approaches is reportd. ^{13}C relaxation experiments were performed to measure correlation times of internuclear ^{13}C-^{1}H motions to probe dynamical fluctuations of the spectroscopically resolvable moieties across virgin, multiparous, and primiparous rats (2 days and 14 days postpartum) (collagen study) and virgin, para1, para3 and multiparous samples (elastin study). ^{2}H T_1-T_2 experiments, based on an inverse Laplace transform (ILT),

were also employed to characterize the distribution and dynamics of water in the collagen and elastin samples studied. Additionally, spectrophotometry, histology, and mass spectrometry were employed to further investigate changes in collagen and elastin due to pregnancy and parity. Spectrophotometry was used to quantify MMP-2, MMP-9, and TIMP-1 expression involved in regulation of elastin during pregnancy and/or parturition in reproductive tract tissues. MALDI mass spectrometry was used to quantify the amount of desmosine in reproductive tract elastic fibers.

This thesis work also explored the alterations of elastin due to photoaging. The effects of photoaging are closely connected to elastin damage through UV exposure. It has been found that the major histopathological alteration to photoaged skin is an accumulation of poorly organized elastin, termed solarelastosis. UV irradiation has been shown to induce the expression of matrix metalloprotenases (MMPs), which cause degradation of extracellular matrix such as elastin and collagen. Irradiation of skin was found to increase the expression of human macrophase elastase (MMP-12) mRNA 11.9 fold within 16 hours of UV exposure [74]. Other studies have found that elastin production is increased after exposure to UV radiation, which may result in large amounts of abnormal elastic material in the skin. In one study, irradiation of mice with ultraviolet B (wavelengths = 290-320 nm) yielded an 8.5 fold increase in promoter activity, while ultraviolet A (wavelengths = 320-400 nm) only resulted in an 1.8 fold increase in promoter activity. These results indicate that ultraviolet B has a significant impact on the accumulation of elastosis, while ultraviolet A contributes as well, but to a lesser extent [75]. In another study, by tagging elastic material with antibodies and conducting immunofluorescence microscopy, it was found that solar elastosis is primarily

derived from elastic fibers and not from preexisting or newly synthesized collagen [76]. The effects of UV-A irradiation on the elastic fibers were investigated by using NMR, mass spectrometry, transmission electron microscopy (TEM), and histology.

This thesis contains seven chapters. Chapter 2 provides a background of the experimental techniques employed. Chapter 3 provides an overview of a novel experimental techniques that we developed to quantify the levels of desmosine in elastin is discussed. Chapter 4 summarizes results from the experimental study relating to the structural and dynamical fluctuations in elastin resulting from parity. In chapter 5, the structural and dynamical alterations in collagen caused by pregnancy and/or parturition are discussed. In Chapter 6 the effects of UV radiation in elastic fibers are discussed. Lastly, in Chapter 7, a general conclusion is drawn and a brief outlook of future work is discussed.

Chapter 2

Overview of experimental techniques

2.1 Nuclear magnetic resonance

Nuclear magnetic resonance (NMR) is a non-destructive analytical tool that has been successfully applied to study molecular structure, sample purity, and reaction mechanisms at the atomic level. The application and development of NMR spectroscopy has enabled a more thorough understanding of topics from molecular structure and dynamics of single molecules to complex molecular systems to biological tissues [77].

Nuclear magnetic resonance is a physical phenomenon utilized to investigate molecular properties of matter by irradiating atomic nuclei in a magnetic field with radio waves. If the nuclear spin angular moment is non-zero, the nucleus can interact with the external magnetic field. For spin-1/2 nuclei, in the presence of the external magnetic field, the degenerate spin state is split into two energy levels: one oriented in the direction of the applied magnetic field and the other opposite to the applied magnetic field. Removal of degeneracy creates a population difference between the upper and lower energy levels given

by the Boltzmann distribution. The signal in NMR spectroscopy results from detecting the radio frequency signal emitted by the spins making transitions from lower to higher energy states and, is proportional to the population difference between the two spin states. The population difference between the two spin states is small, making NMR a very insensitive tool compared to other analytical techniques. For protons at thermal equilibrium at room temperature in an 18.8 Tesla magnet, the population ratio is 0.99872. This small population ratio means that for every 1,000,000 nuclei in the upper energy state there are 1,000,128 nuclei in the lower energy state. Such a small population difference results in a sensitivity problem as only the difference in populations is detected in NMR. The low sensitivity is probably one of the greatest limitations of NMR. However, the sensitivity can be increased by the use of stronger magnetic fields, dynamic nuclear polarization and increasing the number of nuclei in the sample by labeling methods [78].

In order to understand the functional dynamics of biomolecules, knowledge of atomic structure and dynamics is crucial. Techniques useful for resolving structure include X-ray crystallography, solution NMR, and solid state NMR. Each method has certain advantages and limitations. X-ray crystallography is one useful method that can be used on both natural and artificial macromolecules to determine molecular structure. This method does not require isotope labeling. However, this method can only be used to study crystalline samples and requires relatively large amounts of samples for the crystallization process. Therefore, this method cannot be applied to non-crystalline samples like membrane proteins and nucleic acids. For this reason, NMR has become one of the most popular techniques in various fields, such as chemistry, biology, physics, pharmacy, and geology [79]. "NMR,"

in many places, refers to solution state (NMR) experiments, which require the sample to be in the solution phase for testing. Generally, it allows for investigating structural and dynamical information based on interactions, such as isotropic chemical shift, J couplings, and relaxation information (T1, T2, and NOEs). The same type of atoms experiencing different local chemical environments will have different chemical shifts. Compared to solid state NMR (SSNMR), this method has much better resolution with narrower line widths and a much stronger signal intensity because of the rapid isotropic reorientation [80, 81]. The major limitation of solution NMR spectroscopy is the rotational correlation time of the the solvated biomolecule which is proportional to its molecular weight. This method can be employed for the structure determination of small biological macromolecules of molecular weight 30-40 kDa [82]. Structural information can be extracted by NMR from torsional angle and through space distance restraints [83, 84, 85].

Solid-state nuclear magnetic resonance (SSNMR) spectroscopy is a diverse method that can be applied to study crystalline, amorphous or gel-phase systems. It has been applied for the investigation of the structure and dynamics of different biological molecules such as globular [86, 87] and fibrous proteins [88], as well as membrane proteins [89, 90] and lipids [91]. SSNMR is useful for determining structure and dynamics of systems which are inaccessible by solution NMR and X-ray crystallography. The greater temperature range accessibility of SSNMR makes this method advantageous for dynamic studies compared to solution NMR. SSNMR primarily provides structural information by investigating the isotropic chemical shift, chemical shift anisotropy, and dipolar coupling. The development of solid-state NMR methods in the past thirty years has contributed greatly to the understanding of molec-

ular structure and interactions in both a quantitative and qualitative sense. Modern SS-NMR techniques, such as magic angle spinning (MAS) [92, 93], cross-polarization (CP) [94], multiple-pulse sequences, homo- and heteronuclear decoupling and recoupling techniques, etc. not only produce spectra with a resolution close to that of liquid-state spectra, but also capitalize on anisotropic interactions, which are often unavailable for liquid samples [80]. In the sections that follow, some modern techniques of NMR that have been used in this study are discussed in brief. More detailed information on these techniques can be found in various texts [95, 96].

2.1.1 Magic angle spinning (MAS)

In solid state NMR, one may deal with powdered samples which consists of many crystals in random orientations. The anisotropic spin interactions which result in broad or often unresolved SSNMR spectra are the chemical shielding, dipole-dipole coupling, and quadrupole coupling. In order to achieve high resolution spectra and obtain the desired information different techniques have been developed. Magic angle spinning (MAS) is one such technique which removes the chemical shift anisotropy and heteronuclear dipolar coupling effects. This experimental approach is also applied to narrow lines from quadrupolar nuclei and remove effects from homonuclear dipolar couplings by spinning samples at high spinning speeds [95]. Magic angle spinning is used to remove the effects of the angular dependent part of the anisotropic interactions, $(3\ \cos^2\theta\text{-}1)$ in solids; the angle θ describes the orientation of the shielding/dipolar tensor with respect to the applied field. In solution spectra, the effects of chemical shift anisotropy and dipolar-coupling are averaged or partially averaged due to the

rapid molecular tumbling. Sample spinning about an axis θ_R to the applied field leads to an experimentally contrallable time dependence of θ. The time dependence of the nuclear spin interaction is given by,

$$\overline{3cos^2\theta - 1} = \frac{1}{2}(3cos^2\theta_R - 1)(3cos^2\beta - 1) \tag{2.1}$$

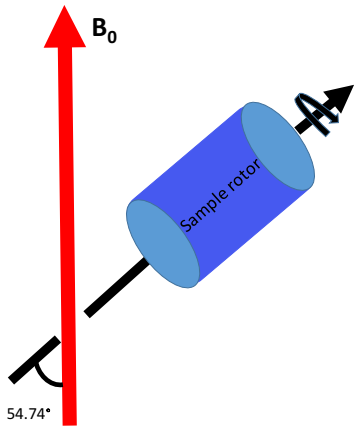

Figure 2.1: Illustrative figure of a sample rotor spinning at the magic angle 57.74°.

where β is the angle between the principal z-axis of the shielding tensor and the spinning axis. When $\theta_R = 54.74°$ the term $\overline{3cos^2\theta - 1} = 0$. Thus, the anisotropic interaction can be eliminated by spinning the sample at a sufficient spinning speed at the magic angle [95]. An illustration of a rotor spinning at the magic angle is shown in Figure 2.1. In case of an insufficient spinning speed, spinning sidebands appear in the spectrum separated by integral multiples of the spinning speed. The effect of MAS on the NMR spectra is shown in Figure 2.2. Thus, line broadening due to chemical shift anisotropy and heteronuclear dipolar coupling can be removed by using MAS. This line broadening otherwise causes a loss of

resolution and decrease in signal to noise ratio in SSNMR.

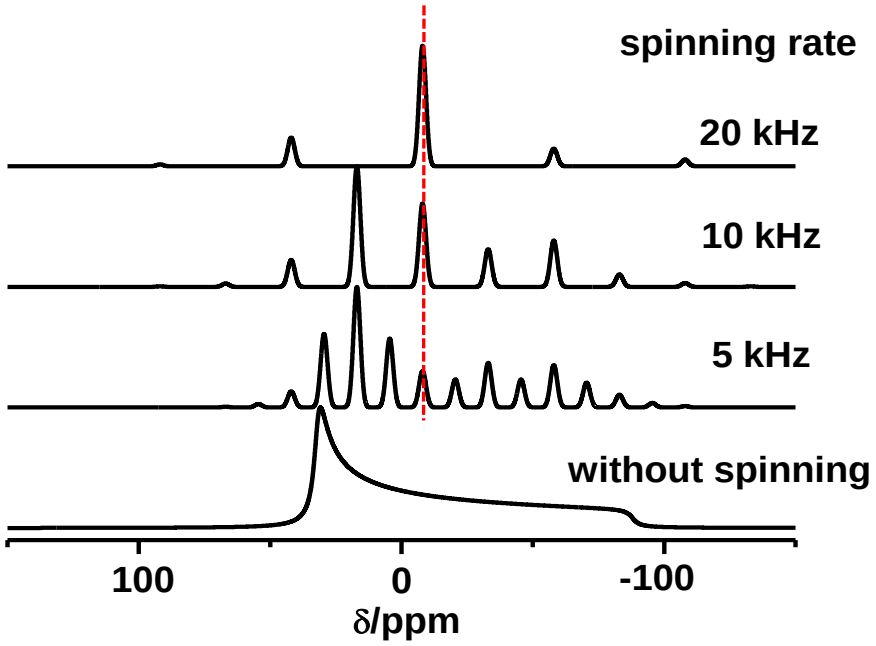

Figure 2.2: Simulated NMR spectra showing the effect of MAS (Image courtesy to Farhana Gul-E-Noor)

2.1.2 Cross polarization

Cross polarization is a widely used technique in SSNMR to assist in observing dilute spins. When combined with MAS, this technique allows for polarization transfer from abundant nuclei such as ^{1}H, ^{19}F and ^{31}P to dilute or rare nuclei such as ^{13}C, ^{29}Si, ^{15}N (isotopic abundances of 1.1%, 4.7%, and 0.03%, respectively) which helps to reduce sensitivity issues in SSNMR. Cross-polarization enhances the signal from dilute spins by a factor of (γ_I/γ_S),

where γ_I and γ_S are the gyromagnetic ratios of abundant and dilute spins, respectively. Moreover, the spin lattice relaxation times of dilute spin 1/2 nuclei are long due to the weakness of homonuclear dipolar interactions. Using the CP technique, where a pulse is applied simultaneously on the abundant spin I and less abundant S spin, the recycle delay depends on T_1(I) and not T_1(S), which is usually much shorter and allows accumulation of many more repetitions in a given time [95].

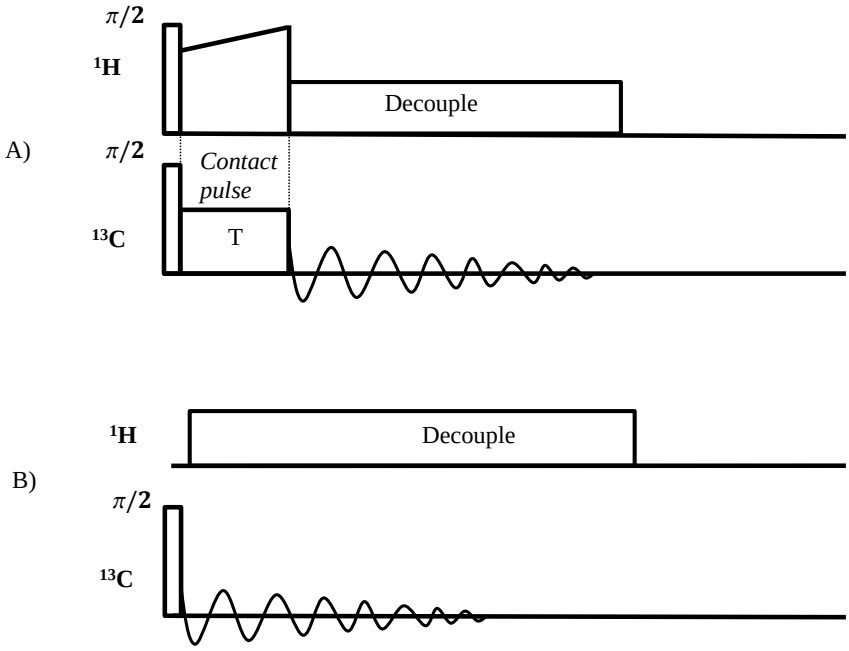

Figure 2.3: A) Pulse sequence for cross-polarization (CP) under magic angle spinning. The amplitude of proton channel was ramped to match the so-called Hartmann-Hann condition. During the contact time T, the ^{1}H magnetization is transferred to ^{13}C spins via dipolar coupling between ^{1}H and ^{13}C spins. B) Direct polarization (DP) pulse sequence used for the study. In DP experiments, $\pi/2$ pulse is only applied to ^{13}C spins. The high power decoupling applied to ^{1}H spins during the acquisition of ^{13}C spins removes the effect of ^{1}H dipolar coupling from the ^{13}C NMR spectrum.

The cross-polarization pulse sequence used for this study is shown in Figure 2.3(A). For the polarization to transfer from abundant nuclei, I, to the less abundant nuclei, S, contact between the two spins must take place. This can be achieved through the Hartmann-Hahn condition [97]. Cross polarization is a double resonance phenomenon in a doubly rotating frame, i. e. the I spins are in a frame in which all the magnetic fields due to I-pulses appear static, and the S spins are in a frame where the fields due to S-pulses also appear static. Transverse magnetization of the spins I is generated by a $\pi/2$ pulse at the frequency ω_{rfI}. Then, another pulse (contact pulse) at ω_{rfI} but with a phase shift of $\pi/2$ is applied to lock the magnetization along the field B_{1I} due to this pulse, the spin-locking field. Simultaneously, another radio frequency field B_{1S} is applied to the S spins, at ω_{rfS}. If now the magnitudes of B_{1I} and B_{1S} are matched by the Hartmann-Hahn condition,

$$\gamma_I B_{1I}(^1H) = \gamma_S B_{1S}(^{13}C) \tag{2.2}$$

each spin species precess with the same frequency ω_1 = -γ B_1 around the axis of its radio frequency field and in its own rotating frame. The polarization can then be transferred from the initially polarized I spins to the S spins. Finally, the S spins are detected while decoupling from the abundant I spins. The acquisition rate is determined by the relaxation time T_1 of the I nuclei, which is generally much smaller than that of the S nuclei [95].

2.1.3 Direct polarization

Direct polarization (DP) is another technique that is often used in SSNMR. The DP pulse sequence used for this study is shown in Figure 2.3 (B). In this method, a simple $\pi/2$ pulse

is applied on the ^{13}C channel followed by acquisition and the high power decoupling in the ^{1}H channel. The DP experiment allows for the observation of both highly mobile as well as restricted spins [95]. Acquiring high signal-to-noise-ratio for ^{13}C NMR spectra through direct polarization is time consuming as ^{13}C spins are dilute and require a relatively long recovery delays between the spectral scans. However, this experimental time can be reduced by using the CP technique described above. CP is mediated by heteronuclear dipolar coupling as discussed in previous paragraph. CP efficiency is good for rigid samples but it does not work well for mobile samples as rapid molecular motion averages out the dipolar coupling. For this work, both CP and DP techniques will be employed to study the structure and dynamics of both collagen and elastin.

2.1.4 ^{13}C NMR relaxation

Molecular motions may be generally described in terms of autocorrelation functions. The spectral density function, $\mathcal{J}_n(\omega)$ is the Fourier transform of the autocorrelation function which is defined as,

$$\mathcal{J}_n(\omega) = \frac{1}{\sqrt{2\pi}} \int_0^\infty \mathcal{G}_n(\tau) e^{-i\omega\tau} d\tau \qquad n = 0, 1, 2, ... \tag{2.3}$$

Assuming a single correlation time govern the relaxation process, the spectral density function may be written as

$$\mathcal{J}_n(\omega) = \frac{2}{5}(1 - y^2)\frac{\tau_c}{1 + (\tau_c\omega)^2}. \tag{2.4}$$

where y is the order parameter that describes the amplitude of motion and τ_c is the correlation time of the ^{1}H-^{13}C internuclear vectors.

The spin lattice relaxation time in rotating frame for two spins I, S in terms of spectral density functions is given by [98],

$$\begin{aligned}\frac{1}{T_{1\rho}^{IS}} = \mu_S^2\Big\{&\frac{1}{2}\Big[\mathcal{J}_0(\omega_I-\omega_S)+3\mathcal{J}_1(\omega_I)+6\mathcal{J}_2(\omega_I+\omega_S)\Big]\\ &+3\mathcal{J}_1(\omega_S)+\frac{1}{3}\Big[\mathcal{J}_0(\omega_e-2\omega_R)+\mathcal{J}_0(\omega_e+2\omega_R)\Big]\\ &+\frac{2}{3}\Big[\mathcal{J}_0(\omega_e-\omega_R)+\mathcal{J}_0(\omega_e+\omega_R)\Big]\Big\}\end{aligned} \tag{2.5}$$

The spin lattice relaxation time T_1^{IS} is given by,

$$\frac{1}{T_1^{IS}} = \mu_S^2\Big[\mathcal{J}_0(\omega_I-\omega_S)+3\mathcal{J}_1(\omega_I)+6\mathcal{J}_2(\omega_I+\omega_S)\Big] \tag{2.6}$$

In the above expressions, ω_e is the frequency of the spin locking field (applied to ^{13}C nuclei), ω_R is the spinning frequency of the rotor, $\mu_s^2 = \frac{\gamma_I^2\gamma_S^2\hbar^2}{4r^6}$, γ_I and γ_S are the gyromagnetic ratios for I and S spins, and ω_I and ω_S are the Larmor frequencies of the ^{1}H and ^{13}C spins, respectively.

The pulse sequence used for the $T_{1\rho}$ collagen experiments is shown in Figure 2.4

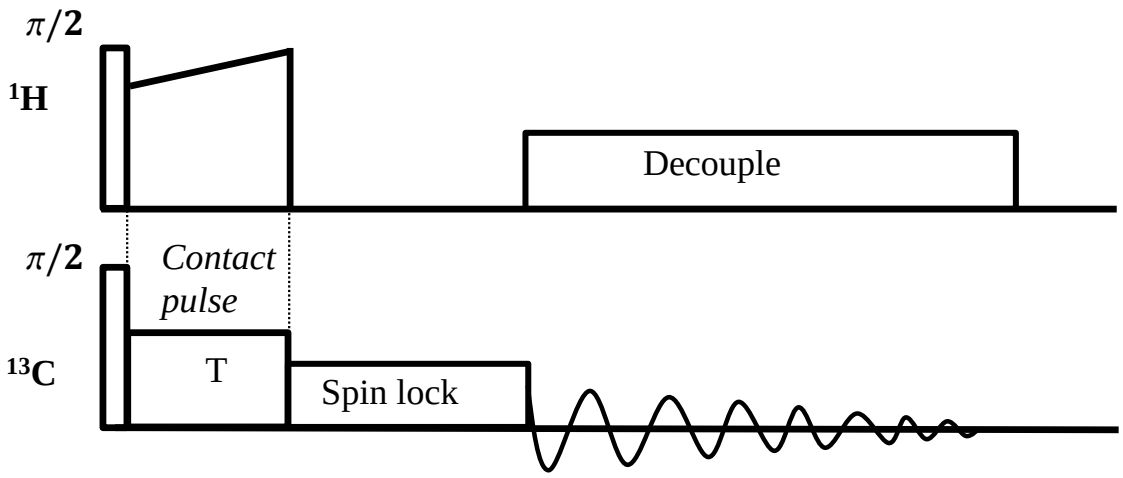

Figure 2.4: ^{13}C $T_{1\rho}$ with ^{1}H-^{13}C cross polarization used for collagen experiments. A similar experiment was implemented for studies on elastin, but without the cross-polarization step.

2.1.5 Two dimensional H^2 NMR relaxometry

The two dimensional T_1-T_2 correlation pulse sequence is composed of two parts: inversion recovery followed by CPMG. The signal is proportional to the (1-2 e^{-t/T_1}) e^{-t/T_2}, where t is the delay in inversion recovery and τ is the delay in CPMG and is given by

$$M(t,\tau) = \int\int (1 - 2e^{-t/T_1})e^{-\tau/T_2} \times F(T_1, T_2)dT_1dT_2 \tag{2.7}$$

Where $F(T_1, T_2)$ is the probability density of molecules. Laplace inversion is used to determine F from the above equation. The algorithm for two dimensional inverse Laplace transform (ILT) transformation has been demonstrated by Song and coworkers [99]. This powerful experimental technique has been previously applied on various systems such as potato tissue [100], cement paste [101], bovine nuchal ligament and aortic elastin [102], spider silk [103], cortical bone [104], and in water saturated sedimentary rock [105]. An example

spectrum using this algorithm is shown in Figure 2.5. Figure 2.5 shows T_1-T_2 spectrum of bulk water and Nugget sandstone obtained by Song and coworkers. For bulk water T_1 =T_2 and there is a single peak where as for the Nugget sand stone there are a number of peaks. The presence of separate peaks in Nugget sandstone are indicative of distinct water environment due to the constraints in movement of water molecules inside sandstone [99].

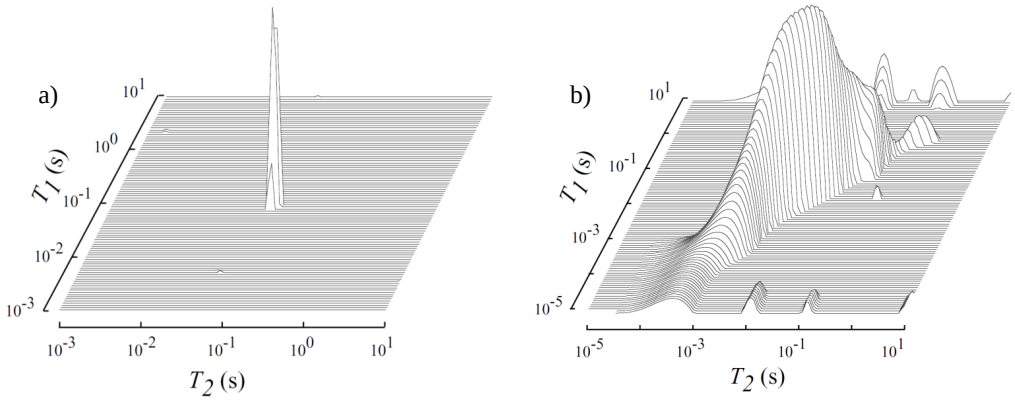

Figure 2.5: T_1-T_2 correlation spectrum for a) bulk water b) Nugget sandstone [99]

The pulse sequence used for H^2 NMR measurements is shown in Figure 2.6. In the T_1-T_2 experiments, the first π pulse inverts the magnetization which relaxes toward thermal equilibrium with a relaxation time T_1 during a delay t_1. The magnetization is then rotated into the transverse plane by $\pi/2$ pulse and the NMR signal is detected. A T_1-T_2 correlation map is obtained using a 2D ILT of the data.

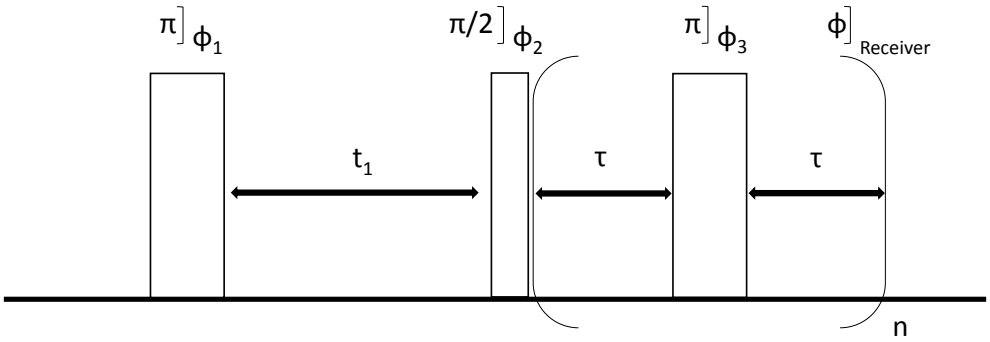

Figure 2.6: NMR pulse sequence used for H^2 2D T_1-T_2 measurements.

The dominant NMR relaxation pathway for the ^{2}H nucleus is quadrupolar as ^{2}H-^{1}H and ^{2}H-^{2}H nuclear dipolar interactions are usually negligible. The T_1 and T_2 relaxation times are given by [106],

$$\frac{1}{T_1} = \frac{3\pi^2}{20} {C_{Q_{eff}}}^2 [2J(\omega_0) + 8J(2\omega_0)] \tag{2.8}$$

$$\frac{1}{T_2} = \frac{3\pi^2}{20} {C_{Q_{eff}}}^2 [3J(0) + 5J(\omega_0) + 2J(2\omega_0)] \tag{2.9}$$

In the above expressions, $C_{Q_{eff}} = \frac{e^2 q_{eff} Q}{h} \Gamma$ is the effective quadrupolar coupling constant, and Γ is a motional averaging parameter. The spectral density is defined by $J(m\omega) = \frac{\tau_c}{1+(m\omega\tau_c)^2}$, where τ_c denotes the correlation time of the nuclear spin and surrounding electric field gradient which is intramolecular in origin. Using the measured T_1 and T_2, the correlation times may be determined by using equation (2.7) and (2.8).

2.2 Other techniques

2.2.1 Mass spectrometry:

Mass spectrometry is a powerful technique that can be used to gather qualitative and quantitative information about the composition of organic, inorganic and large biomolecules such as peptides, proteins, carbohydrates, and polymers in complex mixtures. Mass spectrometry (MS) provides precise mass measurements, and may be applied to analyze sample purity and elucidate molecular structure by measuring the mass-to-charge ratio when a sample is ionized [107, 108, 109].

A mass spectrometer with different components is illustrated in Figure 2.7. From the inlet system, a small amount of sample is inserted into the instrument and converted to gaseous phase. The gaseous phased samples are bombarded with electrons or photons and converted into ions at ion source. The mass analyzer disperses the ions on the basis of mass to charge ratio and the ion detector detects the amount of ion with a given mass-to-charge ratio by measuring a current [110].

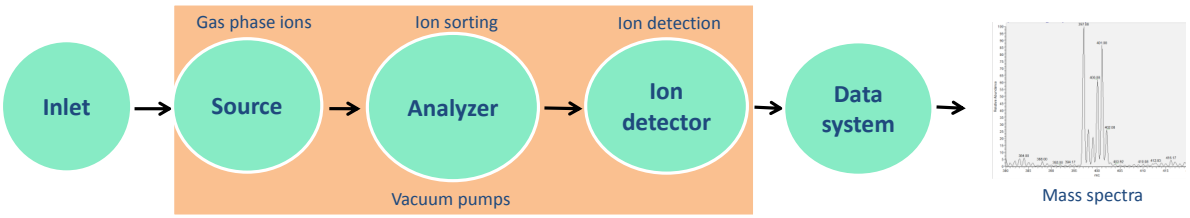

Figure 2.7: Illustrative figure of mass spectrometer with components.

A number of ionization techniques may be used for the mass spectrometry such as Chemical Ionization (CI) [111], Fast Atom Bombardment (FAB) [112], Electron Ionization (EI)

[113], Electrospary ionizaton (ESI) [114] and Matrix Assisted Laser Desorption Ionization (MALDI) [115, 116]. The two most widely used ionization techniques are Electrospray and Matrix assisted laser desorption ionization [117, 118]. For desmosine quantification measurements, the MALDI ionization technique will be used.

Large molecules of molecular weight up to 200 kD can be analyzed by using MALDI [119]. MALDI is used for the analysis of synthetic and natural polymers [120], proteins [121], carbohydrates [122] and relative desmosine quantification [36]. This technique directly ionizes and vaporizes the analyte from the condensed phase. The desorption and ionization in MALDI is induced by a single laser wavelength. The sample is prepared by mixing the analyte and the matrix compound and then spotted on a MALDI plate and dried. A laser beam is focused in dried spot of a MALDI plate, as a result of which analyte ions are ejected from the surface and a spectrum is acquired over each laser pulse. The interpretation of the mass spectra is easy, as MALDI produces mainly singly charged ions. The choice of solvent is important in MALDI as the solubility of analyte in evaporating solvent determines its inclusion in the matrix. The major advantages of MALDI mass is a gentle ionization technique, molecules need not to be volatile and picomole sensitivity can be obtained. Furthermore, MALDI exhibits moderate tolerance to salts and other contaminants. The one disadvantage is that matrix cluster ions obscure low m/z species, and thus the analyte must have low vapor pressure [123].

2.2.2 Spectrophotometry

A spectrophotometer is an instrument that measures the amount of light absorbed after it passes through a sample solution. With the spectrophotometer, the amount of a known chemical substance (concentration) can be determined by measuring the intensity of the light detected, and a standard curve. Based on the range of light source wavelength, there are different types of spectrophotometer. For this study, visible spectrophotometry was used. In visible spectrophotometry, the absorption and transmission can be determined by observing the color of the sample solution.

The basic illustration of the spectrometer is shown in Figure 2.8. It consists of a light source, a monochromator, a wavelength selector, sample solution, light detector, and a digital display. The spectrophotometer basically consists of two instruments - a spectrometer for producing light of desired wavelength and a photometer for detecting the intensity of light. These instruments are arranged in a way that the solution containing the sample is placed in between the spectrometer beam and the photometer. The spectrometer produces the desired wavelength of light. First the light from the source falls in the monochromator to split into several colors and the desired wavelength of light is transmitted by wavelength selector. Once the desired wavelength of light passes through the sample solution, the photometer detects the amount of photons absorbed and the signal is sent to a digital display meter as shown in Figure 2.8 [124, 125].

For concentration measurements, a series of standard solutions of known concentration are made and the spectrophotometer is set to a wavelength of maximum light absorption for the sample. The absorption of the unknown sample is measured and from the standard plot

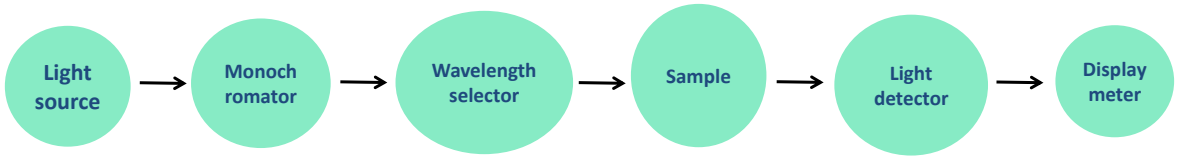

Figure 2.8: Illustrative figure of spectrophotometer with components.

of absorbance versus concentration, the concentration of an unknown sample is measured. This method was used for the measurement of collagen, MMP-2, MMP-9, microfibril and TIMP-1 concentration in different samples of this study.

Spectrophotometry is a widely used quantitative technique in physics, chemistry, biochemistry, and chemical engineering applications. The advantages of the spectrophotometry include its quick analysis ability and easy of use. This tool may also be used for structure elucidation of organic compounds, and impurities present can be detected by full absorption spectrum. Moreover, it can be used in the field of forensic analysis, medicine, pharmacy or food industry. The major drawback of the spectrophotometry is its inability to discriminate between the sample of interest and contaminants that absorb at the same wavelength. Absorption results can be influenced by temperature, pH, impurities and contaminants, which sometimes may lead to inaccurate measurements[124, 126].

Chapter 3

Effects of purification on elastin cross-links

This chapter highlights results published in ref. [36].

Desmosines are cross-linked amino acids unique to the matured elastin and can be used as potential biomakers to determine the extent of tissue damage and elastin breakdown [127]. A wide range of analytical techniques have been applied to measure desmosines such as enzyme linked immunosorbentassays (ELISA) [128, 129], amino acid analysis [130], radioimmunoassay [131, 132], electrophoresis [133], electrokinetic chromatography [134], high performance liquid chromatography (HPLC) [135], liquid chromatography (LC-MS) [136], and LC-tandem mass spectrometry (LC-MS/MS) [137]. Among these, LC-tandem mass spectrometry (LC-MS/MS has been observed to give more selectivity and sensitivity [138, 130]. Labor intensive process to prepare samples as well as relatively long chromatography runs makes the use of LC-MS more challenging. One potential technique to improve desmo-

sine/isodesmosine analysis time maintaining the selectivity and sensitivity is to use matrix assisted laser desorption/ionization (MALDI). MALDI data can be analyzed more rapidly with less chromatographic separation. In this chapter, a novel method to measure the concentration of desmosine in elastic fibers using MALDI-MS^2 quantification is described.

A distinguishing feature of elastin is its resistance to high temperature and pH that usually denature many proteins. Various purification schemes take advantage of these characteristics by heating the tissue in order to purify it from collagen, fat and smooth muscle. A detailed comparison of the purity of the products resulting from five purification schemes has been recently documented by Daamen et al. using amino acid analysis, sulphydryl quantification, and transmission electron microscopy [139]. Their results showed that the purification methods may also result in a product that includes traces of the microfibrillar component of the elastic fiber. In this chapter, I summarize results highlighting alterations of desmosine concentration as measured by MALDI mass spectrometry.

3.1 Sample preparation

Both purified and unpurified bovine nuchal ligament elastin samples were purchased from Elastin Products Company, LLC (Owensville, MO). Elastin Products Company, LLC purified the tissue using the following three methods which are summarized in reference [140]. The unpurified bovine nuchal ligament elastin sample was cleared of muscle and fat and dried by Elastin Products Company, LLC. All samples arrived having an average mesh size of $90\mu m$ (Samples 1 to 3) and $465\mu m$ (Unpurified) and were lyophilized for 72 hours. Experiments on hydrated samples were prepared as follows: the samples were suspended in distilled

water for 48 hours and then centrifuged for 3 minutes to remove bulk water for packing into the NMR rotor. The water to protein concentration of all samples was determined to be approximately 40% by volume. Standard amino acid analysis was performed by J. Myron Crawford's group at the W.M. Keck Biotechnology Resource Laboratory at Yale University using a Hitachi L8900 analyzer. Amino acid analysis on unpurified elastin was performed by New England Peptide (Cambridge, MA) using the same instrumentation.

Sample 1: Autoclaving [141]: The tissue was washed, minced and autoclaved in 20 volumes of distilled water for 45 minutes at one atmospheric pressure. This procedure was repeated 3 to 4 times until no protein trace was detected in the supernatant. Then residue was dried by lyophilization after treating with ethanol. .

Sample 2: Hot alkali [142]: Defatted and minced tissue was suspended in 0.1 N $NaOH$ and mixed. The product is placed in boiling water for 45 minutes and stirred. The sample was then stored at room temperature and washed with cold 0.1N $NaOH$ followed by centrifugation.

Sample 3: Starcher method [143]: 0.05 M Na_2HPO_4 at 7.6 pH, 1% $NaCl$, 0.1%$EDTA$ was used as a buffer to extract the tissue. The purification begins with suspending the tissue in the buffer for 72h. The product is washed twice with distilled water and lyophilzed. 200mg of the lyophilized product was suspended in 30ml of water and autoclaved for 45min at 25 PSI. The next step includes centrifugation and washing the tissue. The product is suspended in 30ml of 0.1M Tris buffer at a pH of 8.2, that contains 0.02 M $CaCl_2$ and incubated with 4mg of trypsin at 37°C for 18h. The sample is centrifuged and the residue is washed and suspended in 10ml of 97% of formic acid. Cyanogen bromide (200mg) is added

and the suspension shaken under a hood at room temperature for 5h. The sample is then centrifuged and the residue is washed twice with water and resuspended in 30ml of 0.05 M Tris buffer at a pH of 8.0 which contains 6 M urea and β-mercaptoethanol (0.5%v/v). The suspension is stirred overnight at room temperature, centrifuged, washed successively with the three washes each of ethanol and acetone, and dried in vacuum over P_2O_5.

3.2 Quantification of desmosine concentration

3.2.1 Elastin hydrolysis

2.1-2.2 mg of each sample was placed in 300μL of 6N HCL and 1μL of 0.5% w/w phenol solution in sealed glass tubes and flushed with argon gas. The samples were incubated at 110 °C for 96 hours. After incubation the solvent was frozen under liquid nitrogen and then lyophilized for 6-8 hours. The sample was then re-suspended in 50μL of solution of 95.5% 0.14M sodium acetate, 0.5% triethylamine, 5% acetonitrile (v/v/v) at a pH of 7.5.

3.2.2 Quantification with labeled desmosine

Resuspended samples were mixed in 1 : 1 (v/v) ratios with standard d_4-desmosine (Toronto Research Chemicals, Toronto, Canada) at a final concentration of 0.250 mg/mL. The mass spectrometric peak intensity ratio in MS^2 mode of desmosine to d_4- desmosine was used to quantify the relative amount of desmosine in each sample.

The solution of standard and matrix was made in the ratio of 1:9 (v/v) and stirred. The standard d_4-desmosine (Toronto Research Chemicals, Toronto, Ontario, Canada) was at a final concentration of 0.250 mg/mL. In addition, 10 μL of this solution were mixed with 1

μL of resuspended solution. The ratio of natural abundance desmosine to d_4-desmosine was used to quantify the amount of desmosine in the sample.

3.2.3 MALDI-MS quantitative analysis

MALDI-MS^2 experiments were performed using a Thermo LTQ XL ion trap mass spectrometer (Thermo Scientific, Waltham, MA, USA) equipped with a vacuum MALDI source. α-Cyano-4-hydroxycinnamic acid (CHCA) was purchased from Sigma-Aldrich (St. Louis, Missouri, USA) and used without additional purification. Solid CHCA was then mixed with a solution of 0.1% trifluoroacetic acid, 70% acetonitrile and 29.9% HPLC grade water until saturated, and used as a matrix solution. $1\mu L$ of the sample was added to 10 μL of solution containing standard desmosine and CHCA matrix solution. The solution of CHCA matrix and standard was prepared in the ratio 1:9 ($1\mu L$ standard in $9\mu L$ of CHCA matrix). Finally, the solution was stirred and $1\mu L$ of the solution was spotted on the MALDI plate and allowed to dry prior to mass spectrometric analysis.

MALDI-MS^2 analysis was conducted using a laser energy of 2.6 μJ, for 150 scans with the AGC set to $10,000$ ions. Precursor ions of unlabeled desmosine (m/z 526.3) and d_4 labeled desmosine standard (m/z 530.3) were selected in a single isolation window (m/z 529 ± 6), and fragmented with a normalized collision energy = 35, activation Q = 0.25, activation time = 30 ms. The most intense product ions, at 397 m/z for unlabeled desmosine and 401 m/z for d_4-desmosine, were used for relative quantification.

3.3 Discussion and conclusions

Amino acid analysis was performed on all the samples in order to analyze their purity [36]. For each sample $0.8\frac{ml}{mg}$ of HCl was used for hydrolysis in vacuum at $110°C$ for $48h$. After drying off the acid, each aliquot was dissolved and serially diluted to load onto the amino acid analyzer. Table 3.1 highlights the results of the amino acid analysis. The results show that elastin is largely composed of glycine, proline, alanine and valine; more than 84% of the residues in a single molecule belong to these four amino acids. Additionally, in less concentration, these measurements reveal that elastin also contains isoleucine, leucine, phenylalanine, and glutamine. Additional traces of amino acids appearing in unpurified bovine ligament elastin, such as histidine, may be evidence of either residual collagen or smooth muscle. Note that the presence of these amino acids also skews the percentage contribution of other tabulated values. These findings for purified samples are in agreement with the theoretical values computed from the cDNA of tropoelastin [144] and with work reported elsewhere [140].

To compare these three purification methods for tissue samples, MS/MS experiments were performed to quantify the amount of desmosine in the samples treated with and without the purification steps. The internal standard, d_4-desmosine, was added prior to the MS/MS experiments where the precursor ions for desmosine and d_4-desmosine were fragmented into their product ions (m/z 397 and 401, respectively), shown in Figure 3.1. In addition, Table 3.1 includes the relative concentration of desmosine in each sample studied in this work. The numbers reported are shown as the ratio of desmosine to d_4-desmosine, normalized to the unpurified sample. Note that this metric is thus sensitive to traces of residual fat and

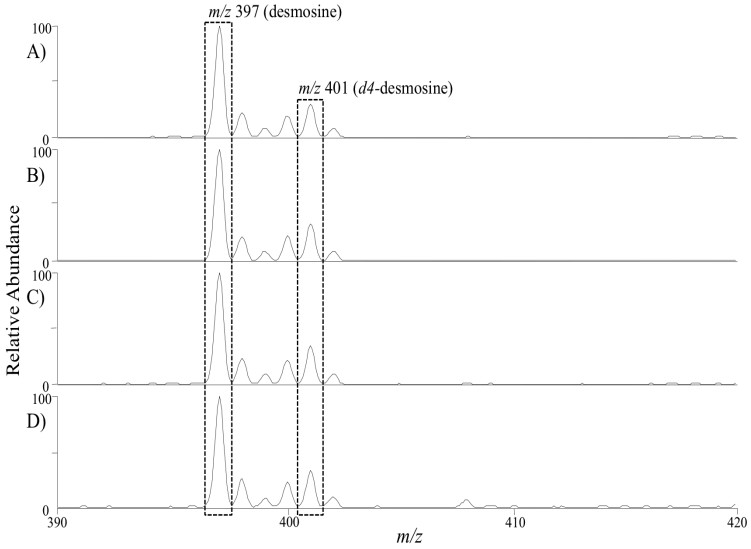

Figure 3.1: Mass spectrometric spectra of hydrated samples treated with various purification methods: A) autoclaving (sample 1), B) hot alkali (sample 2), C) Starcher (sample 3), and D) unpurified. The relative amount of desmosine in the samples was measure by monitoring peak intensity of MS^2 fragmentation of unlabeled desmosine (m/z 397) to d_4- desmosine (m/z 401).

collagen. The results of Table 3.1 indicate that the relative desmosine concentration in the samples are very similar, with similar overlap in error bars; sample 2 (hot alkali protocol) appears to have slightly higher desmosine concentration with respect to all the other samples. The small differences between sample 2 and all the other samples may be attributed to traces of fat and collagen, or differences in the extent of cross-linking across the samples. As the starting tissue was the same in all three isolation schemes, the amount of cross-linking is presumably similar. These results would indicate that sample 2 may contains slightly less residual fat and collagen compared to the other isolation schemes studied. Furthermore, ^{13}C NMR was also applied to study the alterations in the structure and dynamics of the elastin.

^{13}C NMR results show that elastin maintains its structure on purification as no differences in NMR chemical shifts were observed across samples. However, small differences in dynamics and relative signal intensities were observed for some amino acid motifs [36]. Since, the desmosine concentration as well as the structure in samples purified from different schemes are similar within the error limit, purification schemes do not alter cross links.

	res/1000				
	Sample 1	Sample 2	Sample 3	Unpurified	Theory*
Asx	5.6	4.6	4.1	4.2	4
Thr	6.9	5.5	6.8	1.0	11
Ser	7.1	6.4	7.3	0.0	10
Glx	14.5	14.9	14.0	19.7	14
Pro	147.5	149.2	153.2	121.0	119
Gly	335.9	332.6	329.7	325.3	319
Ala	238.3	237.6	238.4	229.1	211
Val	121.8	125.3	123.7	125.5	126
Cys	-	-	-	-	-
Met	0.0	0.0	0.0	0.0	-
IIe	21.9	22.2	22.2	21.1	25
Leu	53.7	54.6	53.9	62.7	60
Tyr	6.9	7.3	7.2	17.4	10
Phe	33.2	34.3	34.6	38.4	29
His	0.0	0.0	0.0	10.4	0
Lys	2.4	1.9	1.9	10.9	53
Arg	4.3	3.6	3.0	13.3	7
Relative desmosine concentration	1.00±0.10	1.09±0.12	0.86±0.10	1.00±0.14	-

Table 3.1: Amino acid analysis of three purified bovine nuchal ligament elastin samples (samples 1-3, described in the text), unpurified elastin and their relative desmosine concentration. The amino acid measurements are reported as "residues per 1000 residues (res/1000)" for ease of comparison with other published results [140]. The theoretical values, shown in column 6, correspond to the amino acids computed from cDNA of bovine tropoelastin [144]. The relative desmosine concentration represents the ratio of desmosine to d_4-desmosine, normalized by the unpurified sample (starting product).

Chapter 4

Pregnancy induced alterations of elastin in the female reproductive tract

4.1 Introduction

Desmosines are cross-linked amino acids unique to mature elastic fibers [127]. Zunga-smith et al. showed that during pregnancy the formation of desmosine does not keep pace with the formation of elastin but rather it lags behind. Immediately after birth, there is a loss of desmosine-poor elastin from the reproductive tract, and consequently the ratio of the desmosine to elastin returns to a normal level [6]. A similar pattern of elastin deposition during pregnancy with reduced proportion of desmosines has been observed in human uteri. Zunga-smith et al. also showed that the collagen and elastin content increases with successive pregnancies; however the cross-link concentration (measured in moles of desmosine plus isodesmosine per 1000 residues of amino acid) was larger in parous (2 pregnancies) nongravid females in comparison to virgin females [145].

A study on reproductive tract collagen, summarized in the next chapter, revealed no structural change as a function of parity and pregnancy at a microscopic level. However, a signature of collagen fiber dissociation with smooth muscle and a change in the density of collagen fibers in multiparous rats was revealed at a macroscopic level by histological methods leading to a redistribution of water due to pregnancy and/or parturition [146]. In another study in our laboratory, it was discovered that postpartum rats had more tortuous elastic fibers than virgin rats, although mode of delivery had no effect on the tortuosity of those fibers. Additionally, it was found that between two days and two weeks postpartum, the fibers of elastin had undergone some mechanistic repair that yielded less tortuous elastic fibers, though still more tortuous than virgin cohorts [59].

To date there has been no experimental study of the alterations of reproductive tract elastin and its associated structural alterations due to pregnancy. This thesis work has provided the first such study. In this chapter, I summarize results from an experimental investigation of the effects of parity on architecture of vaginal elastic fibers in female Sprague-Dawley rats by histological methods. NMR spectroscopic and relaxation techniques were employed to follow the structural and dynamical changes in elastic fibers, respectively. In order to probe structural changes, ^{13}C direct polarization under magic-angle spinning (DPMAS) NMR was applied to probe dynamical fluctuations of the spectroscopically resolvable moieties across virgin and multiparous as well as para1 (one birth) and para3 (3 births) rats studied. ^{2}H T_1-T_2 experiments based on an inverse Laplace transform (ILT) were also performed to characterize the distribution and dynamics of water in uterine horn elastic fibers. The concentration of MMP-2, MMP-9, and TIMP-1 in reproductive tract tissue of

various samples studied was quantified by spectrophotometry. The desmosine content in the uterine horn elastic fibers was studied using MALDI-mass spectrometry.

4.2 Materials and methods

4.2.1 Animals

Animal protocol in this study was endorsed by the Institutional Animal Care and Use Committee at the Albert Einstein college of Medicine. For this study, altogether 70 Sprague-Dawley rats were used. These included virgin (11-14 weeks of age), para1, para3, and multiparous cohorts (9-15 months old). For histological study, virgin, para3, and multiparous cohorts (2 per group) were used. For purification of elastic fibers, in the first set 20 rats of multiparous and virgin cohorts (10 per group) were used. For the second set of purification, virgin , para1, para3, and multiparous cohorts (8 rats per group) were used. 12 rats (4 per group for MMP-2 and MMP-9 measurements while 2 for TIMP-1 measurements) were used for the MMP-2, MMP-9, and TIMP-1 quantification.

4.2.2 Histology and microscopy

A small portion of the upper vaginal wall of three cohorts: virgin, para3, and multiparous were placed overnight in 100 ml of phosphate buffered saline with 30 g sucrose. The sample was then placed in Lieca Cryo-Gel (SPI supplies Product 02694-AB) and sectioned on a Leica CM1850 cryostat at 10 μm and 16 μm with no noticeable difference between the two. The samples were then placed on microscope slides and stained using a commercial stain kit for elastin (Sigma Aldrich REF HT25A-1KT) following a protocol adapted from Downing et

al. [59]. The slides were placed in a stain solution containing 20 ml haematoxylin solution, 3 ml of ferric chloride solution, 8ml of Weigert's iodine solution, and 5 ml of deionized water for 10 min. The slides were then placed in a working ferric chloride solution. Next, the slides were then gently rinsed with water, placed in 100% ethanol for a few seconds, and again gently rinsed with deionized water. The slides were placed Van Geisen solution for 1.5 min, followed by a gentle rinse with 100% ethanol and placed in xylene for a few seconds. Lastly, cover slips were mounted using Eukitt quick-hardening mounting medium (Sigma-Aldrich REF 03989) and left to dry overnight.

4.2.3 MMP-2, MMP-9, and TIMP-1 quantification

Uterine horn tissues from virgin, para1, para3, and multiparous samples were rinsed in 1× PBS solution to remove blood and weighed before homogenization. Tissues from different samples were finely minced and homogenized using a Bio-Gen PRO200 Homogenizer in 4-4.5 ml of PBS at 0°C. The cells were lysed thawing three times and underwent ultrasonication. The homogenates were centrifuged at 5000 rpm for 5 minutes and supernatant was collected for assaying. MMP-2, MMP-9, and TIMP-1 standards were prepared in the range of 0-4000 pg/ml, 0-50 ng/ml, and 0-10 ng/ml from a standard solution provided by Abbexa Ltd (Innovation Centre, Cambridge Science Park, United Kingdom), respectively. All of the samples and standard dilutions procedures were followed from the assay kit provided. The absorbance for the standard and the samples in 96 well plate were measured at wavelength of 450 nm using FLUOstar OPTIMA microplate reader (BMG Labtech, Thermo Fisher Schientific, Waltham, MA).

4.2.4 Isolation of elastic fibers

Two different biological replica sets were used for purification. For the first set of purification, twenty Sprague Dawley rats of two cohorts: virgin and multiparous were used. In a second set, eight Sprague Dawley rats of four cohorts each : virgin, para1, para3, and multiparous were used. The reproductive tracts of each cohort were supplied by Charles River Laboratories, Wilmington, MA. The only difference in the first set and second set of purification was centrifuge speed (first set centrifuge speed 5000 rpm, second set centrifuge speed- 12000 rpm) while filtering the samples in the steps described below. For this study, only the uterine horn of the reproductive tract was used. To remove fat from the sample, the procedure from Mecham et al. was adapted [147]. Saline solution was used to wash the uterine horns and repeated three times. Then, the horns were kept in 100% ethanol for 7-10 minutes and the procedure was repeated twice. The tissue was then placed in a (50/50) mixture of ethanol and diethyl ether (99%) for 7-10 minutes (2 times). Finally, the tissue was placed in diethyl ether for 10 minutes (2 times). The tissues were then lyophilized, weighed, and homogenized using Bio-Gen PRO200 Homogenizer.

Elastic fibers were isolated from the uterine horns following Starcher's method [148, 147]. To extract the homogenized tissue, 0.05 M Na_2HPO_4 buffer (pH 7.6), containing 1% NaCl and 0.1% EDTA was used. The extraction was continued for 72 h with repeating changes of the buffer. The residue was washed with distilled water (three times) to remove the buffer after the final extraction and lyophilized. For 200 mg of the lyophilized tissue 30 ml of water was used and autoclaved for 45 min at 25-lb pressure. After autoclaving, the residue was centrifuged and washed twice with distilled water. The residue was then suspended in 30 ml

of 0.1 M Tris buffer (pH 8.2), containing 0.02 M $CaCl_2$ and incubated with 4 mg of trypsin at 37 °C for 18 h. The sample was centrifuged and the residue was washed (three times) with distilled water, and suspended in 10 ml of 97% formic acid. Cyanogen bromide (200 mg) was added and the suspension was stirred for 5 h in a well ventilated fume hood at room temperature. The sample was then centrifuged, washed (three times) and resuspended in 30 ml of 0.05 M Tris buffer (pH 8.0), containing 6 M urea and β-mercaptoethanol (0.5%, v/v). The suspension was kept at room temperature for 12 h, centrifuged, washed three times with ethanol and acetone, successively. Finally, the elastic fibers from all the cohorts were combined and was stored in distilled water at -20 °C prior to experiments. Purity of the isolated elastin was confirmed by amino acid analysis in the multiparous and purified bovine nuchal ligament elastin which appear similar to each other and to the reported theoretical values by Dameen et. al [144]. Amino acid composition are presented as molar % in Table 4.7 All amino acid analysis was performed by New England Peptide (Gardner, MA).

4.2.5 Sample hydrolysis and quantification with labeled desmosine

The protocol used for desmosine measurements is described in Chapter 3.2.

4.2.6 ^{13}C MAS NMR experimental parameters

^{13}C NMR experiments were carried out at the New York Structural Biology Center on a Bruker Avance (Billerica, MA) spectrometer at (300 ± 1) K . All direct polarization (DP) experiments were performed at a magnetic field strength of 21.10 Tesla using a 3.2 mm center packed rotor and (17 kHz ± 20 Hz) spinning speed. To keep samples hydrated and centered

with respect to the RF coil, silica inserts were used. In all DP experiments, the ^{13}C $\pi/2$ pulse was 5 μs and recycle delay was 9 s. All ^{13}C spectra were acquired using approximately 80 kHz TPPM decoupling [149]. All $T_{1\rho}$ relaxation measurements were acquired in 750 MHz system at (300 $\pm$ 1) K using a 4 mm center packed rotor with an insert to prevent the loss of water as well as to center the sample with respect to the RF coil. The DEPTH sequence was used to mitigate background signals [150, 151]. In all experiments, the ^{13}C $\pi/2$ pulse was 45 μs and recycle delay was 6 s. For the $T_{1\rho}$ experiments, the two different spin locking fields of 50.00 and 25.00 kHz were used. The spin locking time interval used for these measurements varied from 50 μs to 7000 μs. All DP spectra were analyzed using matNMR by using 100 Hz line broadening. Relaxation measurements were analyzed using matNMR with a Gaussian multiplication broadening factor of 150 Hz. ^{13}C NMR spectra presented in this work were referenced to adamantane (TMS scale).

4.2.7 Microfibrillar quantification

The protocol for microfibrillar quantification was adopted from Dameen et al. [152]. Ellmann's reagent was prepared by placing 4 mg of DTNB in 1 ml of 0.1 M Tris HCl (pH 8.0). Cysteine solution in the range of 0-600 μg/ml was used to generate the standard curve from the stock solution of 1200 μg/ml. 40 μl of diluted standards and samples (hydrolysed solutions of virgin and multiparous rat cohorts from desmosine measurements) were placed in a 96 well plate. 220 μl solution containing 20 μl of Ellmann's reagent and 200 μl of Tris HCl was placed into each well. The plate was sealed at room temperature for 20 minutes and absorbance was measured at 410 nm using a FLUOstar OPTIMA microplate reader (BMG

Labtech, Thermo Fisher Schientific, Waltham, MA).

4.2.8 ^{2}H NMR experimental parameters

All ^{2}H T_1-T_2 experiments were carried out at a magnetic field of 4.21 Tesla and ^{2}H resonance frequency of 27.55 MHz using a Doty probe at 25 °C. A portion of sample of elastin used for NMR measurements was soaked in D_2O for ∼72 h before experiments. For all the ^{2}H experiments, ^{2}H $\pi/2$ pulse was 25 μs and interpulse spacing in the CPMG train was 700 μs. The recovery time was logarithmically incremented from 1 ms to 20 ms in 150 steps to measure T_1, and stroboscopic detection of 5120 echo peaks was used for T_2 relaxation time measurement. ^{2}H T_1-T_2 relaxation data were analyzed using 2D ILT algorithm, described elsewhere [153].

4.3 Results and discussion

Histological images of the stained upper vaginal sections for samples studied were taken at 40× magnification as described in the method section and in previous work [59]. Representative histological images for virgin, para3, and multiparous samples are shown in Figure 4.1. In these figures, elastic fibers are stained black, collagen is stained red, and smooth muscles are stained yellow. A careful examination of the images revealed more linear and less fragmented elastic fibers in the virgin sample when compared to the multiparous and para3 samples. These images also show differences in collagen, smooth muscle, and elastic fiber content.

Tortuosity is defined as the integrated path length divided by the end-to-end distance [59]

and given by

$$\tau = \frac{\int_{x1}^{x2} \sqrt{1 + (\frac{dy}{dx})^2}}{\sqrt{(\Delta x)^2 + (\Delta y)^2}} \tag{4.1}$$

where x and y are pixel coordinates and Δx and Δy are end to end distances of a given fiber in the image.

Modeling the elastic fiber as a polymer, the tortuosity of the elastic fiber should correlate with the tension it can bear under stress and hence alter its scaffolding properties. In this model, a flexible polymer can be modeled as a superposition of neighboring monomers which can reorient in any direction allowing for linear to tortuous chain. Hence, polymer tension f is proportional to its end to end length $\langle l \rangle$ and is given by [154],

$$f = \frac{T \langle l \rangle^{3/2}}{N^{3/2} b^{5/2}} \tag{4.2}$$

where N is the number of monomers, T is the temperature and b is the length of individual monomer. For linear fibers, $\tau = 1$ and $\langle l \rangle$ is maximum such that it would provide more support to the tissue compared to highly tortuous fibers ($\tau > 1$). Hence, highly tortuous fibers require decrease in tortuosity before providing same tension under a given strain of the tissue.

For length and tortuosity measurements approximately 100 to 150 images were accumulated for each cohort. The curled nature of the elastic fiber was quantified by measuring the fiber tortuosity defined by equation (4.1). In order to probe the relationship between pregnancy and elasticity of the uterus, the effect of parity as a function of elasticity was investigated. Changes in the upper vaginal wall of Sprague-Dawley rats were tracked for virgin,

para3, and multiparous rat tissue sections. The length and tortuosity were measured using a method as reported previously [59], and presented in Table 4.1. The only modification was such that the median of the length, skewness, and kurtosis was reported to allow for a closer look at the statistical distribution of the data allowing for a more in depth characterization of the statistics of the distribution of the elastic fibers. A histogram of elastic fiber length and tortuosity measurements for each cohort studied is presented in Figure 4.2, 4.3, 4.4, 4.5, 4.6, and 4.7.

Table 4.1 summarizes the measurements of median fiber length and tortuosity for the various samples studied. It also shows the number of fibers over which statistics was accumulated. The numbers reported were determined by tracing fibers from inner, middle, and the outer layer of upper vaginal wall. These data show that the median length of the elastic fibers in multiparous cohorts is shorter than that of the other cohorts studied. From the histogram (Figure 4.2, 4.3, 4.4, 4.5, 4.6, and 4.7), the elastic fiber length in virgin and para 3 cohorts appear to follow a normal distribution while in multiparous sample appear to show two overlapped distributions: one with shorter fibers and another with longer fibers. The skewness of the virgin fiber length is 2.36 while for the multiparous is 5.23 indicating a mean fiber length distribution more asymmetric in the multiparous sample. The kurtosis value in the multiparous sample is 46.12 while in the virgin sample it is 9.29, indicating a heavily right tailed in the multiparous sample. These changes in skewness and kurtosis in the elastic fibers of multiparous tissues may arise from new fibers during or after pregnancy. Data in Table 4.1 shows an increase in tortuosity when comparing virgin, para3, and multiparous tissues. The elastic fiber tortuosity in virgin tissues appears to be slightly more asymmetric

(higher skewness) compared to the multiparous tissues. Additionally, the mean fiber tortuosity is heavily right tailed in the multiparous tissues (higher value of kurtosis) compared to that observed in the virgin tissues. These macroscopic changes have been previously correlated to the stiffness of the tissue [59], and were the stimulus for this study which is aimed at unveiling the microscopic alterations of elastin, the principal protein component of the elastic fiber.

The female reproductive tract undergoes extensive remodeling throughout each reproductive cycle to support placentation. These dynamical changes in the extracellular architecture are partly regulated by the matrix metalloproteinases (MMPs) and associated tissue inhibitors of matrix metalloproteinases (TIMPs) [155]. Thus, an additional goal of this study is to quantify MMP-2, MMP-9 and TIMP-1 expression involved in regulation of elastin during pregnancy and/or parturition. Total MMP-2, MMP-9, and TIMP-1 content in virgin, para1, para3, and multiparous tissues are presented in Table 4.2. From Table 4.2, it was found that MMP-2 and MMP-9 content is highest in the virgin reproductive tract tissue while its associated inhibitor TIMP-1 is similar within our experimental uncertainty. As shown below, these results appear to correlate well with the observed differences in the ^{13}C MAS NMR spectra of elastin from virgin and multiparous cohorts. The higher enzyme concentration in the virgin tissues gives rise to ^{13}C NMR spectra unlike that of mature elastin from other mammalian tissues, including rats.

The levels of MMP-2, MMP-9, and TIMP-1 in the cervix and uterine tissue in nonpregnant virgin and postpartum rats have been previously reported by Lyons et al. [156]. In uterine tissues, the MMP-2 levels in nonpregnant virgin rats were found to be higher

than postpartum rats, as in our measurements. However, in the cervix the nonpregnant and postpartum levels of MMP-2 were similar within statistical uncertainty. MMP-9 levels in postpartum rats in uterine tissues were lower in concentration in comparison to MMP-2 levels, and the levels between nonpregnant virgin and postpartum rats were similar within statistical uncertainty. In our measurements, higher concentration levels were measured in comparison to MMP-2 levels. These differences in concentration may arise from the sensitivity of the assay kit that was used. Referring to [156], the levels of TIMP-1 in nonpregnant and postpartum cervical and uterine tissue were found to be similar within statistical error as our experiments. These trends reported by Lyons et al. document changes due to pregnancy—however, the number of pregnancies in the rats was not included in their study. The results in our study, shown in Table 4.2, track the changes in concentration of MMP-2, MMP-9, and TIMP-1 following one, three, or more than five (multiparous) pregnancies.

During pregnancy the elastin content in the uterus increases several-fold and varies from animal to animal [7, 6, 5, 29, 27]. In the rat uterus, there is a steady increase of elastin content to three times above non-pregnant controls and elevated levels of desmosines are observed at this point [6]. The loss of elastin begins prior to birth and continues on into the postpartum period. However, it has been shown that the formation of desmosine lags behind the pace of formation of elastin. In the postpartum period, the ratio of the desmosine to elastin concentration has been observed to be fall below its nominal (prepartum) value [6].

The desmosine content (per mg lyophilized sample) for virgin, para1, para3, and multiparous samples are presented in Table 4.3. Referring to Table 4.3, the amount of desmosine is highest in the multiparous sample compared with the other three samples studied. Sur-

prisingly, these results also show that the amount of desmosine increases with increase in parity for the various cohorts. The amount of desmosine in multiparous sample is similar to that observed in bovine nuchal ligament elastin. These two samples also exhibit similar structural and dynamical characteristics, as studied by ^{13}C NMR and are discussed below. In a previous study by Gunja-smith et al., the amount of desmosine cross-links in the human uterus were observed to vary with successive pregnancies from age between 18 to 34 yrs [145]. In that study, they observed that nongravid females with successive pregnancies exhibited a higher desmosine concentration in comparison to a virgin female, in agreement with the trends observed in our study. For example, a 33 year old nongravid female with 9 pregnancies exhibited molar concentration of desmosine plus isodemsosine (per 1000 residues of amino acids) of 2.44, whereas a nongravid virgin female had a concentration of 1.64.

To provide insight into the dynamical and structural modifications to elastin in each cohort the NMR ^{13}C chemical shifts and relaxation times were measured. Natural abundance ^{13}C DPMAS NMR spectra were recorded for virgin, para1, para3, and multiparous uterine horn elastic fibers and are shown in Figure 4.8 and Figure 4.9. For the virgin spectra, experiments were performed at 22kHz rather than 17 kHz, as rotor stability was an issue due to small sample sizes. However, spectra from 22kHz MAS and 17 kHz MAS were observed to be similar. The representative aliphatic region of multiparous sample at 300 K with chemical shift assignments following previously reported measurements of elastin and its related peptides is shown in Figure 4.8 [36, 157, 35, 57, 158, 159]. Figure 4.9 compares the aliphatic region for virgin, para1, para3, and multiparous samples as well as elastin spectra from purified bovine nuchal ligament.

The spectra obtained under MAS allows for the assignment of C_α and C_β aliphatic carbons typically from 17 ppm to 70 ppm. In ^{13}C NMR, methyl peaks in between 17 ppm to 20 ppm are assigned to valine and alanine residues. From a study of the elastin mimetic polypeptide $[(VPGVG)_4(VPGKG)_{39}]$, Yao et. al assigned the peak at 19 ppm to val C_γ [160]. They further assigned isotropic chemical sifts of various sites by ^{13}C-^{13}C and ^{15}N-^{13}C correlation experiments. The Pro C_β peak was assigned at 30.5 ppm where as two chemical shifts 31.3 and 30.1 ppm were reported for Val C_β residues. Val C_α and Pro C_α signals were assigned chemical shifts of (57.1, 61.5) and 60.8 ppm, respectively [160]. More recently, Pro C_β and Val C_β in bovine nuchal ligament elastin were assigned chemical shifts of 31.8 and 32.8 ppm, respectively. Pro C_α and Val C_α have been assigned chemical shift of 63.35 and 62.08 ppm, respectively in the same study [161]. Further details relating to structural assignments from ^{13}C NMR are given in [36]. Table 4.4 summarizes the detailed chemical shift analysis and related secondary structure for elastin isolated from virgin, para1, para3, and multiparous rat cohorts used in our study.

Among all the samples studied, the virgin spectrum appears remarkably different compared to the spectra from elastin isolated from multiparous tissues. Referring to Figure 4.9, differences in line widths and signal intensities are observed when comparing the spectra of elastin from virgin and multiparous uterine horns. Overall, all the peaks in the virgin sample appear broader and are less resolved in comparison to the elastin spectra in other cohorts. In the region from $\sim$ 45 ppm to 65 ppm, no peaks are well resolved compared to the multiparous sample. It was noted that this particular region represents the C_α chemical shifts of alanine, which are abundant at the cross-linking sites of elastin in the form of polyalanine segments

such as AAAAA [41]. The signal intensity of glycine (∼43ppm) most abundant amino acid is significantly reduced in the case of the virgin rat. The intensity of this peak increases when comparing para1 to para3 spectra and exhibits highest intensity in elastin isolated from the multiparous tissues. However, the signal intensity of the peak ∼ 28 to 30 ppm (Pro C_β / Val C_γ) is observed to be higher in the virgin sample. The para1 spectrum closely resembles the virgin spectrum while para3 spectrum resembles the multiparous spectrum. The changes in the ^{13}C NMR spectrum of the virgin rat arise from structural alterations mediated by the higher concentration of MMP-2 and MMP-9 in these tissues. The enzymatic activity has been reported to cleave the peptide bonds in elastin and hence alter the amino acid concentration [162]. The intensity variation in the ^{13}C NMR spectra may be caused by these enzyme activities, in addition to the reduction in cross linking discussed earlier.

Due to the low concentration of elastin in the virgin tissues, it may be argued that these samples were not sufficiently pure and might have contained excess collagen. Additional tests were performed to measure the amount of microfibrillar component in the virgin and multiparous rat cohorts. Our findings indicate that the concentration of the microfibrillar component of the elastic fiber was similar. Per unit mass of lyophilized elastic fibers the values measured are: virgin (6.17±0.37)%, multiparous (7.05±0.46)%. Thus, the concentration of microfibrillar constituent in the elastic fibers in these two cohorts was experimentally similar and the changes observed are therefore arising from changes in elastin, not in trace contaminants. Furthermore, as hydroxyproline is one of the main amino acids of collagen, a signal arising from the C_γ nuclei of this amino acid of collagen may be used as a tracer for the purity of our samples (see amino acid analysis in Table 4.7). The ^{13}C NMR spectra from

any of our samples show no such signature, and further confirm the purity of our samples.

The dynamical characteristics of the protein can be described by measuring the average rotational correlation times of the carbon-proton internuclear vectors. The ^{13}C $T_{1\rho}$ relaxation times allows us to access μs range motion, while ^{13}C T_1 are sensitive to picosecond and nanosecond motions [163, 164]. In these experiments, I was not able to measure T_1 relaxation times, as ^{13}C T_1 are long and signal to noise in our natural abundance samples was small. Here, ^{13}C relaxation times were measured in the rotating frame of reference at two different locking fields and correlation times were calculated using equation (2.4) and (2.5) reported in Chapter 2. These equations were tested on bovine nuchal ligament elastin at two different Zeeman fields (900 MHz and 750 MHz) and produced similar correlation times; that is the equations that govern the $T_{1\rho}$ relaxation process are accurate to describe the dynamics of μs range motion in elastin with a single correlation time. The measured correlation times in bovine nuchal ligament elastin at 900 MHz and 750 MHz are presented in Table 4.8.

Tables 4.5 and 4.6 summarize the results of the ^{13}C $T_{1\rho}$ relaxation times measured at two different locking fields (50 kHz and 25 kHz) for four different samples studied. The correlation time for Ala C_β, Val C_γ appear to be longer in the virgin sample (7.92$\pm$2.01 μs) compared to the multiparous sample (1.88$\pm$0.47 μs) pointing to an increase in mobility of these moieties. Similar trends are observed for Ile C_β moieties, where the correlation time is smaller in the multiparous cohorts than virgin cohorts. However, I was not able to measure correlation time for Ala C_β, Val C_γ, and Ile C_β in para1 and para3 samples, due to overlapping peaks. For Gly C_α, Ala C_α, Phe C_α, Val C_α, Pro C_α, and Ile C_α, the correlation time decreases in going from virgin to para1 to para3 to multiparous samples. These results

indicate the increase in mobility of these peaks with increase in parity. In virgin rats, the measured correlation time for Pro C_β and Val C_β is (3.21±1.27 μs) which reduces in the multiparous sample to (1.93±0.41μs). However, the measured correlation time for this peak in para1 (3.15±0.48 μs) and para3 (4.71±0.64 μs) overlap with the virgin sample.

Interestingly, the ^{13}C MAS spectra of elastin from the multiparous rat cohorts and the associated relaxation times and correlation time appear similar to what has been previously observed in bovine nuchal ligament [36] and pig aortic elastin [157]. Additional measurements were performed to check findings on the reproductive tract elastin from virgin and multiparous cohorts and compared them to ^{13}C MAS NMR spectra from elastin isolated from the aorta in these cohorts. Our results showed that the ^{13}CMAS NMR spectra of aortic elastin in virgin and multiparous cohorts were similar (see Figure 4.10 and 4.11).

Additional measurements were performed to study the porosity and morphology of the elastic fiber, by investigating the tumbling nature of water molecules. ^{2}H T_1-T_2 experiments based on an inverse Laplace transform (ILT) have been used by our group to characterize the distribution and dynamics of water in the upper vaginal wall tissue [146], cortical bone [104], spider silk [103], and aortic elastin [165]. This powerful experimental technique has also been applied in potato tissue [100], cement paste [101], and in water-saturated sedimentary rock [166]. The ^{2}H 2D ILT T_1-T_2 map of virgin, multiparous, and bovine nuchal ligament samples acquired at 25 °C are shown in Figure 4.12. Referring to Figure 4.12, four reservoirs of water were observed for the virgin, multiparous, and bovine nuchal ligament samples similar to previous measurements in elastin samples [157, 165]. Using the notation in our earlier work, four peaks were labelled α_1, α_2, β, and γ. The observed $T_1 - T_2$ and the correlation time

τ_c are tabulated in Table 4.9. Using the measured T_1 and T_2, the correlation times for the tumbling motions were calculated using equations (2.8) and (2.9) reported in Chapter two [157]. From Table 4.9, the measured τ_c values for all peaks in multiparous sample are similar or slightly higher compared to bovine nuchal ligament samples. Variation in T_1, T_2, and τ_c of β, γ peaks in multiparous samples in comparison to bovine nuchal ligament elastic fibers arises alterations of the surface morphology of the inner and outer regions of the elastic fiber. However, these values in the virgin samples vary significantly particularly, peaks β and γ, which suggests that the water molecules are in a less mobile environment—these results correlate with the findings from ^{13}C NMR, which showed that backbone and side-chain motion of elastin from the reproductive tact of virgin cohorts was smaller than that of other cohorts. These alterations resulted from the variation in the MMP levels in the tissues, or the alterations in the cross-linking discussed earlier.

Previous work on reproductive tract tissue stiffness from our laboratory, has shown that the tissue stiffness was found to decrease in multiparous as well as 2 days postpartum rats (spontaneous or simulated) in comparison to the virgin rats. However, in 2 weeks postpartum rats (where the elastic fibers are in the course of repair) the tissue stiffness returns back to that observed in virgin rat cohorts [59]. Several studies on prolapsed tissues have also shown that the architecture of elastic fibers may directly impact the macroscopic properties of tissues. Liu et al., observed substantial accumulation of elastin monomers with decreased cross-links in case of LOXL1 deficient mice [60]. Additionally, different groups have observed fragmented and tortuous elastic fibers with reduced elastin content in women with POP [2, 61]. Goepel et al. observed irregular fragmented distributions of elastic fibers in studies

of female stress urinary incontinence [62]. All these observations highlight the important scaffolding role of elastic fibers in the reproductive tract, and that any disturbance in the equilibrium may lead to pelvic floor dysfunction. While the microscopic structure of elastin in multiparous rats appears strikingly similar to elastin in other mammalian tissues, the elastic fibers are fragmented and tortuous, as in UV exposed skin[167]. This study therefore suggests that the macroscopic elastic fiber fragmentation may appear to play a dominant role in providing for tissue stiffness over microscopic alterations (e.g. cross link concentration) of its principal protein component, elastin. Although this work focussed on the effects of parity on reproductive tract elastin, multiparous rats were unavoidably older than virgin rats. Separating the effects of age from pregnancy, and thus understanding the role of elastic fibers in the pelvic floor pathogenesis, requires tracking changes in old virgin rats, which may include effects due to menstruation. Lastly, as multiparous cohorts showed lower MMP levels in comparison to virgin counterparts, results from this study appear to correlate with the finding that tissue MMP levels might provide access to information relating to a patient's predisposition of pelvic floor dysfunction [168].

4.4 Conclusions

This chapter summarizes results on modifications on female reproductive tract elastic fibers, and its principal protein component elastin, as a function of parity in a murine model. Elastin isolated from the reproductive tract of cohorts of virgin Sprague-Dawley rats was compared to para1, para3, or multiparous cohorts. Histological work reveals increasing fragmentation and tortuosity of elastic fibers with increase in parity, which has previously

been associated with the loss of tissue stiffness. MALDI mass spectrometry reveal that the amount of desmosine was observed to increase with increase in parity—the amount of desmosine in multiparous samples was observed to be more than three times than virgin rat cohorts, which is in turn similar to other healthy mammalian tissues (e.g. bovine nuchal ligament elastin). Additionally, virgin rat cohorts reveal significantly different ^{13}C NMR spectra due to higher concentration of MMP-2 and MMP-9 levels compared to cohorts that have given multiple births. ^{13}C NMR spectra of elastin isolated from para1 rat cohorts appears similar to ^{13}C spectra from virgins, while the ^{13}C NMR spectra of elastin isolated from para3 rat cohorts resemble spectra from multiparous cohorts. Furthermore, NMR relaxation measurements show that dynamics of major backbone and side chain carbon nuclei in the major amino acids between virgin rat and multiparous cohorts are different, while the dynamics of elastin in multiparous cohorts resembles that of healthy elastin. Despite the microscopic similarities in elastin between multiparous cohorts and healthy elastin, the macroscopic alterations, which include fragmentation and tortuosity, appear to govern tissue scaffolding properties.

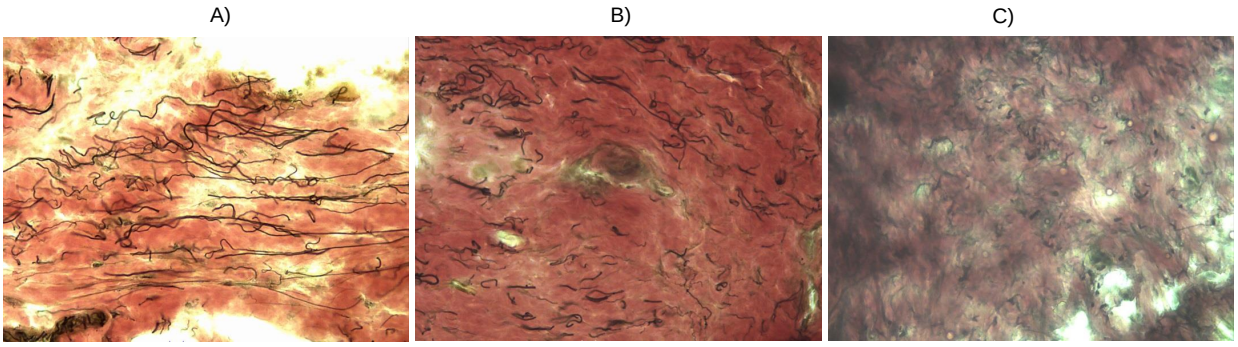

Figure 4.1: Histological images of the stained upper vaginal sections for A) virgin B) para3, and C) multiparous rat cohorts taken at 40× magnification. Elastic fibers are stained black, smooth muscles are stained yellow, and collagen is stained red.

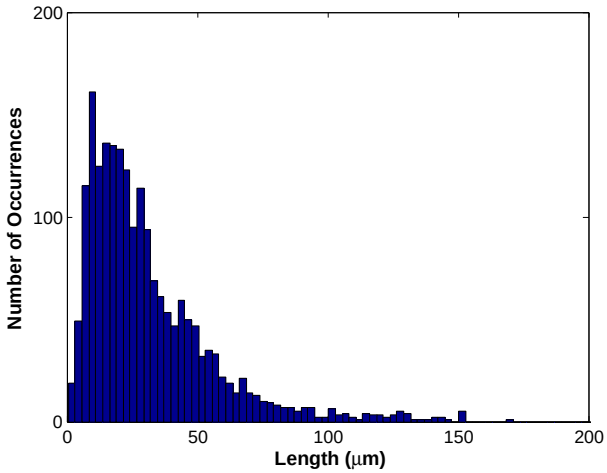

Figure 4.2: Histogram of the elastic fiber length distribution observed in the reproductive tract of virgin rat cohorts.

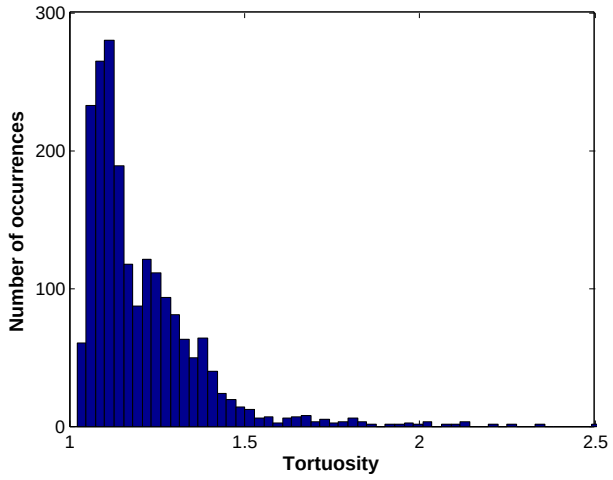

Figure 4.3: Histogram of the elastic fiber tortusity distribution observed in the reproductive tract of virgin rat cohorts.

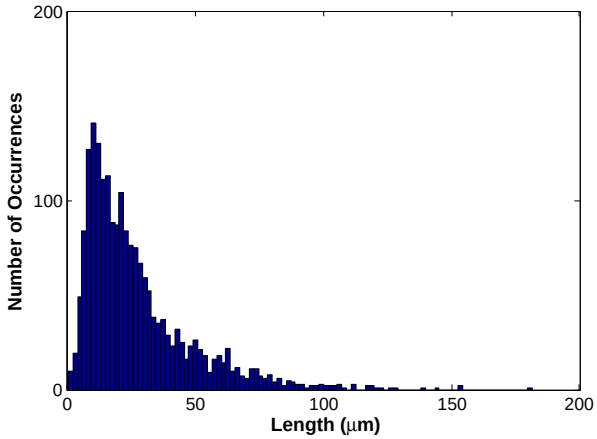

Figure 4.4: Histogram of the elastic fiber length distribution observed in the reproductive tract of para3 rat cohorts.

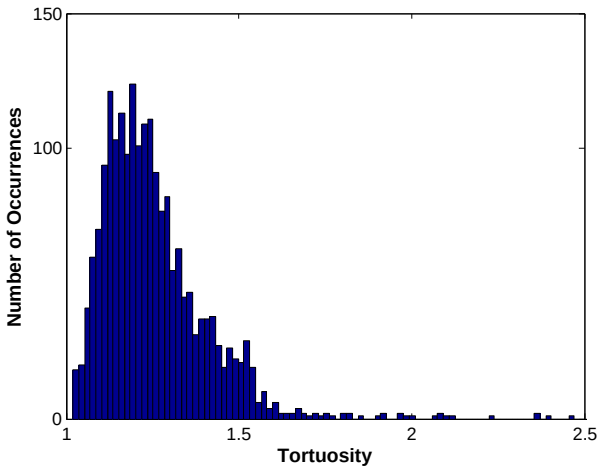

Figure 4.5: Histogram of the elastic fiber tortusity distribution observed in the reproductive tract of multiparous cohorts.

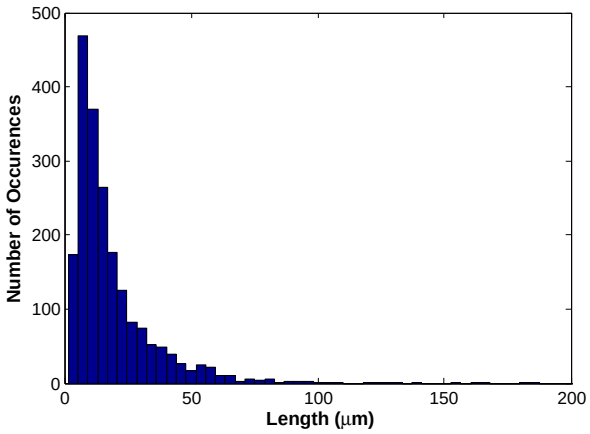

Figure 4.6: Histogram of the elastic fiber length distribution observed in the reproductive tract of multiparous cohorts.

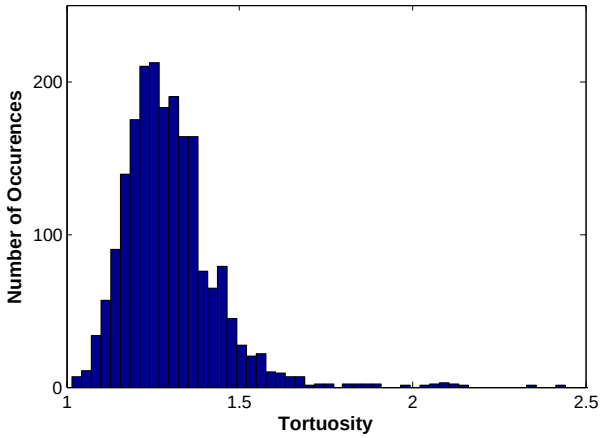

Figure 4.7: Histogram of the elastic fiber tortusity distribution observed in the reproductive tract of multiparous cohorts.

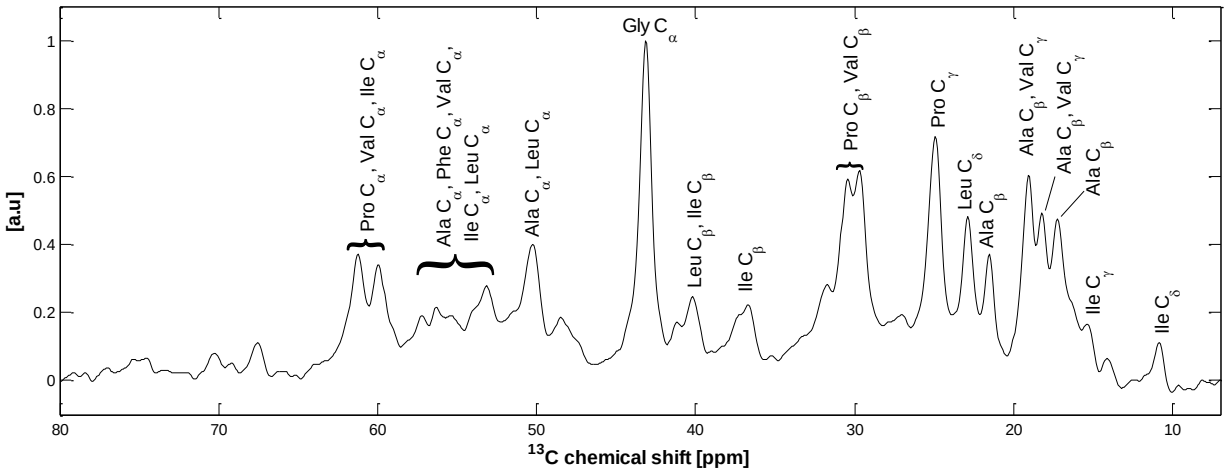

Figure 4.8: Direct polarization magic angle spinning (DPMAS) ^{13}C NMR spectra of the aliphatic region from purified hydrated multiparous uterine horn elastin at spinning speed 17 kHz and at 300 K. Chemical shift assignments of all the peaks were performed following previously published data reported in the literature.

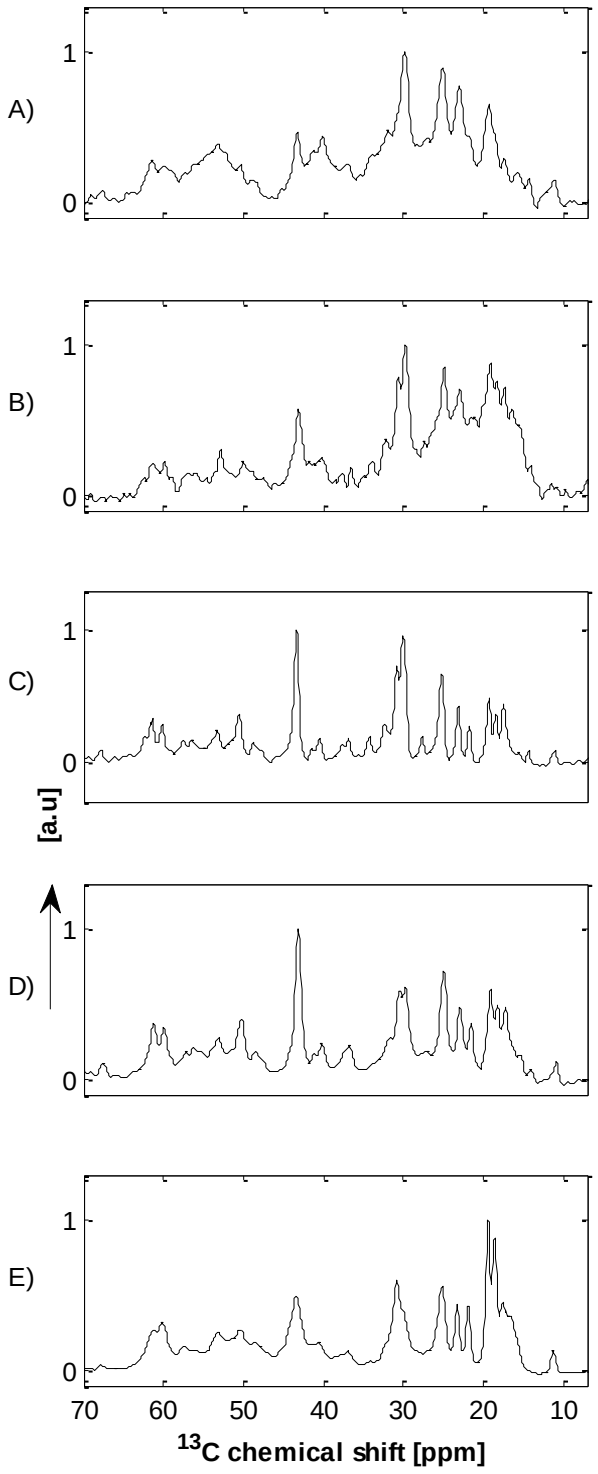

Figure 4.9: DPMAS ^{13}C NMR spectra of the aliphatic region from purified hydrated uterine elastin from A) virgin, B) para1 C) para3, D) multiparous and E) bovine nuchal ligament elastin at spinning speed 17 kHz and at 300 K.

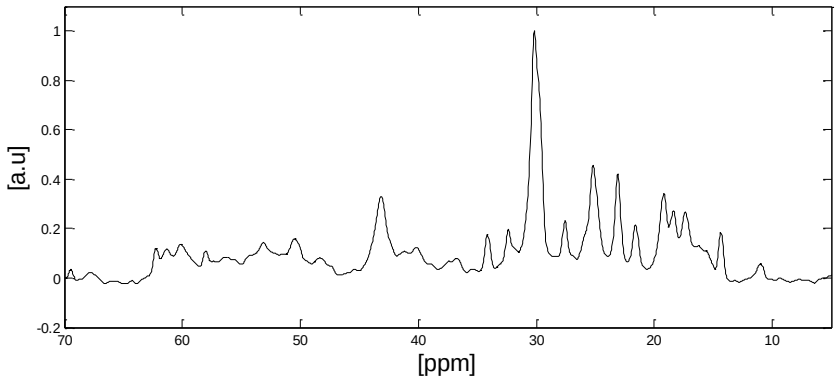

Figure 4.10: Direct polarization magic angle spinning (DPMAS) ^{13}C NMR spectra of the aliphatic region from purified hydrated virgin rat aortic elastin at spinning speed 17 kHz and at 300 K.

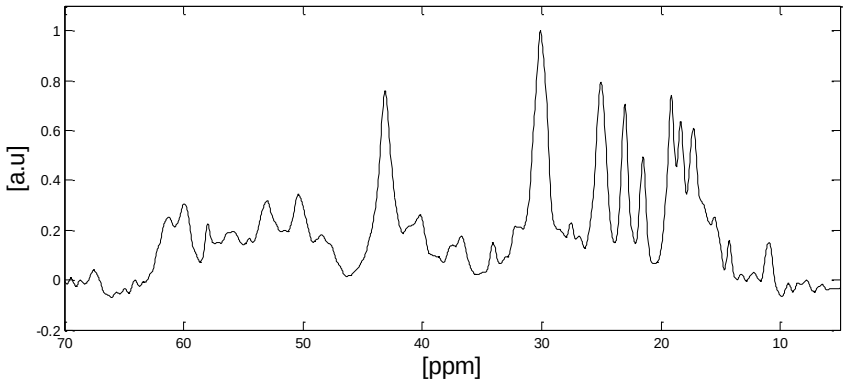

Figure 4.11: Direct polarization magic angle spinning (DPMAS) ^{13}C NMR spectra of the aliphatic region from purified hydrated multiparous aortic elastin at spinning speed 17 kHz and at 300 K.

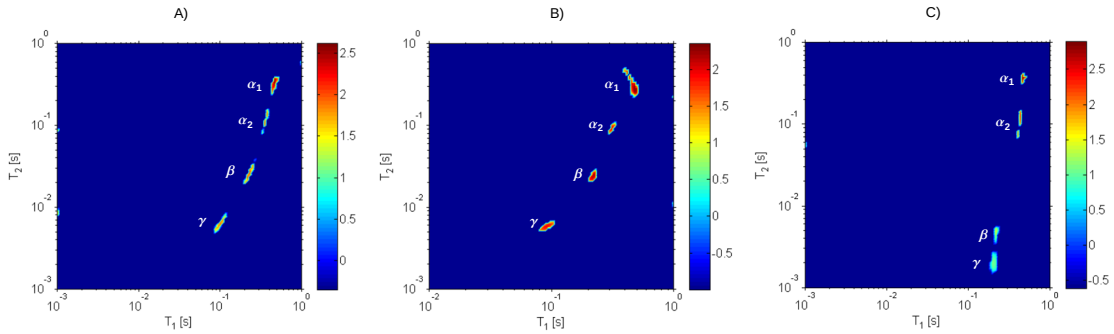

Figure 4.12: 2D ILT map of the ^{2}H T_1 and T_2 results from bovine nuchal ligament, multiparous, and virgin rat cohorts elastic fibers. In all three measurements, four peaks are well resolved and labeled α_1, α_2, β, and γ.

Table 4.1: Statistical characteristics of the elastic fiber length and tortuosity of elastic fibers observed in the vaginal wall of Sprague-Dawley cohorts.

Sample	Median fiber length	Skewness	Kurtosis
Virgin (n=2009)	24.56	2.36	9.29
Para3 (n=2017)	21.38	1.92	5.20
Multiparous (n=1022)	21.18	5.23	46.12
	Median fiber tortuosity	Skewness	Kurtosis
Virgin (n=2009)	1.15	4.20	29.88
Para3 (n=2017)	1.23	2.31	11.06
Multiparous (n=1022)	1.26	4.08	35.46

Table 4.2: Amount of MMP-2, MMP-9, and TIMP-1 in different samples studied. The error bar denotes the variance across the biological replica (n=3 for MMP-2 and MMP-9 and n=2 for TIMP-1).

Sample	MMP-2 content*10^{-7}	MMP-9 content *10^{-7}	TIMP-1 content*10^{-7}
Virgin	2.07±0.64	4.69±2.66	1.29±0.08
Para1	1.26±0.73	2.87±1.10	1.19±0.62
Para3	1.13±0.28	1.83±0.82	1.42±0.16
Multiparous	1.01±0.73	1.59±0.48	1.55±0.28

Table 4.3: Relative desmosine content (per mg lyophilized elastic fibers) from virgin, para1, para3 and multiparous uterine horns elastic fibers and bovine nuchal ligament elastic fibers. Purified bovine nuchal ligament elastic fibers were purchased from Elastin Products LLC (Owensville, MO). The relative amount of desmosine is reported by taking the ratio of unlabeled desmosine to the d_4 desmosine normalized by the amount of desmosine in the lyophilized virgin rat uterine horn elastic fibers. Error bars denote the variance propagated across all measurements. In the table, n is the number of animals used to prepare samples and m is the number of replicate measurements.

Sample	Relative desmosine content
Virgin (n=18, m=4)	1.00±0.05
Para1(n=8, m=2)	2.31±0.05
Para3 (n=8, m=2)	2.60±0.06
Multiparous (n=18, m=4)	3.13±0.13
Bovine nuchal ligament (m=6)	3.40±0.20

Table 4.4: Measured ^{13}C chemical shift for uterine horn elastin of multiparous and virgin rat, and corresponding secondary structural assignments. Structural assignments were performed using literature values [169, 170, 171, 172, 161]

Assignments	Observed chemical shift (ppm)				Structure assignment
	Virgin	Para1	Para3	Multiparous	
Ile C_δ	11.0	11.1	11.1	10.9	RC (Random coil)
Ile C_γ	-	16.4	-		-
Ala C_β	17.3	17.3	17.4	17.2	α-helix or β-sheet/turn or RC
Ala C_β, Val C_γ	-	18.3	18.4	18.2	β-sheet/turn or RC, RC
Ala C_β, Val C_γ	19.2	19.1	19.2	19.1	β-sheet/turn, RC
Ala C_β	21.6	21.4	21.7	21.5	β-sheet
Leu C_δ	22.97	22.96	23.1	22.9	-
Pro C_γ	25.1	24.9	25.2	24.9	-
Pro C_β, Val C_β		27.4	27.6		α-helix,α-helix
Val C_β, Pro C_β	29.8	29.8, 30.6	30.0, 30.8	29.7, 30.5	α-helix or β-sheet/turn or RC, α-helix or β-sheet/turn or RC
Pro C_β, Val C_β	31.9	32.1	32.3	31.7	α-helix or β-sheet/turn or RC,β-sheet/turn or RC
Phe C_β, Ile C_β		34.0	34.3		–
Ile C_β	36.9	36.6	36.8	36.7	β-sheet/turn or RC
Leu C_β, Ile C_β	40.1	40.2	40.4	40.2	α-helix or β-sheet/turn or RC, β-sheet/turn
Gly C_α	43.2	43.2	43.3	43.2	α-helix or β-sheet/turn or RC
Ala C_α	48.8	-	48.8	48.5	β-sheet/turn
Ala C_α, Leu C_α	50.4	50.1	50.5	50.2	α-helix or β-sheet/turn or RC,-
Ala C_α, Phe C_α	53.2	52.9	53.2	53.1	α-helix, β-sheet/turn or RC
Phe C_α, Leu C_α	-	-	56.4	56.3	β-sheet/turn or RC, α-helix
Phe C_α, Val C_α, Ile C_α	-	-	57.5	57.2	α-helix or RC, β-sheet/turn or RC, β-sheet/turn or RC
Val C_α, Pro C_α, Ile C_α	59.9	59.9	60.1	60.1	β-sheet/turn or RC, β-sheet/turn or RC, RC
Val C_α, Pro C_α, Ile C_α	61.3	61.4	61.4	61.4	RC, β-sheet/turn or RC,α-helix or RC

Table 4.5: Tabulated ^{13}C $T_{1\rho}$ relaxation times, of the spectroscopically resolved moieties of the virgin and para1 uterine horn elastin samples at 300 K.

Assignments	Virgin			para1		
	$T_{1\rho}[ms]$ (50.00 kHz)	$T_{1\rho}[ms]$ (25.00 kHz)	$\tau_c[\mu s]$	$T_{1\rho}[ms]$ (50.00 kHz)	$T_{1\rho}[ms]$ (25.00 kHz)	$\tau_c[\mu s]$
Ala C_β, Val C_γ	13.23±1.50	4.54±0.42	7.92±2.01	-	-	-
Leu C_δ	9.56±0.82	4.16±0.34	5.97±1.34	8.83±0.59	7.86±0.56	-
Pro C_γ	4.56±0.29	2.45±0.19	4.48±0.98	5.54±0.24	4.04±0.19	2.58±0.54
Pro C_β, Val C_β	5.28±0.33	3.47±0.25	3.21±1.27	20.24±0.94	13.41±0.43	3.15±0.48
Ile C_β	4.60±0.73	2.76±0.60	3.76±2.74	-	-	-
Leu C_β, Ile C_β	3.71±0.35	1.17±0.16	8.70±2.57	3.62±0.29	1.49±0.14	6.39±0.62
Gly C_α	4.49±0.49	1.90±0.28	6.18±2.23	3.82±0.11	2.42±0.06	3.43±0.33
Ala C_α, Phe C_α	3.98±0.48	1.42±0.08	7.57±1.61	3.55±0.30	1.58±0.12	5.80±1.26
Val C_α, Pro C_α, Ile C_α	4.03±0.68	1.48±0.34	7.32±4.29	4.18±0.30	1.88±0.11	5.73±0.99

Table 4.6: Tabulated ^{13}C $T_{1\rho}$ relaxation times, of the spectroscopically resolved moieties of the para3 and multiparous uterine horn elastin samples at 300 K.

Assignments	para3			Multiparous		
	$T_{1\rho}[ms]$ (50.00 kHz)	$T_{1\rho}[ms]$ (25.00 kHz)	$\tau_c[\mu s]$	$T_{1\rho}[ms]$ (50.00 kHz)	$T_{1\rho}[ms]$ (25.00 kHz)	$\tau_c[\mu s]$
Ala C_β, Val C_γ	-	-	-	11.63±0.43	9.53 ±0.40	1.88±0.47
Leu C_δ	19.67±2.44	10.92±0.87	4.26±1.37	9.81±0.40	6.97±0.30	2.74±0.50
Pro C_γ	9.82±0.60	8.26±0.42	1.73±0.66	6.16±0.17	4.45±0.14	2.64±0.35
Pro C_β, Val C_β	26.42±1.58	13.70±0.46	4.71±0.64	5.89±0.18	4.79±0.18	1.93±0.41
Ile C_β	-	-	-	4.22±0.27	3.18±0.27	2.39±0.90
Leu C_β, Ile C_β	2.65±0.42	2.20±0.17	1.81±1.35	3.75±0.19	3.20±0.25	1.64±0.78
Gly C_α	5.46±0.20	4.59±0.16	1.73±0.43	4.04±0.08	3.14±0.20	2.20±0.15
Ala C_α, Phe C_α	5.01±0.52	3.76±0.31	2.41±1.11	3.96±0.19	2.38±0.16	3.76±0.75
Val C_α, Pro C_α, Ile C_α	5.80±0.63	3.49±0.26	3.75±1.18	4.41±0.20	3.93±0.27	1.35±0.72

Table 4.7: Amino acid analysis of multiparous rat cohorts and purified bovine nuchal ligament elastin sample as measured by New England Peptide. The amino acid measurements are reported as mole %. The theoretical values, shown in column 4, correspond to the amino acids computed from cDNA of bovine tropoelastin [144] .

	% of amino acid		
Amino acid	Multiparous reproductive tract	Bovine nuchal ligament	Theory
Asp	2.38	0.80	0.40
Thr	3.08	0.87	1.10
Ser	2.55	0.90	1.00
Glu	3.58	1.78	1.40
Pro	9.23	11.88	11.90
Gly	31.05	33.93	31.90
Ala	17.94	21.25	21.10
Val	9.26	13.58	12.6
Met	0.00	0.00	-
IIe	3.88	2.58	2.11
Leu	7.89	6.29	6.27
Tyr	3.00	0.82	1.0
Hyp	0.00	0.00	-
Phe	2.45	3.06	3.84
His	0.62	1.18	0.00
Lys	1.33	0.40	5.30
Arg	1.76	0.70	0.70

Table 4.8: Tabulated ^{13}C $T_{1\rho}$ relaxation times (two different locking fields), of the spectroscopically resolved moieties of bovine nuchal ligament elastin samples at 900 MHz system. Correlation times are calculated from $T_{1\rho}$ values and compared with the correlation times in 750 MHz system [36].

Assignments	Bovine nuchal ligament 900 MHz			
	$T_{1\rho}[ms]$ (50 kHz)	$T_{1\rho}[ms]$ (25 kHz)	$\tau_c[\mu s]$	$\tau_c[\mu s]$ [750 MHz]
Ala C_β	3.52±0.13	1.85±0.08	4.64±0.55	—-
Ala C_β, Val C_γ	6.64±0.15	4.17±0.11	3.48±0.31	3.02±0.25
Leu C_δ	2.83±0.13	2.33±0.11	1.85±0.56	1.30±0.24
Pro C_γ	1.42±0.04	1.21±0.04	1.65±0.38	2.27±0.13
Pro C_β, Val C_β	1.42±0.04	1.13±0.03	2.07±0.33	2.71±0.15
Leu C_β	1.09±0.07	0.95±0.07	1.50±0.85	—-
Gly C_α	1.16±0.04	0.85±0.04	2.56±0.49	8.65±0.63
Val C_α, Pro C_α, Ile C_α	1.34±0.10	0.98±0.09	2.57 ±1.02	—-

Table 4.9: Measured T_1, T_2, correlation time (τ_c) of bovine nuchal ligament, multiparous, and virgin rat cohorts elastic fibers. The error bars shown for any of the T_1 and T_2 relaxation times represent the half-width of the peak observed in the 2D ILT maps and have been propagated to the errors in the correlation times.

Assignments		Bovine	Multiparous	Virgin
Peak α_1	T_1 [s]	0.4507±0.0470	0.4653±0.0324	0.4809±0.0168
	T_2 [s]	0.2965±0.0201	0.3121±0.0644	0.3520±0.0245
	τ_c [s] $\times 10^{-8}$	0.3251±0.1000	0.3151±0.1800	0.1851±0.0600
Peak α_2	T_1 [s]	0.2014±0.0140	0.3520±0.0245	0.4183±0.0146
	T_2 [s]	0.1117±0.0117	0.1166±0.0355	0.1061±0.0356
	τ_c [s] $\times 10^{-8}$	0.4251±0.1150	0.7852±0.3550	1.1350±0.1300
Peak β	T_1 [s]	0.0872±0.0061	0.2243±0.0234	0.2232±0.0078
	T_2 [s]	0.0321±0.0055	0.0264±0.0063	0.0046±0.0008
	τ_c [s] $\times 10^{-8}$	0.7052±0.2000	1.7250±0.4400	2.2950±0.2450
Peak γ	T_1 [s]	0.0516±0.0018	0.1010±0.0140	0.2014±0.0140
	T_2 [s]	0.0091±0.0009	0.0063±0.0013	0.0021±0.0004
	τ_c [s] $\times 10^{-8}$	1.3200±0.0140	2.5150±0.5550	6.4710±1.0550

Chapter 5

Pregnancy induced dynamical and structural changes of reproductive tract collagen

This chapter highlights the results published in ref. [146].

5.1 Introduction

Pregnancy induced alterations to the tissues and organs of the female pelvic floor and reproductive tract allow for fetal growth and facilitate spontaneous vaginal birth. For such changes to occur, the extracellular matrix (ECM) of these structures, composed of collagen, elastic fibers, and smooth muscle, may undergo significant remodeling. Collagen, the most abundant ECM protein in the human body, plays a vital role in providing structure and tensile strength to tissues of the female pelvic floor and reproductive tract. Studies of the reproductive tract in humans and rodents have demonstrated that collagen content

of the vagina, cervix, and uterus is drastically altered during gestation, only to return to pre-pregnancy levels following postpartum involution [5, 26, 173]. Additionally, collagen and other ECM proteins remodeled in the reproductive tract during pregnancy and parturition have been associated with altered tissue bio-mechanics that typically results in an increase in tissue distensibility which returns to the non-pregnant state postpartum [173, 174, 59, 175].

The influence of multiparity and aging on the process of remodeling is less clear. Rundgren studied the influence of multiparity and age on the collagen content and bio-mechanics of the reproductive tract by comparing old (22-23 months of age) multiparous versus old nulliparous rats, and young virgin versus old virgin rats. He concluded that age had a greater influence on the physical properties of the uterine horns and cervix, while multiparity had greater influence in the vaginal wall [173]. As multiparity and aging are major risk factors for the development of pelvic floor disorders such as POP and stress urinary incontinence, it is thought that a better understanding of these processes may provide greater insight into the pathogenesis of these conditions [176, 177, 178].

In light of the known alterations to collagen and the bio-mechanical properties of the reproductive tract, we applied NMR methods to study the effects of parturition on collagen. Collagen is a fibrous protein and does not form crystals but the x-ray structures of collagen like proteins and peptides have been reported by Bella et al. [179]. To characterize the structural and dynamical properties of collagen at molecular level, NMR is an ideal tool as ^{13}C chemical shift can be useful for conformational characterization of the secondary structure and NMR relaxation times may be applied to measure dynamical characteristics [180, 181].

The signature molecular structure of collagen consists of 3 α polypeptide chains bound in a triple helix configuration, stabilized by inter-chain hydrogen bonds. These chains are composed of a series of a triplet amino acid pattern: glycine-X-Y, where X and Y can be any amino acid (but are frequently proline and hydroxyproline, respectively) [182]. Collagen exists as either homotrimers or heterotrimers. There have been at least 28 different collagen types described. Collagen I, III and V have been found in the PFCT where I and III are most abundant. Collagen I fibers provide the majority of tissue resistance to tension. Collagen III confers greater flexibility and distension to tissue, while collagen V appears to be of minor importance as it forms small fibers of very low tensile strength. The copolymerization of collagen I with III and V form fibrils that influence the biomechanics of tissue [183]. It is thought that the higher the collagen I/III ratio in the ECM, the greater its strength (compared to a lower ratio). These fibrillar collagens are thought to be the principal determinants of strength in the vaginal wall. Changes in ratios, structure and/or dynamics of these collagens likely contribute to changes in vaginal tissue behavior [184].

A well resolved ^{13}C NMR spectrum of collagen like peptides and collagen fibrils from bovine tendons has been obtained, allowing for structural characterization [185, 186, 187]. In previous studies, NMR ^{13}C NMR chemical shift measurements were used to understand the flexibility of the collagen triple helix, which is sensitive to the ring conformation of the collagen imino residues. In addition, recent ^{13}C solid state NMR was employed to follow the molecular disorder of collagen in articular cartilage, due to Alkaptonuria [188]. Dawson and colleagues also applied ^{31}P NMR to study rat uteri, however, to date, no other study has made use of ^{13}C NMR to study the effect of parity on the molecular structure of collagen in

the reproductive tract [189].

In this chapter, I summarize results from an experimental investigation of the effects of parity on the structure and dynamics of upper vaginal wall collagen derived from Sprague-Dawley rats using NMR spectroscopic and relaxation techniques. ^{13}C CPMAS (cross polarization under magic angle spinning) NMR was employed to probe structural changes. ^{13}C relaxation experiments were also performed to measure correlation times of internuclear ^{13}C–^{1}H motions to probe dynamical fluctuations of the spectroscopically resolvable moieties across virgin and multiparous rats, as well as primiparous rats at two days and 14 days postpartum. ^{2}H T_1–T_2 experiments based on an inverse Laplace transform (ILT) [99] have been performed to characterize the distribution and dynamics of water in the upper vaginal wall tissue. This powerful experimental technique has been previously applied on various systems such as potato tissue [100], cement paste [101], bovine nuchal ligament and aortic elastin [102], spider silk [103], cortical bone [104], and in water saturated sedimentary rock [105]. Lastly, the collagen content in the upper vaginal wall of each of the samples studied was measured by spectrophotometry and histology.

5.2 Materials and methods

5.2.1 Preparation of tissues for NMR

The animal protocol for this study was approved by the Institutional Animal Care and Use Committee at the Albert Einstein College of Medicine. Sixteen Sprague Dawley rats (four per group) were used in total. These included virgin rats (11-14 weeks of age), multiparous

rats (9-15 months old), two day postpartum primiparous rats (para-1 (2 days postpartum)), and fourteen day postpartum primiparous rats (para-1 (14 days postpartum)) following spontaneous vaginal delivery that were not nursing. All animals were sacrificed in a carbon dioxide chamber and their reproductive tracts harvested. Multiparous rats were sacrificed at least two weeks after their final parturition. An approximately 1 cm portion of upper vaginal tissue was excised and used for NMR studies. Lower vaginal tissue and cervix were discarded. Two rats in each group were used. To remove fat from the sample, the following procedure was performed [147]. Each specimen was washed with saline solution three times. Then, the tissue was kept in 100% ethanol for 7-10 minutes and the procedure was repeated twice. The tissue was then placed in a (50/50) mixture of ethanol and diethyl ether (99%) for 7-10 minutes (2 times). Finally, the tissue was placed in diethyl ether for ten minutes (2 times). All samples were defatted following same procedure and to keep samples hydrated, all the samples were stored in distilled water at -20 °C. NMR experiments were performed on water hydrated tissue. Furthermore, careful attention was taken to check the sample mass before and after NMR experiments to avoid dehydration during the experiments.

5.2.2 ^{13}C NMR experimental parameters

^{13}C NMR experiments were performed at a magnetic field strength of 17.61 T using a Bruker Avance (Billerica, MA) spectrometer. Each sample was packed in a 4 mm center packing rotor with an insert to prevent the loss of water as well as to center the sample with respect to the RF coil. All the experiments were performed at (300 ± 1) K. In all experiments, the ^{13}C $\pi/2$ pulse was 5 μs and the spinning frequency was (10 kHz ± 10 Hz). In the CP

experiments, the contact time was set to 0.5 ms and recycle delay was 6 s. The spectra were acquired by accumulating 10000 scans using 80 kHz TPPM decoupling [149]. ^{13}C $T_{1\rho}$ were measured at two different spin-lock rf field strengths (25.00 and 50.00 kHz). The spin locking time interval used for the low field varied from 50 μs to 750 μs and for the high field measurements, the value was varied from 100 μs to 3000 μs. For all ^{13}C T_1 measurements, the delay time τ was varied from 1 ms to 5000 ms in ten steps. Analysis of data was performed using MATLAB and matNMR with a Gaussian multiplication broadening factor of 100 Hz for CP spectra and 150 Hz for relaxation measurements. ^{13}C NMR spectra presented in this work were referenced to adamantane (with TMS at 0 ppm). The mass of hydrated samples used in the NMR experiments for virgin, multiparous, para-1(2 day postpartum) and para-1(14 day postpartum) was roughly (41.8 $\pm$ 0.1) mg, (37.9 $\pm$ 0.1) mg, (54.4 $\pm$ 0.1) mg and (53.9 $\pm$ 0.1) mg respectively.

5.2.3 ^{2}H NMR relaxation

All the ^{2}H T_1-T_2 experiments were performed on a magnetic field strength of 4.70 T using Varian Unity system (Palo Alto, CA) with a Varian liquids double resonance NMR probe at 25 °C. A portion of samples used in ^{13}C NMR experiments were used for ^{2}H NMR experiments. Samples were soaked in D_2O for approximately 48 hours prior to experiments. For all the experiments, the ^{2}H $\pi/2$ pulse was 24 μs and the interpulse spacing in the CPMG train was 700 μs . For the two dimensional T_1-T_2 measurements, the recovery time was logarithmically incremented from 1 ms to 10 s in 100 steps to measure T_1, and stroboscopic detection of 6000 echo peaks was used for the T_2 relaxation time measurement. A two

dimensional inverse Laplace transform (ILT) algorithm described elsewhere was applied to analyze the ^{2}H T_1-T_2 relaxation data [99].

5.2.4 Histology and microscopy

A small sample of the upper vaginal wall was placed overnight in 100 ml of phosphate buffered saline with 30 g sucrose. The sample was then placed in LiecaCryo-Gel (SPI supplies Product Ref-02694-AB), sectioned on a Leica CM1850 cryostat at 10 μm and stained using the Sigma-Aldrich elastic stain kit (REF HT25A-1KT) following a previously reported protocol [59]. The slides were placed in a solution containing 20 ml hematoxylin solution, 3 ml of ferric chloride solution, 8 ml of Weigert iodine solution, and 5 ml of deionized water for 10 minutes. Following this step, the slides were then placed in a working ferric chloride solution consisting of 3ml ferric chloride and 37 ml of deionized water for two minutes. The slides were then gently rinsed with water, placed in 100% ethanol for a few seconds, and again gently rinsed with deionized water. In the last step of the staining procedure, the slides were placed in Van Gieson solution for 1.5 minutes, followed by a gentle rinse with 100% ethanol, placed in xylene for a few seconds. Cover slips were mounted using Eukitt quick-hardening mounting medium (Sigma-Aldrich REF 03989) and the slides were left to dry overnight. The slides were photographed using a National Optical DC4-156-S digital microscope at a magnification of 10×. Approximately 50 images were taken from each sample from different regions of the upper vaginal wall. The photographs were then analyzed by an image processing program developed in MATLAB. All the images for collagen fiber analysis were taken using 100× objective with immersion oil on an Olympus BX41 microscope.

5.2.5 Collagen content quantification

Upper vaginal wall tissue was harvested, defatted, and lyophilized for 24 h, as described above. For the collagen quantification, 3.4-3.5 mg of lyophilized tissue from each sample was placed in 300 μl of 6 M HCl solution in hydrolysis tubes under nitrogen after evacuation. For hydrolysis, the samples were kept in an oil bath at 110 °C for 24 h. After hydrolysis, tubes were opened and allowed to dry at 110 °C. The samples were resuspended in 2 ml of PBS for 1 h at 60 °C. Each sample was centrifuged and the supernatant was used for collagen quantification after 2-fold dilution using 4 M HCl. Collagen standards were prepared in the range from 0-300 μg/ml from the 1200 μg/ml stock solution provided by QuickZyme Biosciences. All of the samples and standard dilution procedures were adapted from a standard assay collagen kit and previously reported protocol [190]. The standard and samples were read in 96-well plate reader at wavelength 584-590 nm (exciting - 584 nm; emitting- 590 nm) using a BMG FLUOstar OPTIMA microplate reader.

5.3 Results and discussion

5.3.1 ^{13}C CPMAS NMR studies of structural and dynamical changes in upper vaginal wall tissue

Natural abundance ^{13}C CPMAS NMR spectra were recorded and shown in Figure 5.1 and 5.2 to investigate possible structural differences in the upper vaginal wall collagen samples studied (virgin, multiparous, para-1 (2 days postpartum), and para-1 (14 days postpartum)). Figure 5.1 (A), (B), (C), and (D) illustrates the aliphatic regions. Figure 5.2 (A), (B), (C),

and (D) show the carbonyl region of the spectra of the different samples studied. Among all the samples, CPMAS spectra were similar in terms of peak positions and overall appearance, and no significant chemical shift differences were observed. The chemical shift assignments of all the peaks are shown in Figure 5.3 (CPMAS NMR spectrum of multiparous rat measured in the present study) and the chemical shift values of all the samples are tabulated in Table 5.1. As the spectral features are very similar to the previously reported collagen spectra (obtained from different materials such as collagen parchment, skin, bone, cartilage, tendons, and collagen like peptides), the assignments of all the peaks were performed following previously published data reported in the literature [180, 191, 186, 67, 185, 187, 192, 193, 194].

Here, the chemical shift assignments of the major amino acids (Gly, Pro, Ala, and Glu) present in collagen were taken into account, as these constitute 72% of the total amino acids. In the spectra, the C_γ Hyp peaks appear at 71.4 ppm for the multiparous rats and the position is fairly constant for virgin and para-1 (2 days postpartum) cohorts Figure 5.1 (A), (B), and (C). However, this peak is not visible (or masked by noise) in the para-1 (14 days postpartum) sample Figure 5.1 (D). It is to be noted that all the experiments were performed on collagen, which has undergone trauma during pregnancy and parturition. As a result, changes in dynamics of side chain moieties may be expected (see ^{13}C T_1) which in turn may alter the ^{13}C signal intensity, as the experiments were performed using cross-polarization. However, additional experiments were performed at higher magnetic field (21.10 T) to resolve the Hyp signal in para-1 (14 and 2 days) samples. This signal is present in both samples and chemical shift reported was the same as that observed at 17.61 T. The region from about 54-60 ppm belongs to several amino acids including two major constituents, e.g. C_α-Pro,

C_α-Hyp. In this region no major changes were observed. The C_α Gly peak, appearing at 43 ppm is well resolved in case of virgin rat and multiparous rats. However, in the case of para-1 (2 days postpartum) and para-1 (14 days postpartum), the C_α Gly signal is not well resolved which may have resulted from a change in collagen content, and/or dynamics discussed further below (see Table 5.5).

The tissues used for all NMR experiments also contained elastin in weak concentration (ca. 1.5% by weight) [148]. Previous NMR studies on hydrated elastin showed that at room temperature the ^{13}C signal intensities obtained by ^{1}H-^{13}C cross-polarization are relatively weak, and only a few peaks are resolvable [57, 36]. The inefficiency of the cross-polarization method for elastin arises from its highly mobile nature in a hydrated state. Thus, the contribution of the ^{13}C signal in this collagen ^{1}H-^{13}C CPMAS spectra from elastin is therefore very small. Lastly, it should be noted that in the preparation of the samples, the tissues were exposed to ethanol briefly. Previous studies of the exposure of ethanol in the ^{1}H NMR spectrum of collagen inside hard tissue (e.g. cortical bone) have been noted [195], and one may rightly inquire if the ethanol treatment may alter the water content of these samples. This collagen spectra do not appear broad and unresolved as dehydrated collagen (see Fig 1 of [196]). In contrast this spectra, which were acquired using a specialized rotor with a center packing system to prevent dehydration during spinning, appear well resolved and similar to the case of hydrated collagen (see Fig 1 of [196]).

Table 5.2 and 5.3 give the results of the $^{13}\mathbf{C}$ $T_{1\rho}$ relaxation times measured at two different locking fields for different samples used in this study. From Table 5.2 it is clear that some of the peaks such as, C_γ-Val, C_γ-Thr, C_γ-Glu, C_β-Arg, and C_β-Val showed significant changes

in their correlation times (τ_c). For virgin rats the measured correlation time for the C_γ-Val or C_γ-Thr is (5.57 ± 1.77) μs and this value is smaller (0.91 ± 0.16) μs in multiparous rats. Similar trends are observed for C_γ-Glu, C_β-Arg or C_β-Val; here the correlation time changes from (4.57 ± 1.05) μs (virgin rat) to (1.87 ± 0.09) μs (multiparous rats), respectively. This measurement indicates that these moieties appear to be in a more mobile environment in the multiparous rats. The correlation time of (4.07 ± 0.81) μs was measured for the C_γ-Val or C_γ-Thr in para-1 (2 days postpartum) rats (Table 5.3), which is close to the value observed in virgin rats. This observation indicates that following parturition (2 days postpartum), C_γ-Val or C_γ-Thr resides in a less mobile state compared to virgin rats. However, it was not possible to measure τ_c for these peaks in the para-1 (14 days postpartum) rats. A different scenario is observed for the C_γ-Glu, C_β-Arg, and C_β-Val, where the correlation time observed in para-1 (2 days postpartum) and para-1 (14 days postpartum) rats are close to the value observed in multiparous rats. For major amino acids, e.g. Gly and Hyp, no marked changes in the correlation time are observed. Changes are also observed in the correlation time for C_γ-Pro, C_β-Glu, or C_γ-Leu (2 days: 2.48 ± 0.41 μs, 14 days: 1.37 ± 0.43 μs) and C_α-Glu, C_α-Asp, or C_α-Ser (2 days: 5.22 ± 1.95 μs, 14 days: 2.47 ± 0.71 μs). The measured para-1 (2 days postpartum) correlation times appear to overlap slightly with the measurements in multiparous rats C_γ-Pro, C_β-Glu, or C_γ-Leu (2.75 ± 0.39 μs) and C_α-Glu, C_α-Asp, or C_α-Ser (4.08 ± 0.71 μs). These observation suggests that remodeling of the ECM resulting from pregnancy and/or parturition alters the dynamical characteristics of specific collagen side chain groups. The data also suggests that the value for para-1 (14 days postpartum) following parturition return somewhat to those observed in virgin rats C_α-Glu, C_α-Asp,

C_α-Ser (3.21 $\pm$ 0.95 μs). Additional changes may have resulted from structural alterations involving structural heterogeneity resulting in overlap of peaks or a redistribution of water in the extracellular matrix, discussed further below, which may not be completely reversible. Recently, marked changes in the dynamics of elastin following in vitro exposure to glucose by ^{13}C NMR relaxation measurements have been observed [157]. Glucose exposure causes elastin to stiffen (as measured by tensile testing) and larger H-C correlation times were observed in comparison to samples in water only. Moreover, evidence of glucose interacting with elastin was observed as a cross-polarized glucose signal was observed in this ^{13}C NMR spectra. In this collagen spectra the broad signal in the range of 70-80 ppm may result from sugars in the tissue (e.g. due to glycosylation). Thus, the effects of glucose on the samples studied may also be a contributor to the alterations observed in the correlation times and may require further investigation.

The ^{13}C spin lattice T_1 relaxation times for virgin and multiparous rats are presented in Table 5.4. Previous studies of ^{13}C spin lattice relaxation times for the collagen fibrils and model peptides showed that different amino acids present in collagen exhibit different relaxation times [66]. Referring to Table 5.4, small changes in T_1 values are observed for some of the moieties such as the C_α-Glu, C_α-Asp, or C_α-Ser, C_δ-Hyp, or C_α-Leu peaks. The T_1 values appears slightly larger in multiparous rats in comparison to virgin rat for the C_α-Glu, C_α-Asp, or C_α-Ser peaks. However, for C_δ-Hyp, or C_α-Leu peaks the T_1 observed in the multiparous rat tissues (5.32$\pm$0.41μs) appears smaller in comparison to the measured value in the virgin rat tissues (7.44$\pm$1.11 μs). As discussed below, evidence of trauma to the tissue following pregnancy was observed as revealed by histology (Figure 5.4). The

changes in the relaxation times may arise from a redistribution of water due to this trauma from pregnancy which may alter the dynamical characteristics of these particular side chain motifs. For other moieties (Table 5.4) no significant differences in T_1 values were observed between the multiparous and virgin rats. T_1 values in human skin collagen at 300 MHz have been previously measured [66]. Using measured correlation times, the expected T_1 relaxation time at a 300 MHz Larmor frequency was back calculated and found that T_1 values for the upper vaginal wall collagen were smaller than that observed in human skin. These differences may arise from advanced glycation end products that are known to make collagen stiffer [197] and may alter the NMR relaxation times.

5.3.2 Collagen content in upper vaginal wall tissues

The collagen content (per milligram lyophilized tissue of upper vaginal wall) for virgin, multiparous, para-1 (2 days postpartum), and para-1 (14 days postpartum) rats are presented in Table 5.5. Two biological replicas for the virgin and multiparous cohorts, and three for para-1 (2 days postpartum) and para-1 (14 days postpartum) cohorts were used for this study. Referring to Table 5.5, we found that the virgin rat tissues contained higher collagen content (83%) compared to the other three samples. This observation was expected, as after delivery collagen content has been reported to reduce below the non-pregnant value [5]. It has been reported that collagen content in the reproductive tract increases rapidly at the tenth day of pregnancy which reaches the highest level just before parturition and decreases precipitously after parturition that continues approximately up to 16 days [5]. However, the rapid degradation of collagen which starts after parturition varies in different regions

of reproductive tract. It has been found that in the uterine horns this rapid degradation starts 12 hours postpartum whereas the collagen content of the cervix does not begin to degrade until 24-48 hours postpartum [69]. According to observations made in the work by Harkness et al. [69], one would expect that the collagen content should be higher in para-1 (2 days postpartum) rats than in the virgin rats; this was not observed in this study (Table 5.5). It is to be noted that in this analysis, the upper vaginal wall was used. Therefore, this region might have a different time scale for collagen degradation. This study shows that the degradation is much faster and collagen content returns below the non-pregnant control value in two days. However, this degradation continues and the collagen content is even lower in para-1 (14 days postpartum) rats.

Additionally, in these measurements, the multiparous rats showed higher collagen content values compared to para-1 (2 days postpartum) and para-1 (14 days postpartum) cohorts. There are several factors that might affect the collagen content in the multiparous rats such as age, the number of fetuses in the uterus, parity, and weight [70, 69, 5, 71, 198]. With increase in age and parity, collagen deposition increases which might explain the higher values observed in the multiparous rats. Previously, most of the collagen content in rat uteri were reported based on the wet weight of the upper vaginal wall tissue, but in this study, we calculated the collagen content based on the dry weight of the tissue. Smith et al. calculated the percentage of collagen in rat uteri based on the dry weight for the different ovarian cycles and found the highest collagen content in the metestrus phase 28.6% [198]. In contrast, in the cervix of the rat uterus, the collagen content was reported to be 50% based on the sample dry weight [199]. Thus, these results clearly indicate that the collagen

content varies in different parts of the reproductive tract and may explain the differences between previously reported values and the numbers reported in this work.

5.3.3 Histological analysis

Representative histological images of the stained upper vaginal wall from virgin and multiparous rats at 100× magnification are shown in Figure 5.4 (A) and (B), respectively. In these figures, collagen fibers are stained pink, smooth muscle is stained yellow, and elastic fibers are stained black. A qualitative assessment of the images we studied (150 in total) revealed that collagen fibers are more sparsely distributed and disarrayed in multiparous rats compared to the virgin rats. Moreover, collagen fibers in multiparous rats appeared slightly thicker than those of virgin rats, but no quantitative measurements could be made. Most notably, the analysis of all the images we took indicated that there is a signature of collagen fiber dissociation with smooth muscles in multiparous rats but no evidence of collagen fiber fragmentation could be observed. These results are in agreement with the previous observations where the collagen fiber in cervix of pregnant rat appears to be disarrayed and disassociated with smooth muscles [200]. Previously, we reported changes in the elastic fibers of virgin and multiparous rats; an increase in elastic fiber tortuosity and decrease in elastic fiber length was observed when comparing multiparous and virgin rats cohorts [59]. We speculate that the changes in collagen density and thickness, as well as the observed dissociation of collagen fibers with smooth muscle in multiparous rats may be an additional contributor to the decrease in stiffness of the tissue as observed in previous studies [59, 174, 201, 12]. However, these changes appear small in comparison to changes

observed in elastic fibers following pregnancy and parturition [59].

A software was developed to calculate the percentage of collagen content in the virgin and multiparous rats; crudely estimated the values to 64.5±11.1 and 60.3±22.4, respectively based on the pixel color. These values varied from the more precise spectrophotometric measurements discussed above (Table 5.5) and the differences between the two methods may arise from the threshold for distinguishing collagen from elastin and smooth muscle, or the particular sections we used from histology.

5.3.4 Dynamics and distribution of water in rat upper vaginal wall tissues

The ^{2}H 2D ILT T_1 -T_2 relaxation methods were employed to investigate the dynamics and distribution of water in each of the upper vaginal tissues studied. However, we also performed one dimensional ^{2}H NMR experiments and no spectroscopic information was obtainable (^{2}H NMR spectrum of the ^2H_2O hydrated multiparous rat tissues is shown in Figure 5.5. Figure 5.6 shows 2D ILT T_1 -T_2 correlation maps of ^2H_2O hydrated samples acquired at 25 °C. In the 2D ILT map of the virgin rat tissue (Figure 5.6 A), three water reservoirs (labeled a, b, and c) apart from bulk (T_1 and T_2 value of approximately 403 and 352 ms) water were resolved. The peak denoted bulk water, exhibits isotropic motion as $T_1 \approx T_2$, where as the other peaks (labeled a, b, c, and d) exhibit unequal relaxation times and are indicative of anisotropic motion which may arise from the restrictions within the collagen matrix. Each peak corresponds to a different environment of water molecules in the samples indicating different dynamical characteristics of water. In the para-1 (2 days postpartum), para-1

(14 days postpartum), and multiparous cohorts, a fourth water environment (labeled d in Figure 5.6) is observed. To perform these experiments upper vaginal wall tissue was used; this experimental technique does not allow assigning the reservoirs of water to a particular structural motif of collagen, or association with collagen or elastin. Thus, all observable peaks may correspond to water present near collagen, elastin, or other ECM components.

From histological analysis discussed above, collagen fibers appear to be dissociated with the smooth muscle and changes in the collagen density or thickness is observed between virgin to multiparous rat cohorts. Thus, the appearance of water reservoir 'd' in Figure 5.6 (B, C, and D) may presumably arise from a redistribution of water or changes in collagen and/or elastin in the upper vaginal tissue/extracellular matrix following pregnancy and parturition. Lastly, the relaxation measurements and correlation times of peaks a, b, c, and d for all the samples studied are presented in Table 5.6.

We further attempted to correlate the measured relaxation and correlation times with the previously reported values in bovine nuchal ligament elastin samples [102, 202] and commercially available rat tail collagen. The T_1-T_2 ILT map of ^2H in ^2H_2O hydrated elastin showed four water reservoirs including the bulk water (similar to virgin rat samples) and were denoted α_1, α_2, β, and γ. In this study, we only considered peaks β and γ for comparison, as α_1 and α_2 correspond to the bulk water, and water between the elastin fibers, respectively [102, 202]. The measured relaxation times for peak β (T_1 = 66 ms and T_2 = 19.9 ms) and γ (T_1 = 34 ms and T_2 = 5.3 ms) differ with the values observed for peak b and c in the current study for virgin rat sample. Additionally, T_1-T_2 experiments were also performed in pure rat tail collagen and the measured T_1, T_2 and τ_c values did not correlate

with that observed in the tissues we used, which are comprised of collagen and elastin. These observations indicate that water in the upper vaginal wall tissue is experiencing a different environment and exhibit different dynamics than water in pure collagen and in pure elastin samples. However, in the present study no observable differences in the correlation times of peak a, b, c, and d across the samples studied based on pregnancy and parturition were observed. The measured relaxation times and correlation times across the samples were found to be similar within experimental uncertainty, indicating that the there are changes in the ECM which alter the redistribution of water, while preserving the structure of existing domains.

5.4 Conclusions

This chapter summarizes results from a study of the structural and dynamical modifications of rat reproductive tract collagen with respect to parity. ^{13}C CPMAS NMR spectra indicated no observable chemical shift differences despite the significant remodeling of vaginal wall and pelvic floor connective tissues during pregnancy and parturition. These results showed that the structure of collagen is preserved after pregnancy. However, some marked differences were observed in the dynamics of some amino acids. An increased mobility in some of the amino acid side chain moieties (e.g., C_γ-Val, C_γ-Glu, etc.) in the multiparous rats was observed in comparison to the virgin rats. For some of the amino acids such as the C_α-Glu, C_α-Ser, etc., the T_1 value was larger in the multiparous rat, in comparison to the virgin rat. However, we observed a decrease in T_1 value for the C_δ-Hyp or C_α-Leu peaks. Moreover, ^{2}H T_1 -T_2 measurements show the presence of four water reservoirs in the case of multiparous, para-

1 (2 days postpartum), and para-1 (14 days postpartum) while only three reservoirs were observed in the virgin rat. The redistribution of the water in the extracellular matrix due to pregnancy and/or parturition may be responsible for the appearance of an additional water reservoir, which might have influenced the dynamics of some of the amino acid side chains. Spectrophotometric measurements showed that the virgin rat had the highest percentage of collagen content among the samples. A signature of the collagen fiber dissociation, as well as possible changes in the density and thickness of the collagen fiber were observed in multiparous and virgin rat samples.

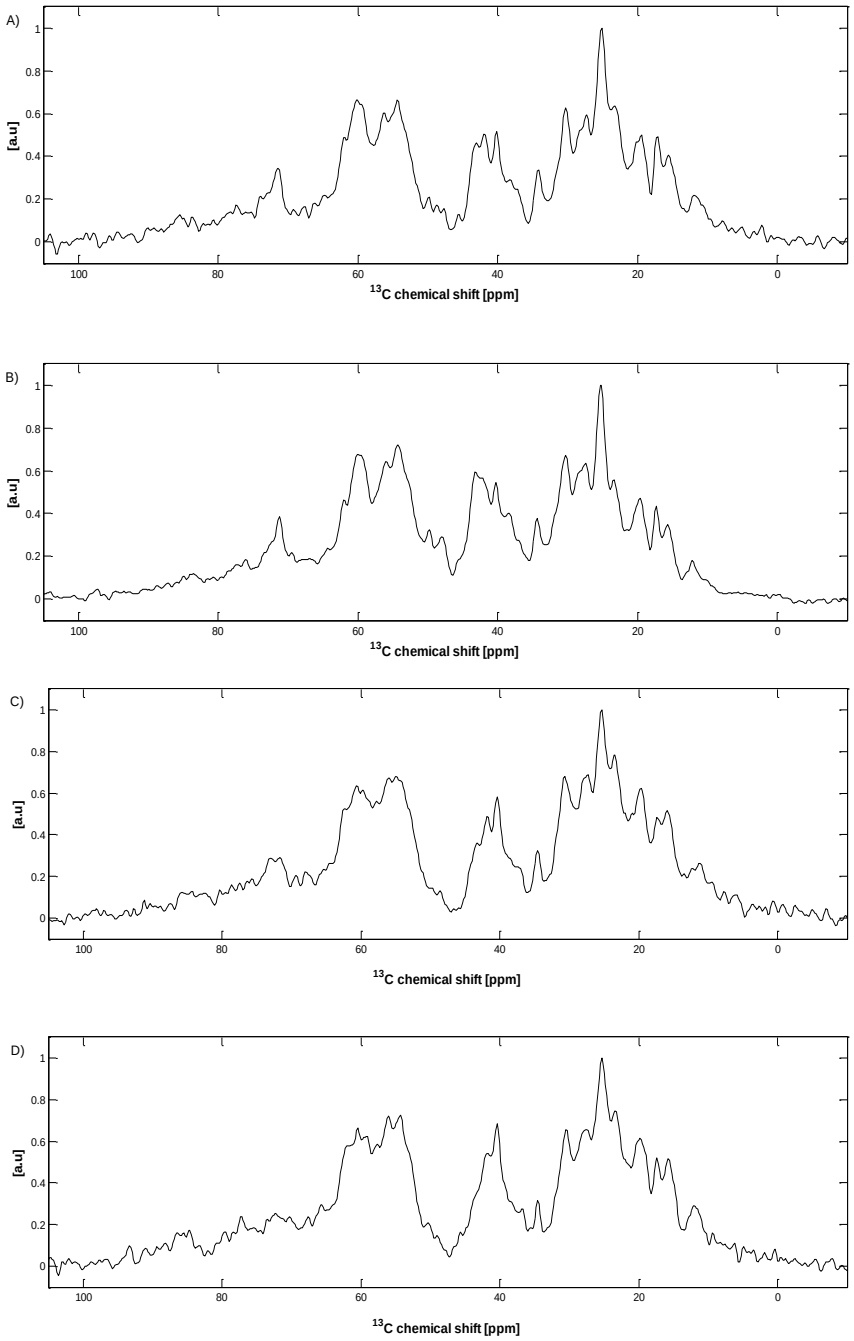

Figure 5.1: Cross Polarization ^{13}C MAS NMR spectra of (A) virgin, (B) multiparous, (C) para-1 (2 days postpartum), and (D) para-1 (14 days postpartum) aliphatic regions. No peaks were resolvable from the range of 150 to 100 ppm. Spectra were acquired by accumulating 10000 scans at 10 kHz spinning speed at a magnetic field strength of 17.61 T. The differences in the spectra are discussed in the text and peak assignments are tabulated in Table 5.1.

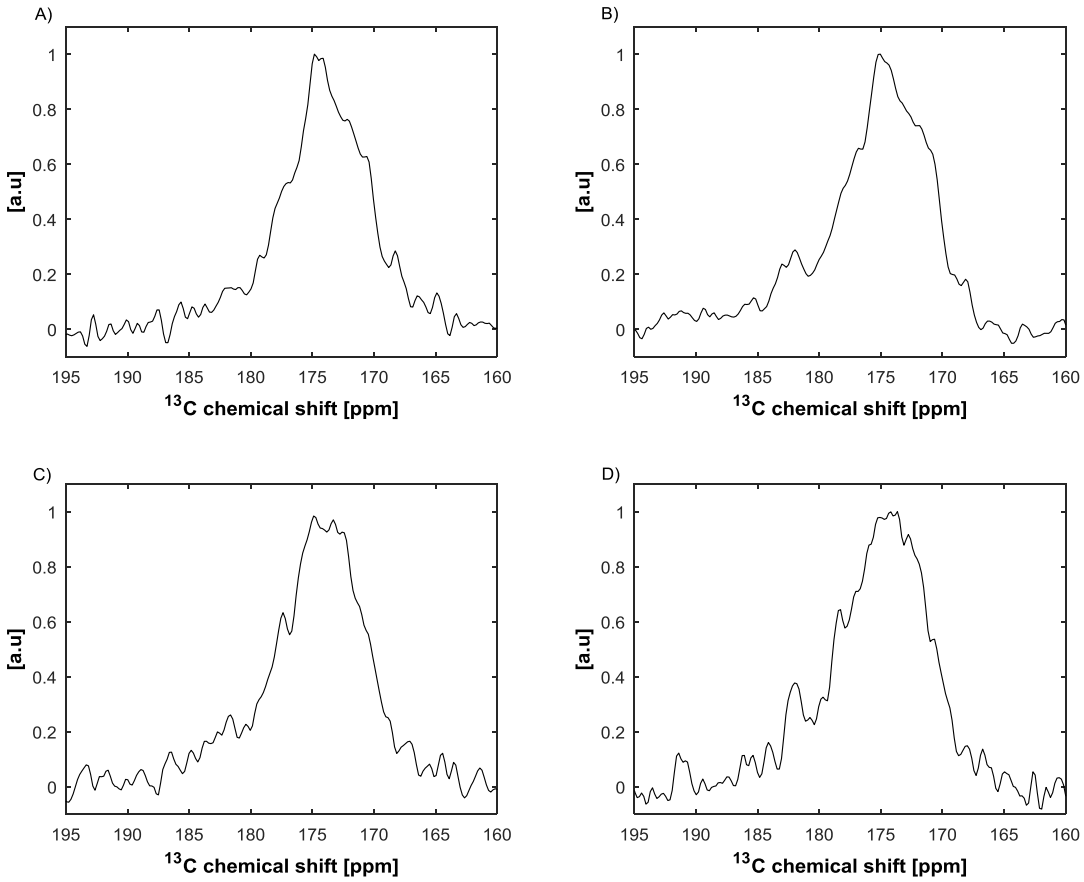

Figure 5.2: Cross Polarization ^{13}C MAS NMR spectra of (A) virgin, (B) multiparous, (C) para-1 (2 days postpartum), and (D) para-1 (14 days postpartum) carbonyl regions. Spectra were acquired by accumulating 10000 scans at 10 kHz spinning speed at a magnetic field strength of 17.61 T.

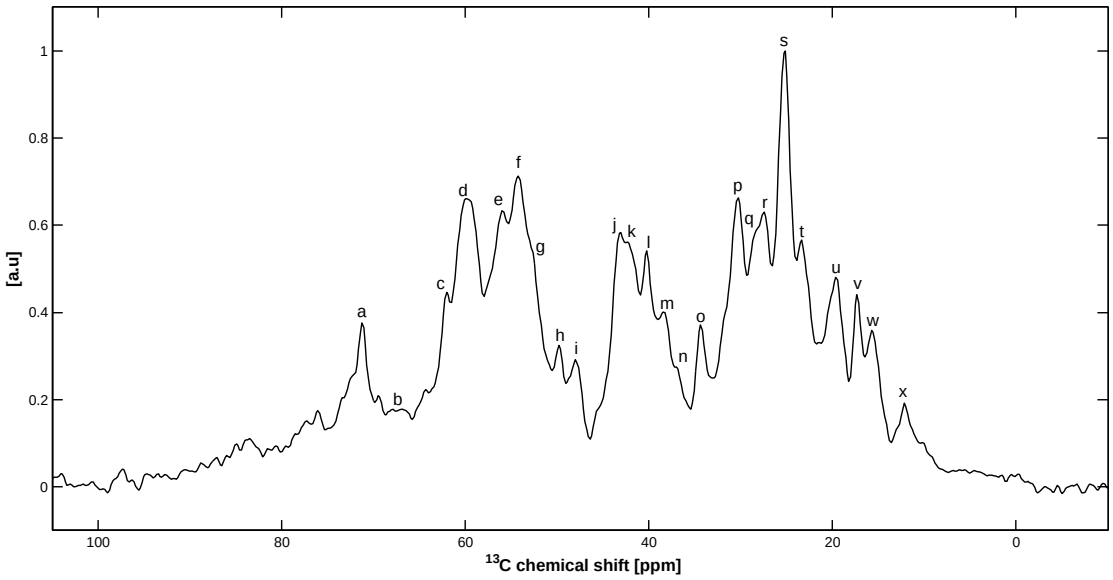

Figure 5.3: Cross Polarization ^{13}C MAS NMR spectra of the multiparous rat tissue at 300 K. No peaks were resolvable from the range of 100 to 165 ppm. The spectrum was acquired by accumulating 10000 scans at 10 kHz spinning speed at a magnetic field of 17.61 T. Chemical shift assignments are tabulated in Table 5.1.

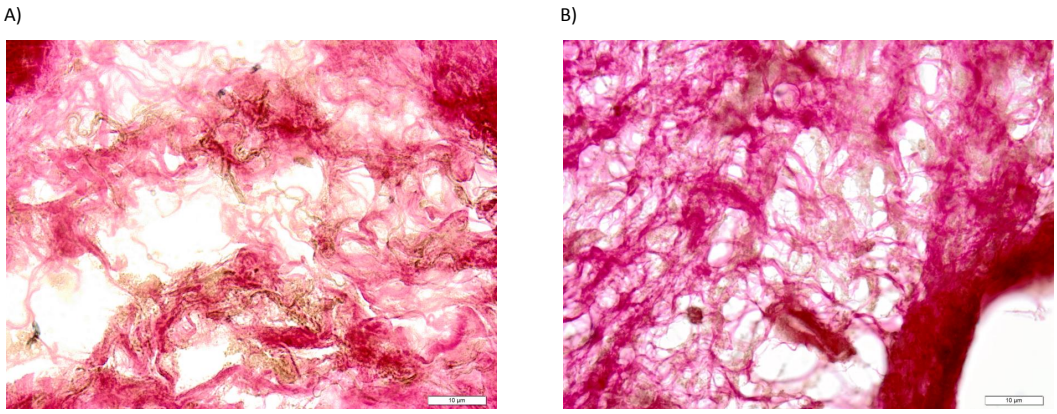

Figure 5.4: Representative histological image (at 100×) of the upper vaginal wall of the A) multiparous and B) virgin Sprague-Dawley rat sectioned at 10 μm. Collagen fibers are stained pink, smooth muscle is stained yellow and elastic fibers are stained black. Histological images show possible collagen fiber disassociation with smooth muscle and a change in density of collagen fibers in multiparous and virgin rats.

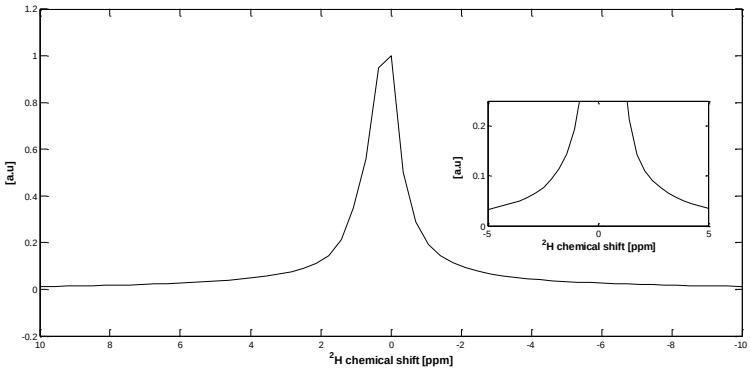

Figure 5.5: ^{2}H NMR spectrum ^2H_2O in collagen from the upper vaginal wall tissue of multiparous rats. Spectra were obtained without spinning at a field of 4.69 T.

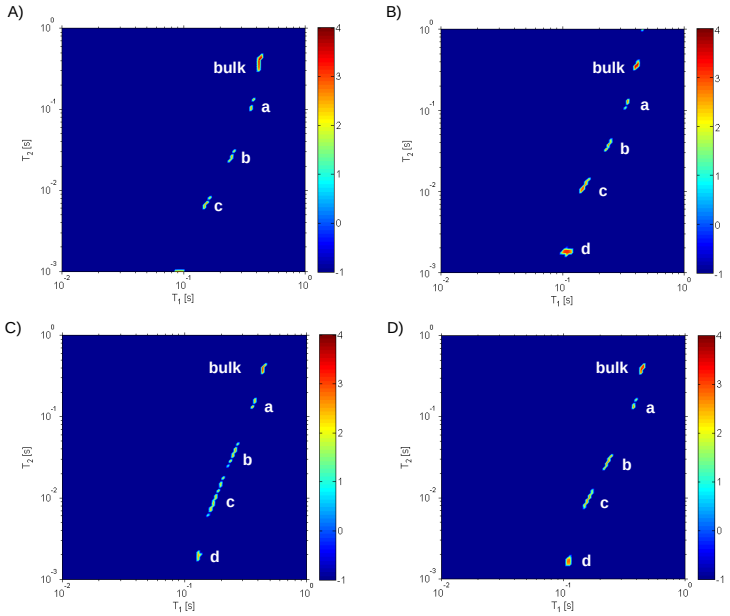

Figure 5.6: 2D ILT map of the ^{2}H T_1-T_2 results from A) virgin B) multiparous C) para-1 (2 days postpartum), and D) para-1 (14 days postpartum) rats. In all the samples except virgin rats, four peaks are well resolved (ignoring bulk water). This fourth peak labeled 'd' may arise from changes in the extracellular matrix which may include changes collagen, elastin, or both. The color bar to the right (in each figure) represents the signal intensity on logarithmic scale. The numerical values of the T_1 and T_2 and correlation times are provided in Table 5.6.

Table 5.1: Tabulated results of the chemical shifts observed at 300 K for the virgin, multiparous, para-1 (2 days postpartum), and para-1 (14 days postpartum) rat upper vaginal wall collagen.

Fig notation	Observed chemical shift				Assignment
	Virgin	Multiparous	para-1 (2 days postpartum)	para-1 (14 days postpartum)	
a	71.4	71.4	72.1	-	C_γ-Hyp
b	67.2	67.2	67.2	67.2	C_β-Thr
c	62.0	62.0	62.4	62.0	C_β-Ser
d	60.1, 59.5	60.1, -	60.6, 59.7	60.5, 59.2	C_α-Pro, C_α-Thr, C_α-Hyp, C_α-Phe
e	56.2	56.0	56.0	56.0	C_δ-Hyp*, C_α-Leu
f	54.4	54.6	54.8	54.3	C_α-Glu, C_α-Asp, C_α-Ser
g	52.6	-	-	52.6	C_α-Arg
h	49.8	49.8	49.8	50.3	C_α-Ala
i	48.7	48.0	48.5	48.9	C_δ-Pro
j	43.1	43.1	43.2	43.2	C_α-Gly
k	42.0	42.3	41.9	41.9	C_δ-Arg
l	40.2	40.2	40.4	40.4	C_β-Leu
m	38.2	38.4	38.5	38.4	C_β-Asp, C_β-Leu, C_β-Phe
n	37.4	37.2	37.2	36.9	C_β-Hyp
o	34.2	34.4	34.5	34.5	C_β-Ile
p	30.3	30.3	30.6	30.5	C_β-Pro, C_β-Lys, C_β-Val
q	28.1	28.1	28.0	28.0	C_γ-Glu, C_β-Arg, C_β-Val
r	27.2	27.4	27.3	27.4	C_β-Val
s	25.1	25.1	25.3	25.3	C_γ-Pro, C_β-Glu, C_γ-Leu
t	23.3	23.3	23.5	23.4	C_γ-Arg, C_γ-Leu, C_δ-Leu
u	19.4	19.4	19.6	19.8	C_γ-Val, C_γ-Thr
v	17.1	17.3	17.3	17.4	C_β-Ala
w	15.5	15.5	15.9	15.8	$C_{\gamma 2}$-Ile
x	12.0	12.0	11.3	12.0	C_δ-Ile

* The C_δ Hyp* chemical shift range has been reported to lie in the range of 54.3 and 58.3 ppm [187, 67].

Table 5.2: Tabulated ^{13}C $T_{1\rho}$ relaxation times (two different locking fields shown in parenthesis), for virgin and multiparous rat upper vaginal wall collagen samples at 300 K. Correlation times were determined using equations (2) and (3) as described in the text.

Assignment	Virgin			Multiparous		
	$T_{1\rho}[ms]$ (50.00kHz)	$T_{1\rho}[ms]$ (25.00kHz)	$\tau_c[\mu s]$	$T_{1\rho}[ms]$ (50.00kHz)	$T_{1\rho}[ms]$ (25.00kHz)	$\tau_c[\mu s]$
$C_{\gamma 2}$-Ile	5.37±0.79	3.24±0.30	3.73±1.56	-	-	-
C_β-Ala	5.04±0.65	3.42±0.31	3.01±1.35	-	-	-
C_γ-Val, C_γ-Thr	6.50±0.98	2.98±0.24	5.57±1.77	5.35±0.41	5.05±0.49	0.91±0.16
C_γ-Pro, C_β-Glu, C_γ-Leu	2.20±0.10	1.44±0.07	3.23±0.58	2.20±0.06	1.56±0.06	2.75±0.39
C_γ-Glu, C_β-Arg, C_β-Val	2.40±0.19	1.27±0.07	4.57±1.05	1.90±0.09	1.56±0.10	1.87±0.09
C_β-Pro, C_β-Val , C_β-Lys	2.13±0.16	1.99±0.06	1.01±0.70	2.00±0.09	1.47±0.12	2.53±0.78
C_β-Ile	4.40±0.90	2.35±0.13	4.51±1.74	-	-	-
C_β-Leu	3.32±0.39	2.61±0.13	2.14±0.96	2.23±0.14	1.70±0.13	2.32±0.84
C_α-Gly	1.77±0.16	1.19±0.12	3.07±1.20	1.05±0.05	0.92±0.09	1.46±0.91
C_α-Glu, C_α-Asp, C_α-Ser	2.04±0.16	1.34±0.10	3.21±0.95	2.26±0.10	1.29±0.08	4.08±0.71
C_α-Pro, C_α-Hyp, C_α-Thr, C_α-Phe	1.99±0.15	1.12±0.09	4.17±1.06	2.31±0.10	1.18±0.08	4.82±0.79
C_γ-Hyp	2.07±0.26	1.31±0.05	3.43±1.00	2.31±0.21	1.42±0.17	3.61±1.40

Table 5.3: Tabulated ^{13}C $T_{1\rho}$ relaxation times (two different locking fields shown in parenthesis), for para-1 (2 days postpartum) and para-1 (14 days postpartum) rats upper vaginal wall tissue samples at 300 K. Correlation times were determined using equations (2) and (3) as described in the text.

Assignment	para-1 (2 days postpartum)			para-1 (14 days postpartum)		
	$T_{1\rho}[ms]$ (50.00kHz)	$T_{1\rho}[ms]$ (25.00kHz)	$\tau_c[\mu s]$	$T_{1\rho}[ms]$ (50.00kHz)	$T_{1\rho}[ms]$ (25.00kHz)	$\tau_c[\mu s]$
$C_{\gamma 2}$-Ile	6.49±0.76	5.01±0.51	2.24±1.13	5.57±0.31	3.63±0.75	3.25±1.85
C_γ-Val, C_γ-Thr	6.75±0.55	3.86±0.17	4.07±0.81	-	-	-
C_γ Pro,C_β-Glu,C_γ-Leu	2.44±0.06	1.81±0.08	2.48±0.41	2.07±0.06	1.84±0.07	1.37±0.43
C_γ-Glu, C_β-Arg, C_β-Val	1.97±0.07	1.74±0.09	1.41±0.55	1.77±0.07	1.36± 0.11	2.27±0.72
C_β-Leu	-	-	-	3.13±0.08	2.48±0.25	2.09±0.77
C_α-Gly	1.56±0.06	1.42±0.28	1.20±0.40	-	-	-
C_α-Glu, C_α-Asp, C_α-Ser	2.18±0.23	1.05±0.15	5.22 ±1.95	2.10±0.10	1.56±0.11	2.47 ± 0.71
C_α-Pro, C_α-Hyp, C_α-Thr, C_α-Phe	2.07 ±0.18	1.30±0.16	3.48±1.39	1.75±0.04	1.13±0.05	3.31±0.42
C_γ-Hyp	1.59±0.07	1.10±0.06	2.89±0.69	2.04±0.14	1.81±0.12	1.38±0.87

Table 5.4: Tabulated ^{13}C T_1 relaxation times of rat upper vaginal wall collagen for the virgin and multiparous rats at 300 K.

Assignment	Virgin T_1[s]	Multiparous T_1[s]
C_γ-Pro, C_β-Glu, C_γ-Leu	1.52±0.08	1.44±0.05
C_β-Pro, C_β-Val, C_β-Lys	1.40±0.14	1.42±0.08
C_β-Leu	1.64±0.19	1.31±0.13
C_α-Gly	2.79±0.35	2.34±0.21
C_α-Glu, C_α-Asp, C_α-Ser	5.71±0.64	6.63±0.54
C_δ-Hyp ,C_α-Leu	7.44±1.11	5.32±0.41
C_α-Pro, C_α-Hyp, C_α-Thr, C_α-Phe	7.07±0.97	6.85±0.53
C_γ-Hyp	4.49±1.19	3.06±0.34

Table 5.5: Collagen content (measured per unit dry sample mass) of rat upper vaginal wall for the virgin, multiparous, para-1 (2 days postpartum), and para-1 (14 days postpartum) cohorts determined by spectrophotometry, as described in the methods section. In the table, n is the number of biological replicas used for this study, and the percentages shown are normalized to the dry sample weight prior to hydrolysis.

Sample	Total collagen (%)
Virgin (n=2)	83.6±1.87
Multiparous (n=2)	68.3±0.61
Para1(2 days) (n=3)	63.1±0.32
Para1(14 days) (n=3)	54.1±0.31

Table 5.6: Measured T_1, T_2 and correlation times (τ_c) obtained from virgin, multiparous, para-1 (2 days postpartum), and para-1 (14 days postpartum) upper vaginal wall tissue samples. The error bars shown for any of the T_1 and T_2 relaxation times represent the half-width of the peak observed in the 2D ILT maps and have been propagated to the errors in the correlation times.

Assignment		Virgin	para-1 (2 days postpartum)	para-1 (14 days postpartum)	Multiparous
Peak a	T_1 [ms]	367.96±25.70	367.95±25.70	385.45±26.90	333.75±15.20
	T_2 [ms]	116.10±24.22	147.60±25.75	147.60±25.75	119.70±20.85
	τ_c [s] $\times 10^{-8}$	0.74±0.22	0.58±0.18	0.61±0.18	0.65±0.17
Peak b	T_1 [ms]	247.95±23.10	248.80±34.69	231.55±26.90	236.70±22.05
	T_2 [ms]	26.82±5.61	35.60±13.34	27.93±6.79	38.02±7.94
	τ_c [s] $\times 10^{-8}$	1.64±0.35	1.37±0.61	1.53±0.41	1.27±0.30
Peak c	T_1 [ms]	155.75±14.50	180.65±33.70	159.60±18.60	152.35±17.70
	T_2 [ms]	7.12±1.49	11.81±6.51	9.95±3.08	12.09±2.94
	τ_c [s] $\times 10^{-8}$	2.69±0.52	2.20±1.52	2.27±0.69	1.97±0.48
Peak d	T_1 [ms]	-	132.25±9.20	109.75±7.65	109.75±15.02
	T_2 [ms]	-	1.88±0.26	1.70±0.29	1.75±0.24
	τ_c [s] $\times 10^{-8}$	-	4.93±0.64	4.74±0.07	4.60±0.80

Chapter 6

Ultraviolet radiation reduces desmosine cross-links in elastin

This chapter highlights the results published in ref. [167].

6.1 Introduction

Elastin, the principal protein component of the elastic fiber, is an extracellular matrix protein of human tissues that require elasticity such as the arteries, lungs, and skin. Elastin plays an important role in providing these tissues, and others, the ability to stretch while maintaining healthy cells [16, 19, 41, 17, 203]. In the skin, the majority of elastin is located in the reticular dermis. Mature elastin is a system of interconnected fibers that are encompassed by other proteins such as elaunin fibers and oxytalan fibers [204]. Tropoelastin, the monomer of elastin, is a large 72 kDa protein which is cross-linked by desmosine or isodesmosine to form elastin. The vast majority of elastin is produced during fetal development, and the

first few years of life, after which the expression of tropoelastin sharply decreases [205]. Consequently, connective tissues rely on elastin that is formed early in life [206]. When the skin is damaged through UV exposure and/or oxidation it may lose elasticity, and low levels of tropoelastin production may result in irreparable damage. Recent research into repairing damaged elastic fibers has focused on integrating tropoelastin into the skin; one challenge in this approach relates to transferring the protein across the epidermis. Another approach has been to increase tropoelastin expression through the use of small molecules such as all-*trans* retinoic acid [207, 208].

While the relationship between UV radiation and photoaging of skin has been established, the exact change that elastin undergoes when exposed to UV radiation is still unclear. One common belief is that elastic fibers are denatured or cleaved by UV radiation, and that most of the elastotic material is produced after exposure to UV radiation or its disorganized structure gives aged skin its characteristic wrinkled appearance. In previously reported studies, electron microscopy, histology, TEM (transmission electron microscopy), and SEM (scanning electron microscopy) have been applied to probe macroscopic changes to the elastic fiber in aged and photodamaged skin [209, 210, 211, 212]. For all biological damage associated to sun exposure, UV-B contributes 80% whereas UV-A contributes only 20% even though approximately 95% of terrestrial UV-radiation is UV-A [213]; more work is needed to better understand the microscopic changes that UV-A irradiation causes to the structure of elastin. We conducted this *in vitro* study to uncover changes on elastic fibers that undergo when exposed to high intensity UV-A irradiation. Elastic fibers were then examined histologically and by TEM to observe the macroscopic changes that resulted from irradiation. ^{13}C

solid state NMR spectroscopy was performed to measure possible structural alterations of elastin. Mass spectrometry was also implemented to quantify changes in the relative amount of desmosine cross-links. These combined methods provide new information relating to the detrimental effects of UV-A irradiation to the structure of the elastic fiber and of elastin.

6.1.1 Materials and methods

6.1.2 Sample preparation

Bovine nuchal ligament elastic fibers purchased from Elastin Products Company were used for this study. These samples were purified by Elastin Products Company using a known protocol[147] and were free of fat, collagen, smooth muscle cells, and other connective tissue. In a prior study, we showed that the protocol used for isolating elastin did not alter the structure of the protein, or the concentration of cross-links [36]. Elastic fibers were completely immersed in distilled water while being irradiated with a 3U40W UV-A lamp (Cnlight Co, China) with a center wavelength of 365 nm which was placed 10 cm above the sample. During irradiation, the system was covered with a shield to ensure that the sample was isolated from other light and were submerged in water during irradiation. The irradiation intensity was 12 mW/cm^2 and samples were continuously irradiated for 9 days. The intensity of the UV-A lamp is therefore 2.85 times higher than that of the sun, when directly overhead (located at the zenith).

6.1.3 Histology and microscopy

Unirradiated elastic fibers and fibers following 9 days of UV-A irradiation were used for the histological study. For histology, a small amount of sample was placed overnight in 100 ml phosphate buffered saline. The samples were then placed in Lieca Cryo-Gel (SPI supplies Product Ref-02694-AB), sectioned on a Leica CM1850 cryostat at 10 μm, and stained using the Sigma-Aldrich elastic stain kit (REF HT25A-1KT) following a modified version of a previously reported protocol [59]. The slides were gently rinsed with 95% ethanol, and then placed in xylene for a few seconds. Cover slips were then mounted using an Eukitt quick-hardening mounting medium (Sigma-Aldrich REF 03989) and left to dry overnight. All sections were photographed using a National Optical DC4-156-S digital microscope at a magnification of 10×.

6.1.4 Transmission electron microscopy (TEM)

Bovine nuchal ligament elastic fibers were immersed in 0.1 M phosphate buffered solution (pH-7.4) for 1 hour. All the samples were stained with osmium tetroxide and embedded in epoxy resin. Samples were sliced along the plane that was perpendicular to the fiber axis, with a thickness of 60 nm and examined in a JEM-2000EX transmission electron microscope. The accelerating voltage used was 120 kV.

6.1.5 ^{13}C NMR experimental parameters

Prior to the NMR experiments, unirradiated and 9 days UV-A irradiated samples were immersed in distilled water and solid-state NMR experiments were carried out on hydrated

samples. ^{13}C NMR experiments were performed using a Bruker Avance (Billerica, MA) spectrometer at a magnetic field strength of 21.10 T. All the experiments were carried out using a 4 mm center packing rotor with an insert to keep the samples hydrated, as well as to center the samples with respect to the RF coil. ^{13}C MAS (magic angle spinning) spectra were measured using a DEPTH sequence (to suppress background carbon signals arising from rotor inserts and the probe head) [150, 151] with 80 kHz TPPM decoupling [149] at (300 ± 1) K and direct polarization. The spinning speed was set to 14.50 kHz for all the samples and spectra were acquired by accumulating 18800 scans. The ^{13}C $\pi/2$ pulse was 54 μs and the recycle delay was 6 s. Analysis of data was performed using MATLAB and matNMR with a Gaussian multiplication broadening factor of 100 Hz. ^{13}C NMR spectra were referenced to adamantane (TMS = 0 ppm).

6.1.6 Sample hydrolysis and quantification with labeled desmosine

Elastic fiber samples for this study were lyophilized for 24 hours prior to hydrolysis. Approximately, 2.1 to 2.2 mg of each sample was placed into a solution containing 300 μl of 6 M HCl and 1 μl of 0.5% w/w phenol solution. The sample and solution mixture was placed into a vacuum hydrolysis tube, flushed with nitrogen gas, and then evacuated. The samples were kept at 110 °C for 96 h, afterward the solvent was frozen in liquid nitrogen and lyophilized for 8 to 10 h. After lyophilization, each sample was suspended in a 50 μl solution of 94.5% 0.14 M sodium acetate, 0.5% triethylamine, and 5% acetonitrile (v/v/v) at a pH of 7.5. Resuspended samples were diluted to 100 fold. Labeled d_4-desmosine standard (Toronto Research Chemicals, Toronto, Canada) at final concentration of 10 pmol/μl was mixed with the

diluted samples in three different ratios 1:1, 3:1, and 1:3. The relative amount of desmosine in each sample was quantified with respect to mass spectrometric peak intensity of standard desmosine in MS^2 mode. For statistical analysis of the data, t-test was used assuming data followed a normal distribution, and using the standard deviations in each samples studied. Null hypothesis probability was measured indicating the level of significance of the data.

6.1.7 MALDI-MS quantitative analysis

MALDI-MS^2 experiments were performed using a Thermo LTQ XL ion trap mass spectrometer (Thermo Scientific, Waltham, MA, USA) equipped with a vacuum MALDI source. α-Cyano-4-hydroxycinnamic acid (CHCA) purchased from Sigma-Aldrich (St. Louis, Missouri, USA) was recrystallized and used to prepare the matrix solution. Solid CHCA was added in a solution of 0.1% trifluoroacetic acid, 70% acetonitrile, and 29.9% HPLC grade water until saturation. The solution was centrifuged and supernatant liquid was used as the matrix solution. 1 μl of sample mixture containing different ratio of standard and sample were placed in 9 μl of CHCA matrix solution. The final solution was vortexed, and 1 μl of mixture was spotted on the MALDI plate. Spotted points were air dried prior to inserting the plate into the MALDI mass spectrometer for analysis.

MALDI-MS^2 analysis was performed using a laser energy of 3.1 μJ, for 150 scans with the AGC set to 10,000 ions. Precursor ions of unlabeled desmosine (m/z = 526.3) obtained from hydrolysis of the elastic fibers studied and d_4 labeled desmosine standard (m/z = 530.3) (Toronto Research Chemicals, Toronto, Canada) were selected in a single isolation window (m/z = 529$\pm$6), and fragmented with a normalized collision energy = 35, activation

Q = 0.25, and activation time = 30 ms. The most intense product ions, at m/z = 397 for unlabeled desmosine and m/z = 401 for d_4-desmosine, were used for relative quantification.

6.2 Results and discussion

6.2.1 UV-A induced alterations of the elastic fiber

To follow the effect of UV-A exposure on elastic fibers, bovine nuchal ligament fibers with and without UV-A irradiation were investigated. Representative histological images of 9 days UV-A irradiated and unirradiated elastic fibers are shown in Figure 6.1. From the figure, it is clear that in an unirradiated sample multiple dense layers of elastic fibers are arranged in a regular fashion; the fibers appear relatively straight and are not fragmented. This regular pattern is dramatically disrupted after UV-A irradiation by 9 days (Figure 6.1 , right panel). UV-A exposure results in fragmentation of elastic fibers and alters the regularly ordered arrangement of the fibers as well. Moreover, elastic fibers appear thinner compared to that of unirradiated samples; the observed alterations in the elastic fibers due to UV-A irradiation follows the work previously reported in the literature [211, 210]. It is known that the level of elastase increases due to UV-irradiation *in vivo* which initiates elastin degradation [210, 214, 215]. Imayama et al. applied SEM and TEM to study the elastic fibers of dermal connective tissue and showed that UV-irradiation alters the elastic fiber by formation of new elastic fibers which later form an irregular network [210]. In their study, they irradiated the soles of Sprague-Dawely rats with UV-B (130 mJ/cm^2 for 3 min/day up to 12 weeks) and therefore it was possible to follow the formation of new elastin. In

the present *in vitro* study, cells have been removed by the purification step, consequently, elastic fibers are not repaired. Thus, this *in vitro* measurement allows for characterization of alterations that occur as a result of break down in the cross-links of elastin, discussed below, due to UV-A exposure, which in turn degrade their structure.

TEM was used to follow the macroscopic alterations of UV-A exposure on elastic fibers. Figure 6.2 shows TEM images of the sample without UV-A exposure and with 9 days of UV-A exposure. In the images, the elastic fibers are in white denoted 'a', the interstitial spaced between fibers is denoted 'c' and cracks within or on an edge of fibers denoted 'b'. Due to UV-A irradiation, pronounced cracks are observed in the 9 days irradiated sample, both in the interior of the elastic fiber and on the edges. Similar to the histological measurements, elastic fibers appear thinner in the 9 days irradiated sample, compared to the unirradiated sample.

UV-A exposure may initiate microscopic changes of the structure or dynamics of the principal protein, elastin, in the elastic fiber. To follow these changes, ^{13}C MAS NMR experiments were carried out. Chemical shift assignments of all major amino acids (e.g. glycine, proline, valine) that comprise the spectra shown in Figure 6.3 were made following previously reported measurements of elastin and its related peptides [36, 157, 35, 57, 158, 159]. A detailed discussion of the peak assignments and structures observable in elastin has been reported elsewhere [36, 161]. Experimental studies of the structure of elastin by modern NMR methodology is difficult due to the large, highly cross-linked nature of the protein. Even with isotopic labeling, degeneracies present in the spectra make structural elucidation challenging—in the present work we apply magnetic resonance spectroscopy to

reveal secondary structural changes or dynamics due to UV-A exposure. The aliphatic regions of the ^{13}C MAS NMR spectra of unirradiated and 9 days irradiated samples is shown in Figure 6.3. All ^{13}C peaks in these samples (unirradiated and 9 days irradiated) appear in the same position and no significant chemical shift differences were observed. These measurements reveal that any microstructural changes of elastin following 12 mW/cm^2 of UV-A irradiation for 9 days do not appear to alter the ^{13}C NMR chemical shifts of the most abundant amino acids that comprise the protein.

6.2.2 Biochemical changes of elastin due to UV-A exposure

The detrimental effects of UV rays on the cell and extracellular components (e.g., elastin, collagen, etc) of skin are already known to some extent [214, 216, 211, 217, 209, 213]. Sun exposed skin showed abnormalities which include fiber disintegration, thickening, and proliferation of the elastic fiber [209]. A marked decrease in the linearity of the elastic fiber is also observed due to UV exposure [211]. Chatterjee et al. observed skin wrinkling when hairless mice were exposed to UV-B irradiation and followed different biochemical parameters. Biochemical parameters such as water, elastin, and glycosaminoglycan content was observed to increase where as the collagen content remained the same after UV-B irradiation [214]. However, a different study showed that both UV-A and UV-B irradiation increase the concentration of elastin while the collagen content remain unaffected [217]. To obtain qualitative assessment of the macroscopic damage in elastic fiber that occurs in 9 days of UV-A exposure and to relate these changes to the actinic damage, we compare the UV-A irradiation from the lamp used in this study with that of the sun over the same period of

time. Taking the total intensity of light on earth surface (1400 W/m^2) one finds that the energy deposition from the UV-A lamp was 2.85 times higher compared to that of continuous exposure to the sun for a duration of 9 days. For this calculation we assumed that only 3% of the incident solar energy is UV radiation, and that the sun is at the zenith [218]. This computation does not account for any attenuation of the UV radiation, e.g. through the dermis, which may act as a layer of protection to the elastic fibers and reduce the intensity of the incident radiation.

Desmosine and isodesmosine are the major cross-linking domains of elastin and their relative concentrations may be used as a measure of biochemical changes. The effects of UV radiation on isolated desmosine and isodesmosine have been reported previously by Baurain and coworkers [219]. Their study showed photolytic reaction results free lysine due to breaking down of pyridinium rings of (iso)desmosine. However, the production of lysine depends on several factors such as irradiating wavelength, pH, and irradiation time. The formation of lysine was 35% when they irradiated desmosine at 274 nm for 25 min, whereas, for isodesmosine the irradiation dose was 285 nm for 50 min and yield was 78%. At the wavelengths of 320-400 nm (UV-A), the absorbance in desmosine is ≤ 0.05 [219]. In the present study, we quantify the reduction of desmosine due to UV-A in bovine nuchal ligament elastic fibers by MS/MS experiments. In these measurements, the unirradiated sample was used as a control. The relative amount of desmosine in the 9 days UV-A irradiated sample was normalized with the amount of desmosine in the unirradiated sample and the result is presented in Table 6.3. From the table, the relative amount of desmosine in the 9-days irradiated sample was found to decrease by approximately 11%. The decrease in the relative

content of desmosine arises from the breakdown of cross-links as a result of the irradiation, as each measurement was made per unit mass of the lyophilized sample prior to hydrolysis.

A previous *in vivo* study on hairless mice skin showed that the desmosine content increases when treated with UV-A or UV-B [217, 214]. Chatterjee et al. observed an increase in elastin content per unit area of mice skin with UV-B exposure (40 mJ/cm^2) of 18 weeks irradiating three times a week [214]. However, Johnston et al. did not observe any statistically significant difference in the relative desmosine content when purified elastin was treated using 1 and 10 J of UV-A [217]. In the current *in vitro* study, an 11% decrease in desmosine content is observed in 9 consecutive days of UV-A irradiation using approximately 42 kJ, whereas in the previous work by Johnson et al. 1 J for 6.25 min was employed [217]. Though it is known that UV-B is more detrimental to the asthetic and mechanical functionality of skin, studies till now have demonstrated that UV-A causes minimal damage to skin. However, the results obtained in the present study show that UV-A may play a greater role in photoaging of skin than previously believed. Thus, the findings of this work indicate that cross-linking of tropoelastin is measurably reduced following UV-A irradiation and this breakdown may alter its biomechanical characteristics during prolonged exposure if not repaired. Chung and coworkers [74] have observed a marked increase in MMP-12 activity following UV exposure, which cause degradation of extracellular matrix such as elastin and collagen. The reduction of desmosine following UV-A exposure revealed in this in vitro study of elastic fibers, indicates that additional alterations are present before MMP-12 is expressed and other biological processes are initiated.

Similar to photoaged skin, cutis laxa is characterized by loose, redundant, inelastic, and

permanently wrinkled skin. Cutis laxa is a clinically and genetically heterogenous connective tissue disease [220]. It is known that in cutis laxa, abnormal mutant tropelastin (120 kDa) deposits result in disruption of the elastin-microfibrillar interaction and interferes with elastic fiber function [221]. A common feature of cutis laxa is a dramatic reduction in elastin content without significant alterations to the collagen component of connective tissue; elastic fibers appear scarce, thin, fragmented, and with less microfibrillar components [222, 220, 223]. The morphological changes to the elastic fiber as a result of cutis laxa are quite similar to the changes observed in UV exposed elastin. In addition to these morphological changes, a biomechanical study of cutis laxa shows reduction in the elastic modulus by 32 % and viscoelastic modulus by 53%, whereas retraction time increased by 85% compared to the control, indicating mechanical changes occur that are similar to the changes observed in aged skin [224, 225]. In the present *in-vitro* study the biochemical analysis also showed that UV-A irradiation breaks the cross-links in elastin which may play a significant role in the already known mechanical degradation of photoaged skin [226].

6.3 Conclusions

Results in this chapter highlight changes in elastic fibers due to UV-A exposure. TEM measurements show that UV-A exposure results in cracks of the elastic fiber pointing to macroscopic alterations. Mass spectrometric measurements show a decrease in desmosine content by 11% in a 9-days UV-A irradiated sample; this change arises from a breakdown of cross-links. Histological images show disruption in the regular array of elastic fibers as well as fibers appear shorter and thinner following UV-A exposure. ^{13}C NMR magic angle

spinning methods were applied to study possible secondary structural changes or dynamics of the major amino acids of elastin, the principal protein component of the elastic fiber. NMR measurements indicated that while the amount of desmosine in the UV-A irradiated sample was reduced in comparison to the unirradiated sample, the NMR chemical shifts of the most abundant amino acids of the protein and the observable line-widths appear the same. While previous *in vivo* studies pointed to an increase in desmosine in the skin when treated with UV-A or UV-B, this *in vitro* study shows a reduction of desmosine of the elastic fiber. These microscopic changes, coupled with the fragmentation of the elastic fiber, are likely to play a significant role in the already known loss of elasticity in aged, UV exposed skin.

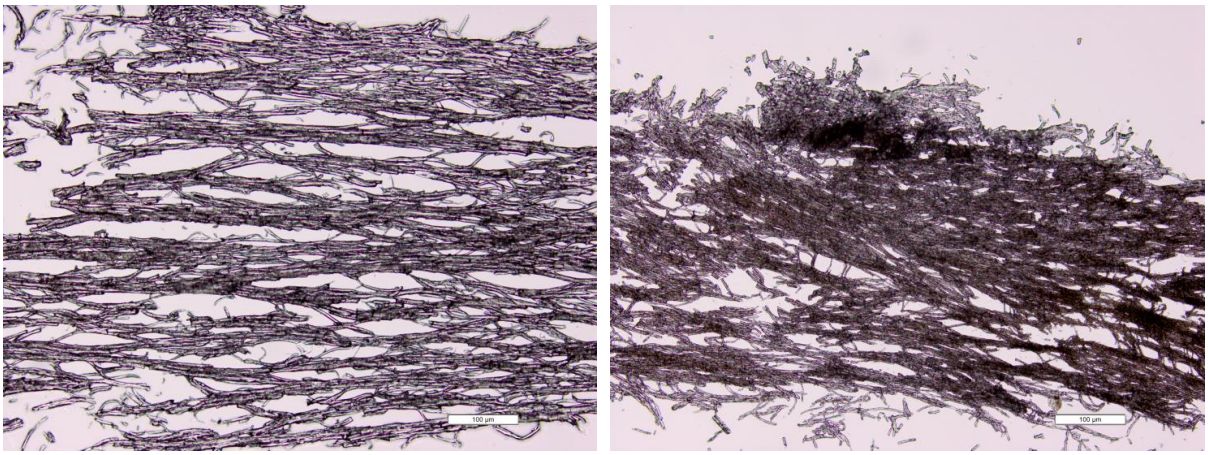

Figure 6.1: Histological images of unirradiated (left) and 9 days UV-A irradiated (right) bovine nuchal ligament elastic fibers. Images were photographed at 10 × magnification and elastic fibers are stained black. The onset of fragmentation and disruption in ordering of elastic fibers is evident following UV-A exposure. The scale bar in the figures shown is 100 μm.

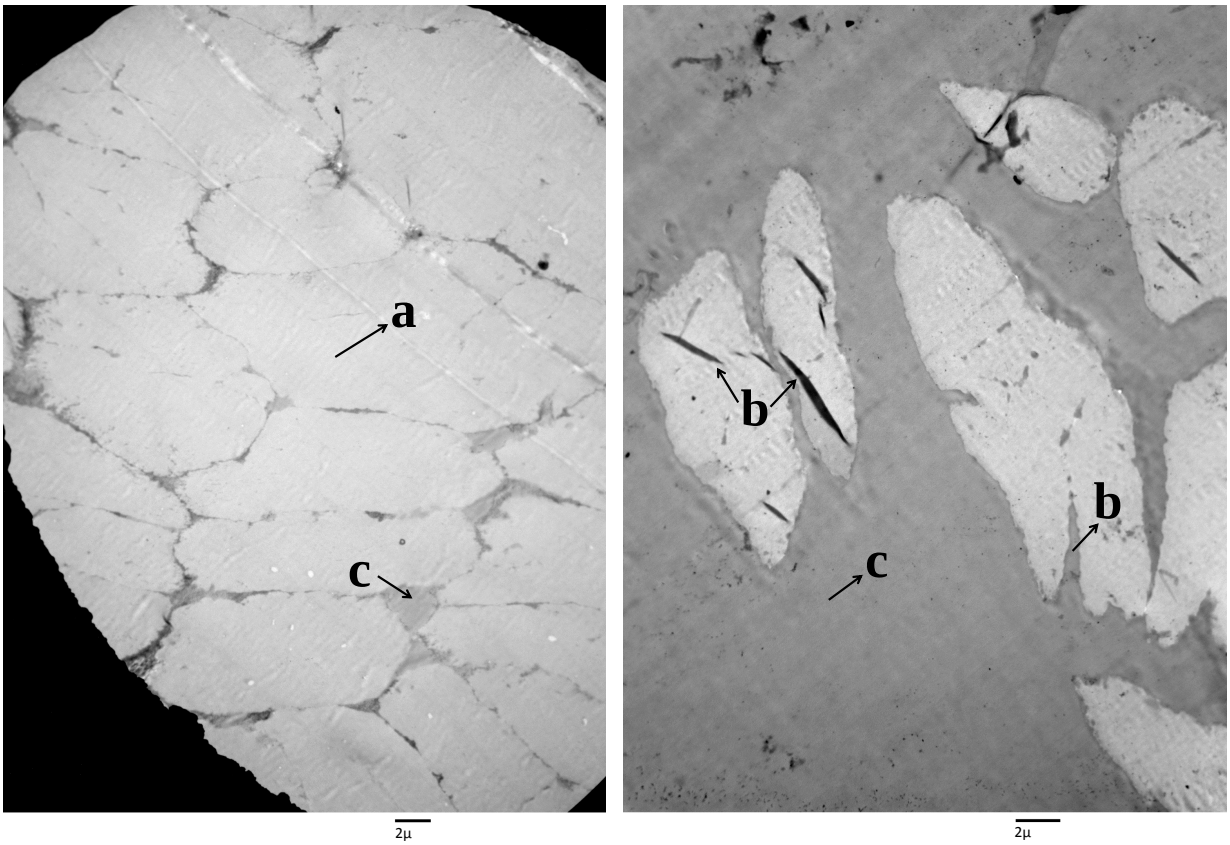

Figure 6.2: TEM images of (left) unirradiated and (right) 9 days UV-A irradiated elastin samples taken cross-sectionally (fiber axis points into the page). In the images, the light gray color (a) denotes an elastic fiber, (b) cracks on the edge or within the elastic fiber are as a result of UV-A exposure, and (c) the interstitial space between fibers.

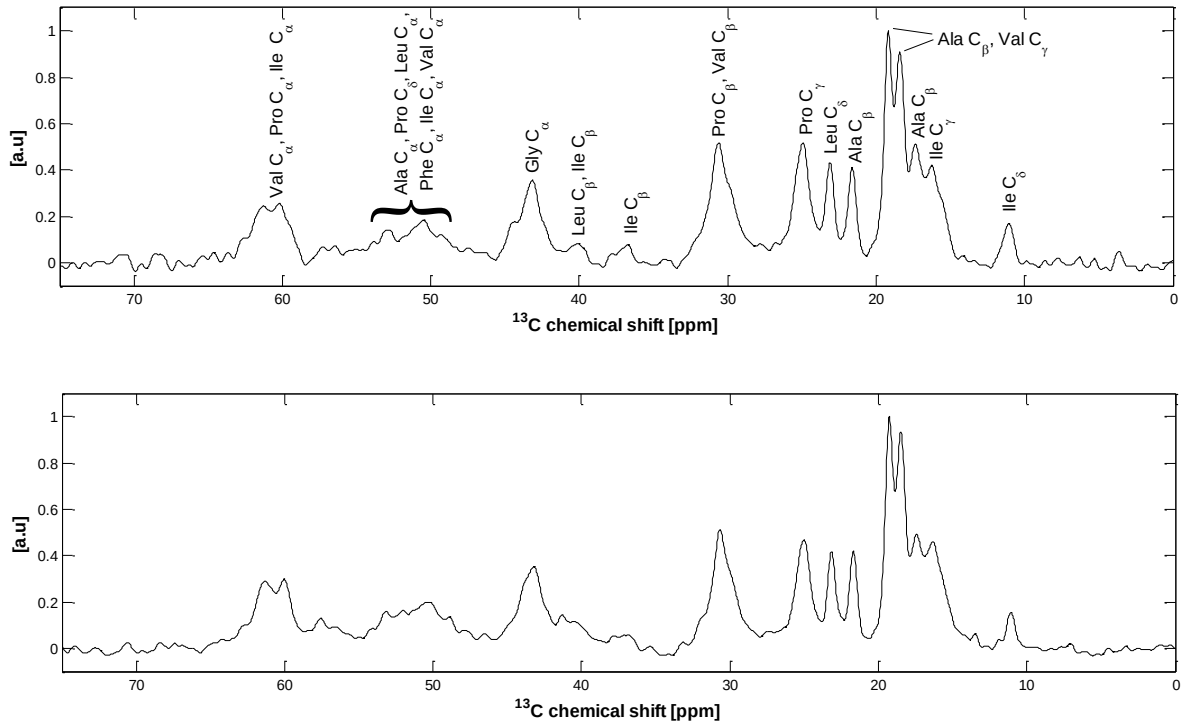

Figure 6.3: ^{13}C MAS NMR spectra of aliphatic region of unirradiated (top) and 9 days UV-A irradiated (bottom) elastic fibers recorded at 300 K. Peak assignments were made using values published in the literature, as discussed in the text. The spectrum was acquired by accumulating 18800 scans at 14.50 kHz magic angle spinning speed at a magnetic field strength of 21.10 T.

Table 6.1: Relative desmosine content (per mg lyophilized mass) in unirradiated and 9 days UV-A irradiated bovine nuchal ligament elastic fibers studied. The relative amount of desmosine is reported by taking the ratio of unlabeled desmosine to the d_4 desmosine normalized by the amount of desmosine in the unirradiated sample. Average values were calculated considering all the data points in each dilution for three different sets of hydrolysis for each sample. Error bars denote the variance propagated across all measurements (9 measurements: 3 different dilution ratios). The results of a t-test are presented in the table indicating the probability that the measurements are statistically different comparing 9 days irradiated and unirradiated sample.

Sample	Amount of Desmosine	t-test(%)
no irradiation	1.00±0.01	-
9 days irradiation	0.89±0.04	99.9

Chapter 7

Conclusions and future work

In conclusion, this thesis reports on the structural and dynamical alterations in female reproductive tract collagen and elastin with respect to parity. This work has provided gynecological community with detailed quantitative measurements relating to change in the structure and dynamics of elastin and collagen as a function of number of births. It also provides scientific community a novel method to measure the concentration of desmosine in tissues and other bodily fluids. The main results from various works in this thesis are described below.

The work relating to elastin study has provided information relating to the structural and dynamical modifications of the female reproductive tract elastin as a function of parity, in a murine model. Histological work, together with 2H NMR relaxation methods, reveal highly fragmented and tortous elastic fibers in the multiparous sample which has been experimentally shown to influence the loss of tissue stiffness [59]. MALDI mass spectrometry measurements reveal that the amount of desmosine was observed to increase with increase in parity. Surprisingly the amount of desmosine in multiparous reproductive tract elastic fibers

was observed to be more than three times than from virgin rat cohorts, which is in turn similar to other healthy mammalian tissues (e.g. bovine nuchal ligament elastin). From ^{13}C NMR measurements, virgin reproductive tract elastin exhibit very different NMR spectra due to higher concentration of MMP-2 and MMP-9 in tissues compared to cohorts that have given multiple births. Para1 rat cohorts resemble virgin spectra, while the para3 rat cohorts resemble multiparous spectra. NMR relaxometry measurements show the dynamics of major backbone and side chain carbon nuclei in the major amino acids vary significantly in virgin rat cohorts in comparison to the multiparous cohorts. Multiparous rat elastin dynamics is similar to bovine nuchal ligament elastin or healthy mammalian elastin. Surprisingly, macroscopic alterations of the elastic fibers evident in histological work, which include changes in length and tortuosity, appear to play a dominant role in tissue scaffolding. Alterations in elastin's microscopic structure, which include the concentration of cross-links, appear to play a secondary role and may not directly influence the mechanistic properties of the tissue. As the reproductive tract of virgin rats has been shown to be stiffer in experiments [59], elastic fragmentation and collagen concentration taken together may have a combined contribution to the scaffolding of tissue.

This thesis also provides the first study of the effect of parity on reproductive tract collagen by ^{13}C CPMAS NMR. The spectra that were obtained showed no observable chemical shift differences indicating that the structure of collagen remains preserved after pregnancy. NMR relaxometry measurements show that the dynamics of major amino acids, (e.g.glycine) remained unaltered with respect to parity. However, the effect of pregnancy appears to redistribute water in the extracellular matrix. This observation was made evident by the

appearance of an additional water reservoir in postpartum and multiparous rat cohorts by ^{2}H T_1 -T_2 measurements. Spectrophotometric measurements showed that the virgin rat had the highest percentage of collagen content among the samples, which may contribute to tissue stiffness. A signature of the collagen fiber dissociation, as well as possible changes in the density and thickness of the collagen fiber were observed in multiparous cohorts as shown by histology.

This thesis has provided an experimental method for quantifying the concentration of desmosine in tissues and bodily fluids using MALDI mass spectrometry. The alterations of elastic fibers due to UV-A exposure were investigated and results are summarized below. UV-A exposure results in cracks of the elastic fiber as shown by TEM measurements. Mass spectrometric measurements show a decrease in desmosine content by 11% in a 9-days UV-A irradiated sample which arises from a breakdown of cross-links. Histological images show that UV-A exposure leads to a disruption of the regular array of elastic fibers and, in addition, fibers appear short and thinner in exposed tissues. These findings appear to correlate with the alterations observed in the reproductive tract elastic fibers. Large alterations in fiber fragmentation and length appear to diminish the ability to provide a scaffold in UV exposed skin.

More work needs to be done to fully understand the weakening of the pelvic floor connective tissue and hence, the causes of pelvic floor disorders. Perhaps effects of other physiological conditions such as aging, obesity, etc. may cause change in the structure and hence, the function of the reproductive tract. Several groups have studied biomechanical properties of the aorta with respect to age [227, 228, 229, 230]. In the aorta (both in human and rat),

it has been shown that increase in age causes aortic tissue to be stiffer and less elastic [229]. Aging, which is driven by free radical exposure, has also been shown to affect the biomechanical properties of the reproductive tract tissues [173]. Rundgren et al. reported that aging and multiparity have different influence on different parts of the reproductive tract. Age had a greater influence on the physical properties of cervix and uterine horns while multiparity had greater effects on the vaginal walls [173]. To date, no study has been performed to characterize the effects of age on the structure and dynamics of reproductive tract elastic fibers, and may be a worthwhile study. Although the work in this thesis focused on the effects of parity on reproductive tract elastin, unavoidably multiparous rats were older than virgin rats. Effects of aging could be separated by investigating the elastic fibers from old virgin rats and studying the structure and dynamics using similar techniques that has been used in this thesis. Such a study may help to separate out effect of age on elastic fibers from pregnancy and thus better understand the role of elastic fibers in the pelvic floor disorder. It has been shown (from this study as well) that MMP and TIMP levels change and appear to alter the structure of the extracellular matrix in the reproductive tract [155]. An additional project for future work that would shed light on the effects of these matrix metalloproteinases would be to focus on studies of prolapsed tissues, perhaps from human subjects and/or mouse models and measure the MMP and inhibitor levels using ELISA techniques. By comparing levels of MMP's and/or TIMP's of prolapsed tissue with that of healthy subjects, it may be possible to determine a patient's predisposition to pelvic floor dysfunction. Recent work has shown that patients who exhibit some form of pelvic floor dysfunction exhibit detectable differences in MMP-1 levels, in comparison to women without POP [168].

The ovary and uterus are known to undergo extensive tissue remodeling throughout each reproductive cycle [155]. The MMP system has been reported to regulate the dynamic structural changes throughout the menstrual or estrous cycle [155]. This remodeling is accomplished partly by the MMP system regulated by the cyclic hormonal signals associated with the estrous or menstrual cycle which modulate remodeling [155]. An additional effort would be to separate out the effects of the menstruation from age and pregnancy and better understand the role of the MMP system as regulators of growth, cellular differentiation and, specialized tissue function in all aspects of ovarian and uterine physiology [155].

Bibliography

[1] J. E. Jelovsek, C. Maher, and M. D. Barber, "Pelvic organ prolapse," The Lancet, vol. 369, no. 9566, pp. 1027–1038, 2007.

[2] C. Goepel, "Differential elastin and tenascin immunolabeling in the uterosacral ligaments in postmenopausal women with and without pelvic organ prolapse," Acta histochemica, vol. 110, no. 3, pp. 204–209, 2008.

[3] A. H. MacLennan, A. W. Taylor, D. H. Wilson, and D. Wilson, "The prevalence of pelvic floor disorders and their relationship to gender, age, parity and mode of delivery," BJOJ: An International Journal of Obstetrics & Gyanecology, vol. 107, no. 12, pp. 1460–1470, 2000.

[4] Y. Wen, Y. Zhao, S. Li, M. Polan, and B. Chen, "Differences in mRNA and protein expression of small proteoglycans in vaginal wall tissue from women with and without stress urinary incontinence," Human Reproduction, vol. 22, no. 6, pp. 1718–1724, 2007.

[5] M. L. Harkness and R. Harkness, "The collagen content of the reproductive tract of the rat during pregnancy and lactation," The Journal of Physiology, vol. 123, no. 3, pp. 492–500, 1954.

[6] Z. Gunja-Smith, J. Lin, and J. F. Woessner, "Changes in desmosine and pyridinoline crosslinks during rapid synthesis and degradation of elastin and collagen in the rat uterus," Matrix, vol. 9, no. 1, pp. 21–27, 1989.

[7] M. Chvapil, V. Melanová, and H. Sommernitz, Physiology of Connective Tissue. Butterworths London, 1967.

[8] F. Regassa and D. E. Noakes, "Changes in the weight, collagen concentration and content of the uterus and cervix of the ewe during pregnancy," Research in Veterinary Science, vol. 70, no. 1, pp. 61–66, 2001.

[9] S. Hunskaar, K. Burgio, A. Clark, M. Lapitan, R. Nelson, U. Sillen, and D. Thom, "Epidemiology of urinary (UI) and faecal (FI) incontinence and pelvic organ prolapse (POP)," Incontinence, vol. 1, pp. 255–312, 2005.

[10] S. L. Hendrix, A. Clark, I. Nygaard, A. Aragaki, V. Barnabei, and A. McTiernan, "Pelvic organ prolapse in the women's health initiative: gravity and gravidity," American Journal of Obstetrics and Gynecology, vol. 186, no. 6, pp. 1160–1166, 2002.

[11] P. G. Drewes, H. Yanagisawa, B. Starcher, I. Hornstra, K. Csiszar, S. I. Marinis, P. Keller, and R. A. Word, "Pelvic organ prolapse in fibulin-5 knockout mice: pregnancy-induced changes in elastic fiber homeostasis in mouse vagina," The American Journal of Pathology, vol. 170, no. 2, pp. 578–589, 2007.

[12] D. D. Rahn, M. D. Ruff, S. A. Brown, H. F. Tibbals, and R. A. Word, "Biomechanical properties of the vaginal wall: effect of pregnancy, elastic fiber deficiency, and pelvic

organ prolapse," American Journal of Obstetrics & Gynecology, vol. 198, no. 5, pp. 590–e1, 2008.

[13] C. K. Wieslander, S. I. Marinis, P. G. Drewes, P. W. Keller, J. F. Acevedo, and R. A. Word, "Regulation of elastolytic proteases in the mouse vagina during pregnancy, parturition, and puerperium," Biology of Reproduction, vol. 78, no. 3, pp. 521–528, 2008.

[14] S. Partridge, "Elastin," Advances in Protein Chemistry, vol. 17, pp. 227–302, 1963.

[15] B. Li and V. Daggett, "Molecular basis for the extensibility of elastin," Journal of Muscle Research and Cell Motility, vol. 23, no. 5-6, pp. 561–573, 2002.

[16] J. Rosenbloom, W. Abrams, and R. Mecham, "Extracellular matrix 4: the elastic fiber.," The FASEB Journal, vol. 7, no. 13, pp. 1208–1218, 1993.

[17] W. F. Daamen, J. Veerkamp, J. Van Hest, and T. Van Kuppevelt, "Elastin as a biomaterial for tissue engineering," Biomaterials, vol. 28, no. 30, pp. 4378–4398, 2007.

[18] K. Ohgo, W. P. Niemczura, and K. K. Kumashiro, "Probing the natural-abundance ^{13}C populations of insoluble elastin using ^{13}C- ^{1}H heteronuclear correlation (HETCOR) NMR spectroscopy," Macromolecules, vol. 42, no. 18, pp. 7024–7030, 2009.

[19] F. W. Keeley, C. M. Bellingham, and K. A. Woodhouse, "Elastin as a self–organizing biomaterial: use of recombinantly expressed human elastin polypeptides as a model for investigations of structure and self–assembly of elastin," Philosophical Transactions of the Royal Society B, vol. 357, no. 1418, pp. 185–189, 2002.

[20] J. Gosline, M. Lillie, E. Carrington, P. Guerette, C. Ortlepp, and K. Savage, "Elastic proteins: biological roles and mechanical properties," Philosophical Transactions of the Royal Society B: Biological Sciences, vol. 357, no. 1418, pp. 121–132, 2002.

[21] G. Ellis and K. Packer, "Nuclear spin-relaxation studies of hydrated elastin," Biopolymers, vol. 15, no. 5, pp. 813–832, 1976.

[22] E. C. Davis, "Stability of elastin in the developing mouse aorta: a quantitative radioautographic study," Histochemistry, vol. 100, no. 1, pp. 17–26, 1993.

[23] L. Sharrow, D. Tinker, J. M. Davidson, and R. B. Rucker, "Accumulation and regulation of elastin in the rat uterus," Experimental Biology and Medicine, vol. 192, no. 2, pp. 121–126, 1989.

[24] O. Shynlova, J. A. Mitchell, A. Tsampalieros, B. L. Langille, and S. J. Lye, "Progesterone and gravidity differentially regulate expression of extracellular matrix components in the pregnant rat myometrium," Biology of Reproduction, vol. 70, no. 4, pp. 986–992, 2004.

[25] J. Fata, A.-V. Ho, K. Leco, R. Moorehead, and R. Khokha, "Cellular turnover and extracellular matrix remodeling in female reproductive tissues: functions of metalloproteinases and their inhibitors," Cell. Mol. Life Sci., vol. 57, no. 1, pp. 77–95, 2000.

[26] J. F. Woessner and T. H. Brewer, "Formation and breakdown of collagen and elastin in the human uterus during pregnancy and post-partum involution," Biochemical Journal, vol. 89, no. 1, p. 75, 1963.

[27] B. Starcher and S. Percival, "Elastin turnover in the rat uterus," Connective Tissue Research, vol. 13, no. 3, pp. 207–215, 1985.

[28] P. Leppert and S. Y. Yu, "Three-dimensional structures of uterine elastic fibers: scanning electron microscopic studies," Connective Tissue Research, vol. 27, no. 1, pp. 15–31, 1991.

[29] F. Regassa and D. Noakes, "Changes in the weight, collagen concentration and content of the uterus and cervix of the ewe during pregnancy," Research in Veterinary Science, vol. 70, no. 1, pp. 61–66, 2001.

[30] K. Wasano and T. Yamamota, "Tridimensional architecture of elastic tissue in the rat aorta and femoral artery—a scanning electron microscope study," Journal of Electron Microscopy, vol. 32, no. 1, pp. 33–44, 1983.

[31] T. Tsuji, "A new elastic system component, elastic sheet ĂŹin the human dermis. an electron microscopic study," British Journal of Dermatology, vol. 118, no. 3, pp. 347–352, 1988.

[32] D. Urry and T. Parker, "Mechanics of elastin: molecular mechanism of biological elasticity and its relationship to contraction," in Mechanics of Elastic Biomolecules, pp. 543–559, Springer, 2003.

[33] K. K. Kumashiro, M. S. Kim, S. E. Kaczmarek, L. B. Sandberg, and C. D. Boyd, "^{13}C cross-polarization/magic angle spinning NMR studies of α-elastin preparations show

retention of overall structure and reduction of mobility with a decreased number of cross-links," Biopolymers, vol. 59, no. 4, pp. 266–275, 2001.

[34] K. Ohgo, W. P. Niemczura, J. Ashida, M. Okonogi, T. Asakura, and K. K. Kumashiro, "Heterogeneity in the conformation of valine in the elastin mimetic $(LGGVG)_6$ as shown by solid-state ^{13}C NMR spectroscopy," Biomacromolecules, vol. 7, no. 12, pp. 3306–3310, 2006.

[35] X. Yao and M. Hong, "Structure distribution in an elastin-mimetic peptide $(VPGVG)_3$ investigated by solid-state NMR," Journal of the American Chemical Society, vol. 126, no. 13, pp. 4199–4210, 2004.

[36] A. Papaioannou, M. Louis, B. Dhital, H. Ho, E. Chang, and G. Boutis, "Quantitative comparison of structure and dynamics of elastin following three isolation schemes by ^{13}C solid state NMR and MALDI mass spectrometry," Biochimica et Biophysica Acta (BBA)-Proteins and Proteomics, vol. 1854, no. 5, pp. 391–401, 2015.

[37] L. Debelle and A. Tamburro, "Elastin: molecular description and function," International Journal of Biochemistry, vol. 31, no. 2, pp. 261–272, 1999.

[38] A. Andrady and J. Mark, "Thermoelasticity of swollen elastin networks at constant composition," Biopolymers, vol. 19, no. 4, pp. 849–855, 1980.

[39] J. M. Gosline, "Hydrophobic interaction and a model for the elasticity of elastin," Biopolymers, vol. 17, no. 3, pp. 677–695, 1978.

[40] M. Lillie and J. Gosline, "The effects of hydration on the dynamic mechanical properties of elastin," Biopolymers, vol. 29, no. 8-9, pp. 1147–1160, 1990.

[41] L. Debelle and A. J. Alix, "The structures of elastins and their function," Biochimie, vol. 81, no. 10, pp. 981–994, 1999.

[42] D. Urry and T. Parker, "Mechanics of elastin: molecular mechanism of biological elasticity and its relationship to contraction," in Mechanics of Elastic Biomolecules, pp. 543–559, Springer, 2003.

[43] D. He, M. Chung, E. Chan, T. Alleyne, K. C. Ha, M. Miao, R. J. Stahl, F. W. Keeley, and J. Parkinson, "Comparative genomics of elastin: Sequence analysis of a highly repetitive protein," Matrix Biology, vol. 26, no. 7, pp. 524–540, 2007.

[44] D. Urry, Arterial Mesenchima and Arterioscleresis. Wiley Online Library, 1974.

[45] A. Tamburro, V. Guantieri, L. Pandolfo, and A. Scopa, "Synthetic fragments and analogues of elastin. ii. conformational studies," Biopolymers, vol. 29, no. 4-5, pp. 855–870, 1990.

[46] S. Partridge, H. Davis, and G. Adair, "The chemistry of connective tissues. 2. soluble proteins derived from partial hydrolysis of elastin," Biochemical Journal, vol. 61, no. 1, pp. 11–21, 1955.

[47] K. M. Baig, M. Vlaovic, and R. A. Anwar, "Amino acid sequences c-terminal to the cross-links in bovine elastin.," Biochemical Journal, vol. 185, pp. 611–616, 1980.

[48] J. A. Foster, L. Rubin, H. M. Kagan, C. Franzblau, E. Bruenger, and L. B. Sandberg, "Isolation and characterization of cross-linked peptides from elastin," Journal of Biological Chemistry, vol. 249, no. 19, pp. 6191–6196, 1974.

[49] G. E. Gerber and R. A. Anwar, "Comparative studies of the cross-linked regions of elastin from bovine ligamentum nuchae and bovine, porcine and human aorta.," Biochemical Journal, vol. 149, pp. 685–695, 1975.

[50] L. Debelle, A. J. Alix, S. M. Wei, M.-P. Jacob, J.-P. Huvenne, M. Berjot, and P. Legrand, "The secondary structure and architecture of human elastin," European Journal of Biochemistry, vol. 258, no. 2, pp. 533–539, 1998.

[51] L. B. Dyksterhuis, E. A. Carter, S. M. Mithieux, and A. S. Weiss, "Tropoelastin as a thermodynamically unfolded premolten globule protein: the effect of trimethylamine N-oxide on structure and coacervation," Archives of Biochemistry and Biophysics, vol. 487, no. 2, pp. 79–84, 2009.

[52] S. Vieth, C. M. Bellingham, F. W. Keeley, S. M. Hodge, and D. Rousseau, "Microstructural and tensile properties of elastin-based polypeptides crosslinked with genipin and pyrroloquinoline quinone," Biopolymers, vol. 85, no. 3, pp. 199–206, 2007.

[53] B. Bochicchio, A. Aït-Ali, A. M. Tamburro, and A. J. Alix, "Spectroscopic evidence revealing polyproline ii structure in hydrophobic, putatively elastomeric sequences encoded by specific exons of human tropoelastin," Biopolymers, vol. 73, no. 4, pp. 484–493, 2004.

[54] D. W. Urry, B. Starcher, and S. M. Partridge, "Coacervation of solubilized elastin effects a notable conformational change," Nature, vol. 222, pp. 795–796, 1969.

[55] W. Fleming, C. Sullivan, and D. Torchia, "Characterization of molecular motions in ^{13}C -labeled aortic elastin by ^{13}C -^{1}H magnetic double resonance," Biopolymers, vol. 19, no. 3, pp. 597–617, 1980.

[56] D. Demuth, N. Haase, D. Malzacher, and M. Vogel, "Effects of solvent concentration and composition on protein dynamics: ^{13}C MAS NMR studies of elastin in glycerol–water mixtures," Biochim. Biophy. Acta-Proteins and Proteomics, vol. 1854, no. 8, pp. 995–1000, 2015.

[57] A. Perry, M. P. Stypa, B. K. Tenn, and K. K. Kumashiro, "Solid-State ^{13}C NMR reveals effects of temperature and hydration elastin," Biophysical Journal, vol. 82, no. 2, pp. 1086–1095, 2002.

[58] K. Ohgo, W. P. Niemczura, T. Muroi, A. K. Onizuka, and K. K. Kumashiro, "Wideline separation (WISE) NMR of native elastin," Macromolecules, vol. 42, no. 22, pp. 8899–8906, 2009.

[59] K. T. Downing, M. Billah, E. Raparia, A. Shah, M. C. Silverstein, A. Ahmad, and G. S. Boutis, "The role of mode of delivery on elastic fiber architecture and vaginal vault elasticity: a rodent model study," Journal of the Mechanical Behavior of Biomedical Materials, vol. 29, pp. 190–198, 2014.

[60] X. Liu, Y. Zhao, B. Pawlyk, M. Damaser, and T. Li, "Failure of elastic fiber homeostasis leads to pelvic floor disorders," The American Journal of Pathology, vol. 168, no. 2, pp. 519–528, 2006.

[61] D. D. Rahn, J. F. Acevedo, S. Roshanravan, P. W. Keller, E. C. Davis, L. Y. Marmorstein, and R. A. Word, "Failure of pelvic organ support in mice deficient in fibulin-3," Am. J. Pathol., vol. 174, no. 1, pp. 206–215, 2009.

[62] C. Goepel and C. Thomssen, "Changes in the extracellular matrix in periurethral tissue of women with stress urinary incontinence," Acta Histochemica, vol. 108, no. 6, pp. 441–445, 2006.

[63] M. D. Shoulders and R. T. Raines, "Collagen structure and stability," Annual Review of Biochemistry, vol. 78, p. 929, 2009.

[64] D. Huster, "Solid-state NMR studies of collagen structure and dynamics in isolated fibrils and in biological tissues," Annual Reports on NMR Spectroscopy, vol. 64, pp. 127–159, 2008.

[65] P. Fratzl, Collagen: structure and mechanics. Springer Science & Business Media, 2008.

[66] H. Saitô, I. Ando, and A. Naito, Solid State NMR Spectroscopy for Biopolymers: Principles and Applications. Springer, 2006.

[67] A. E. Aliev, "Solid-state NMR studies of collagen-based parchments and gelatin," Biopolymers, vol. 77, no. 4, pp. 230–245, 2005.

[68] M. L. Harkness and R. Harkness, "The distribution of the growth of collagen in the uterus of the pregnant rat," The Journal of Physiology, vol. 132, no. 3, p. 492, 1956.

[69] R. D. Harkness and B. E. Moralee, "The time-course and route of loss of collagen from the rat's uterus during post-partum involution," The Journal of Physiology, vol. 132, no. 3, pp. 502–508, 1956.

[70] E. Burack, J. Wolfe, W. Lansing, and A. Wright, "The effect of age upon the connective tissue of the uterus, cervix, and vagina of the rat," Cancer Research, vol. 1, no. 3, pp. 227–235, 1941.

[71] K.-Y. T. Kao and T. H. McGavack, "Connective tissue: I. age and sex influence on protein composition of rat tissues," Experimental Biology and Medicine, vol. 101, no. 1, pp. 153–157, 1959.

[72] R. Kearney, J. M. Miller, J. A. Ashton-Miller, and J. O. DeLancey, "Obstetrical factors associated with levator ani muscle injury after vaginal birth," Obstetrics and Gynecology, vol. 107, no. 1, p. 144, 2006.

[73] A. Kökçü, F. Yanik, M. Cetinkaya, T. Alper, B. Kandemir, and E. Malatyalioglu, "Histopathological evaluation of the connective tissue of the vaginal fascia and the uterine ligaments in women with and without pelvic relaxation," Archives of Gynecology and Obstetrics, vol. 266, no. 2, pp. 75–78, 2002.

[74] J. H. Chung, J. Y. Seo, M. K. Lee, H. C. Eun, J. H. Lee, S. Kang, G. J. Fisher, and J. J. Voorhees, "Ultraviolet modulation of human macrophage metalloelastase in

human skin in vivo," Journal of Investigative Dermatology, vol. 119, no. 2, pp. 507–512, 2002.

[75] E. F. Bernstein, D. B. Brown, F. Urbach, D. Forbes, M. D. Monaco, M. Wu, S. D. Katchman, and J. Uitto, "Ultraviolet radiation activates the human elastin promoter in transgenic mice: A novel in vivo and in vitro model of cutaneous photoaging," Journal of Investigative Dermatology, vol. 105, no. 2, pp. 269–273, 1995.

[76] V. L. Chen, R. Fleischmajer, E. Schwartz, M. Palaia, and R. Timpl, "Immunochemistry of elastotic material in sun-damaged skin," Journal of Investigative Dermatology, vol. 87, no. 3, pp. 334–337, 1986.

[77] H. Saitô, I. Ando, and A. Naito, Solid State NMR Spectroscopy for Biopolymers: Principles and Applications. Springer, 2006.

[78] T. L. James, "Fundamentals of NMR," Online Textbook: Department of Pharmaceutical Chemistry, University of California, San Francisco, pp. 1–31, 1998.

[79] J. R. Deschamps, "X-ray crystallography of chemical compounds," Life Sciences, vol. 86, no. 15, pp. 585–589, 2010.

[80] D. D. Laws, H.-M. L. Bitter, and A. Jerschow, "Solid-state NMR spectroscopic methods in chemistry," Angewandte Chemie International Edition, vol. 41, no. 17, pp. 3096–3129, 2002.

[81] T. C. Pochapsky and S. Pochapsky, NMR for physical and biological scientists. Garland Science, 2008.

[82] V. Tugarinov, W.-Y. Choy, V. Y. Orekhov, and L. E. Kay, "Solution NMR-derived global fold of a monomeric 82-kda enzyme," Proceedings of the National Academy of Sciences of the United States of America, vol. 102, no. 3, pp. 622–627, 2005.

[83] K. Wüthrich, "NMR studies of structure and function of biological macromolecules (nobel lecture)," Angewandte Chemie International Edition, vol. 42, no. 29, pp. 3340–3363, 2003.

[84] V. Kanelis, J. D. Forman-Kay, and L. E. Kay, "Multidimensional NMR methods for protein structure determination," IUBMB Life, vol. 52, no. 6, pp. 291–302, 2001.

[85] G. M. Clore and A. M. Gronenborn, "Determination of three-dimensional structures of proteins in solution by nuclear magnetic resonance spectroscopy," Protein Engineering Design and Selection, vol. 1, no. 4, pp. 275–288, 1987.

[86] V. Chevelkov, Y. Xue, R. Linser, N. R. Skrynnikov, and B. Reif, "Comparison of solid-state dipolar couplings and solution relaxation data provides insight into protein backbone dynamics," Journal of the American Chemical Society, vol. 132, no. 14, pp. 5015–5017, 2010.

[87] J. R. Schnell, H. J. Dyson, and P. E. Wright, "Structure, dynamics, and catalytic function of dihydrofolate reductase," Annual Review of Biophysics and Biomolecular Structure, vol. 33, pp. 119–140, 2004.

[88] C. P. Jaroniec, C. E. MacPhee, V. S. Bajaj, M. T. McMahon, C. M. Dobson, and R. G. Griffin, "High-resolution molecular structure of a peptide in an amyloid fibril

determined by magic angle spinning NMR spectroscopy," Proceedings of the National Academy of Sciences of the United States of America, vol. 101, no. 3, pp. 711–716, 2004.

[89] P. J. Judge and A. Watts, "Recent contributions from solid-state NMR to the understanding of membrane protein structure and function," Current Opinion in Chemical Biology, vol. 15, no. 5, pp. 690–695, 2011.

[90] E. P. Vogel, J. Curtis-Fisk, K. M. Young, and D. P. Weliky, "Solid-state nuclear magnetic resonance (NMR) spectroscopy of human immunodeficiency virus gp41 protein that includes the fusion peptide: NMR detection of recombinant fgp41 in inclusion bodies in whole bacterial cells and structural characterization of purified and membrane-associated fgp41," Biochemistry, vol. 50, no. 46, pp. 10013–10026, 2011.

[91] W. Hu, A. Som, and G. N. Tew, "Interaction between lipids and antimicrobial oligomers studied by solid-state NMR," The Journal of Physical Chemistry B, vol. 115, no. 26, pp. 8474–8480, 2011.

[92] E. R. Andrew, A. Bradbury, and R. Eades, "Nuclear magnetic resonance spectra from a crystal rotated at high speed," Nature, vol. 182, no. 4650, p. 1659, 1958.

[93] C. Tripon, M. Aluas, X. Filip, and C. Filip, "Polarization transfer from remote protons in ^{13}C CP/MAS," Journal of Magnetic Resonance, vol. 183, no. 1, pp. 68–76, 2006.

[94] A. Samoson, T. Tuherm, and J. Past, "Ramped-speed cross polarization MAS NMR," Journal of Magnetic Resonance, vol. 149, no. 2, pp. 264–267, 2001.

[95] M. J. Duer, Introduction to solid-state NMR spectroscopy. Wiley-Blackwell, 2005.

[96] B. C. Gerstein and C. R. Dybowski, Transient techniques in NMR of solids: an introduction to theory and practice. Academic Press, 1985.

[97] S. Hartmann and E. Hahn, "Nuclear double resonance in the rotating frame," Physical Review, vol. 128, no. 5, p. 2042, 1962.

[98] R. Kurbanov, T. Zinkevich, and A. Krushelnitsky, "The nuclear magnetic resonance relaxation data analysis in solids: General $R_1/R_{1\rho}$ equations and the model-free approach," The Journal of Chemical Physics, vol. 135, no. 18, p. 184104, 2011.

[99] Y.-Q. Song, L. Venkataramanan, M. Hürlimann, M. Flaum, P. Frulla, and C. Straley, "T_1-T_2 correlation spectra obtained using a fast two-dimensional laplace inversion," Journal of Magnetic Resonance, vol. 154, no. 2, pp. 261–268, 2002.

[100] B. Hills, A. Costa, N. Marigheto, and K. Wright, "T_1 - T_2 NMR correlation studies of high-pressure-processed starch and potato tissue," Applied Magnetic Resonance, vol. 28, no. 1-2, pp. 13–27, 2005.

[101] P. McDonald, J.-P. Korb, J. Mitchell, and L. Monteilhet, "Surface relaxation and chemical exchange in hydrating cement pastes: a two-dimensional NMR relaxation study," Physical Review E, vol. 72, no. 1, p. 011409, 2005.

[102] C. Sun and G. S. Boutis, "Measurement of the exchange rate of waters of hydration in elastin by 2D T_2–T_2 correlation nuclear magnetic resonance spectroscopy," New Journal of Physics, vol. 13, no. 2, p. 025026, 2011.

[103] O. T. Ukpebor, A. Shah, E. Bazov, and G. S. Boutis, "Inverse temperature transition of elastin like motifs in major ampullate dragline silk: MD simulations of short peptides and NMR studies of water dynamics," Soft Matter, vol. 10, no. 5, pp. 773–785, 2014.

[104] F. Gul-E-Noor, C. Singh, A. Papaioannou, N. Sinha, and G. S. Boutis, "Behavior of water in collagen and hydroxyapatite sites of cortical bone: fracture, mechanical wear, and load bearing studies," The Journal of Physical Chemistry C, vol. 119, no. 37, pp. 21528–21537, 2015.

[105] R. L. Kleinberg, S. A. Farooqui, and M. A. Horsfield, "T_1/T_2 ratio and frequency dependence of NMR relaxation in porous sedimentary rocks," Journal of Colloid and Interface Science, vol. 158, no. 1, pp. 195–198, 1993.

[106] E. W. Lang, H.-D. Lüdemann, and L. Piculell, "Nuclear magnetic relaxation rate dispersion in supercooled heavy water under high pressure," The Journal of Chemical Physics, vol. 81, no. 9, pp. 3820–3827, 1984.

[107] A. M. Hawkridge and D. C. Muddiman, "Mass spectrometry–based biomarker discovery: toward a global proteome index of individuality," Annual Review of Analytical Chemistry, vol. 2, p. 265, 2009.

[108] H.-C. Chang, "Ultrahigh-mass mass spectrometry of single biomolecules and bioparticles," Annual Review of Analytical Chemistry, vol. 2, pp. 169–185, 2009.

[109] K. E. Burnum, S. L. Frappier, and R. M. Caprioli, "Matrix-assisted laser desorption/ionization imaging mass spectrometry for the investigation of proteins and peptides," Annual Review of Analytical Chemistry, vol. 1, pp. 689–705, 2008.

[110] P. Dainese and P. James, "Protein identification by peptide-mass fingerprinting," in Proteome research: mass spectrometry, pp. 103–123, Springer, 2001.

[111] W. Richter and H. Schwarz, "Chemical ionization- a highly important productive mass spectrometric analysis method," Chemischer Informationsdienst, vol. 9, no. 36, 1978.

[112] H.-D. Beckey, Principles of Field Ionization and Field Desorption Mass Spectrometry: International Series in Analytical Chemistry. Elsevier, 2013.

[113] J. T. Watson and O. D. Sparkman, Introduction to mass spectrometry: instrumentation, applications, and strategies for data interpretation. John Wiley & Sons, 2007.

[114] R. B. Cody, J. Tamura, and B. D. Musselman, "Electrospray ionization/magnetic sector mass spectrometry: calibration, resolution, and accurate mass measurements," Analytical Chemistry, vol. 64, no. 14, pp. 1561–1570, 1992.

[115] M. Karas and F. Hillenkamp, "Laser desorption ionization of proteins with molecular masses exceeding 10,000 daltons," Analytical Chemistry, vol. 60, no. 20, pp. 2299–2301, 1988.

[116] F. Hillenkamp, M. Karas, R. C. Beavis, and B. T. Chait, "Matrix-assisted laser desorption/ionization mass spectrometry of biopolymers," Analytical Chemistry, vol. 63, no. 24, pp. 1193A–1203A, 1991.

[117] J. B. Fenn, M. Mann, C. K. Meng, S. F. Wong, and C. M. Whitehouse, "Electrospray ionization for mass spectrometry of large biomolecules," Science, vol. 246, no. 4926, pp. 64–71, 1989.

[118] M. Karas, D. Bachmann, U. e. Bahr, and F. Hillenkamp, "Matrix-assisted ultraviolet laser desorption of non-volatile compounds," International Journal of Mass Spectrometry and Ion Processes, vol. 78, pp. 53–68, 1987.

[119] D. C. Schriemer and L. Li, "Detection of high molecular weight narrow polydisperse polymers up to 1.5 million daltons by MALDI mass spectrometry," Analytical Chemistry, vol. 68, no. 17, pp. 2721–2725, 1996.

[120] U. Bahr, A. Deppe, M. Karas, F. Hillenkamp, and U. Giessmann, "Mass spectrometry of synthetic polymers by UV-matrix-assisted laser desorption/ionization," Analytical Chemistry, vol. 64, no. 22, pp. 2866–2869, 1992.

[121] K. Strupat, M. Karas, F. Hillenkamp, C. Eckerskorn, and F. Lottspeich, "Matrix-assisted laser desorption ionization mass spectrometry of proteins electroblotted after polyacrylamide gel electrophoresis," Analytical Chemistry, vol. 66, no. 4, pp. 464–470, 1994.

[122] B. Stahl, M. Steup, M. Karas, and F. Hillenkamp, "Analysis of neutral oligosaccharides by matrix-assisted laser desorption ionization mass spectrometry," Analytical Chemistry, vol. 63, no. 14, pp. 1463–1466, 1991.

[123] R. Johnson, "Models for matrix-assisted desorption by a laser-pulse," International Journal of Mass Spectrometry and Ion Processes, vol. 139, pp. 25–38, 1994.

[124] C. I. M. Blue, "Introduction to the spectrophotometer," Cell, 2006.

[125] L. Sommer, Analytical absorption spectrophotometry in the visible and ultraviolet: the principles. Elsevier, 2012.

[126] T. Spectronic, "Basic UV-vis theory, concepts and applications," Thermo Spectronic, pp. 1–28, 2012.

[127] J. Uitto, "Biochemistry of the elastic fibers in normal connective tissues and its alterations in diseases," Journal of Investigative Dermatology, vol. 72, no. 1, pp. 1–10, 1979.

[128] T. Watanabe, K. Ishimori, A. Verplanke, H. Matsuki, and H. Kasuga, "An enzyme-linked immunosorbent assay (ELISA) for the quantitation of urinary desmosine.," The Tokai Journal of Experimental and Clinical Medicine, vol. 14, no. 4, pp. 347–356, 1989.

[129] F. Cocci, M. Miniati, S. Monti, E. Cavarra, F. Gambelli, L. Battolla, M. Lucattelli, and G. Lungarella, "Urinary desmosine excretion is inversely correlated with the extent of emphysema in patients with chronic obstructive pulmonary disease," The International Journal of Biochemistry and Cell Biology, vol. 34, no. 6, pp. 594–604, 2002.

[130] M. Luisetti, S. Ma, P. Iadarola, P. Stone, S. Viglio, B. Casado, Y. Lin, G. Snider, and G. Turino, "Desmosine as a biomarker of elastin degradation in copd: current status and future directions," European Respiratory Journal, vol. 32, no. 5, pp. 1146–1157, 2008.

[131] T. Darnule, M. McKee, A. Darnule, G. Turino, and I. Mandl, "Solid-phase radioimmunoassay for estimation of elastin peptides in human sera," Analytical Biochemistry, vol. 122, no. 2, pp. 302–307, 1982.

[132] D. E. McClintock, B. Starcher, M. D. Eisner, B. T. Thompson, D. L. Hayden, G. D. Church, and M. A. Matthay, "Higher urine desmosine levels are associated with mortality in patients with acute lung injury," American Journal of Physiology-Lung Cellular and Molecular Physiology, vol. 291, no. 4, pp. L566–L571, 2006.

[133] S. Viglio, P. Iadarola, A. Lupi, R. Trisolini, C. Tinelli, B. Balbi, V. Grassi, D. Worlitzsch, G. Doring, F. Meloni, et al., "MEKC of desmosine and isodesmosine in urine of chronic destructive lung disease patients," European Respiratory Journal, vol. 15, no. 6, pp. 1039–1045, 2000.

[134] S. Viglio, G. Zanaboni, M. Luisetti, R. Trisolini, R. Grimm, G. Cetta, and P. Iadarola, "Micellar electrokinetic chromatography for the determination of urinary desmosine and isodesmosine in patients affected by chronic obstructive pulmonary disease," Journal of Chromatography B: Biomedical Sciences and Applications, vol. 714, no. 1, pp. 87–98, 1998.

[135] W. R. Cumiskey, E. D. Pagani, and D. C. Bode, "Enrichment and analysis of desmosine and isodesmosine in biological fluids," Journal of Chromatography B: Biomedical Sciences and Applications, vol. 668, no. 2, pp. 199–207, 1995.

[136] S. Ma, Y. Y. Lin, and G. M. Turino, "Measurements of desmosine and isodesmosine by mass spectrometry in COPD," Chest, vol. 131, no. 5, pp. 1363–1371, 2007.

[137] M. Boutin, C. Berthelette, F. G. Gervais, M.-B. Scholand, J. Hoidal, M. F. Leppert, K. P. Bateman, and P. Thibault, "High-sensitivity nanoLC- MS/MS analysis of urinary desmosine and isodesmosine," Analytical Chemistry, vol. 81, no. 5, pp. 1881–1887, 2009.

[138] S. Ma, G. M. Turino, T. Hayashi, H. Yanuma, T. Usuki, and Y. Y. Lin, "Stable deuterium internal standard for the isotope-dilution LC–MS/MS analysis of elastin degradation," Analytical Biochemistry, vol. 440, no. 2, pp. 158–165, 2013.

[139] W. F. Daamen, T. Hafmans, J. H. Veerkamp, and T. H. V. Kuppevelt, "Comparison of five procedures for the purification of insoluble elastin," Biomaterials, vol. 22, no. 14, pp. 1997–2005, 2001.

[140] R. P. Mecham, "Methods in elastic tissue biology: elastin isolation and purification.," Methods, vol. 45, pp. 32–41, May 2008.

[141] S. Partridge, H. Davis, and S. Adair, "The Chemistry of Connective Tissues," Biochemical Journal, vol. 6, no. 1946, 1952.

[142] O. Lowry, D. Gilligan, and E. Katersky, "The determination of collagen and elastin in tissues, with results obtained in various normal tissues from different species," Journal of Biological Chemistry, vol. 139, no. 2, 1941.

[143] B. C. Starcher and M. J. Galione, "Purification and comparison of elastins from different animal species," Analytical Biochemistry, vol. 74, no. 2, pp. 441 – 447, 1976.

[144] W. F. Daamen, T. Hafmans, J. H. Veerkamp, and T. H. V. Kuppevelt, "Isolation of intact elastin fibers devoid of microfibrils," Tissue Engineering, vol. 11, no. 7-8, pp. 1168–1176, 2005.

[145] Z. Gunja-Smith and J. F. Woessner, "Content of the collagen and elastin cross-links pyridinoline and the desmosines in the human uterus in various reproductive states," American Journal of Obstetrics and Gynecology, vol. 153, no. 1, pp. 92–95, 1985.

[146] B. Dhital, F. Gul-E-Noor, K. T. Downing, S. Hirsch, and G. S. Boutis, "Pregnancy-induced dynamical and structural changes of reproductive tract collagen," Biophysical Journal, vol. 111, no. 1, pp. 57–68, 2016.

[147] R. P. Mecham, "Methods in elastic tissue biology: elastin isolation and purification," Methods, vol. 45, no. 1, pp. 32–41, 2008.

[148] B. C. Starcher and M. J. Galione, "Purification and comparison of elastins from different animal species," Analytical Biochemistry, vol. 74, no. 2, pp. 441–447, 1976.

[149] A. E. Bennett, C. M. Rienstra, M. Auger, K. V. Lakshmi, and R. G. Griffin, "Heteronuclear decoupling in rotating solids," The Journal of Chemical Physics, vol. 103, no. 16, pp. 6951–6958, 1995.

[150] J. Feng and J. A. Reimer, "Suppression of probe background signals via b_1 field inhomogeneity," Journal of Magnetic Resonance, vol. 209, no. 2, pp. 300–305, 2011.

[151] M. R. Bendall and R. E. Gordon, "Depth and refocusing pulses designed for multipulse NMR with surface coils," Journal of Magnetic Resonance, vol. 53, no. 3, pp. 365–385, 1983.

[152] W. Daamen, T. Hafmans, J. Veerkamp, and T. Van Kuppevelt, "Comparison of five procedures for the purification of insoluble elastin," Biomaterials, vol. 22, no. 14, pp. 1997–2005, 2001.

[153] L. Venkataramanan, Y.-Q. Song, and M. D. Hurlimann, "Solving Fredholm integrals of the first kind with tensor product structure in 2 and 2.5 dimensions," IEEE Transactions on Signal Processing, vol. 50, no. 5, pp. 1017–1026, 2002.

[154] P.-G. De Gennes, Scaling concepts in polymer physics. Cornell university press, 1979.

[155] T. E. Curry Jr and K. G. Osteen, "The matrix metalloproteinase system: changes, regulation, and impact throughout the ovarian and uterine reproductive cycle," Endocrine Reviews, vol. 24, no. 4, pp. 428–465, 2003.

[156] C. A. Lyons, K. D. Beharry, K. C. Nishihara, Y. Akmal, Z. Y. Ren, E. Chang, and M. P. Nageotte, "Regulation of matrix metalloproteinases (type iv collagenases) and

their inhibitors in the virgin, timed pregnant, and postpartum rat uterus and cervix by prostaglandin e2-cyclic adenosine monophosphate," American Journal of Obstetrics and Gynecology, vol. 187, no. 1, pp. 202–208, 2002.

[157] M. C. Silverstein, K. Bilici, S. W. Morgan, Y. Wang, Y. Zhang, and G. S. Boutis, "^{13}C, ^{2}H NMR studies of structural and dynamical modifications of glucose-exposed porcine aortic elastin," Biophysical Journal, vol. 108, no. 7, pp. 1758–1772, 2015.

[158] K. K. Kumashiro, T. L. Kurano, W. P. Niemczura, M. Martino, and A. M. Tamburro, "^{13}C CPMAS NMR studies of the elastin-like polypeptide $(LGGVG)_n$," Biopolymers, vol. 70, no. 2, pp. 221–226, 2003.

[159] K. Ohgo, J. Ashida, K. K. Kumashiro, and T. Asakura, "Structural determination of an elastin-mimetic model peptide,$(val\text{-}pro\text{-}gly\text{-}val\text{-}gly)_6$, studied by ^{13}C CP/MAS NMR chemical shifts, two-dimensional off magic angle spinning spin-diffusion NMR, rotational echo double resonance, and statistical distribution of torsion angles from Protein Data Bank," Macromolecules, vol. 38, no. 14, pp. 6038–6047, 2005.

[160] M. Hong, D. Isailovic, R. McMillan, and V. Conticello, "Structure of an elastin-mimetic polypeptide by solid-state NMR chemical shift analysis," Biopolymers, vol. 70, no. 2, pp. 158–168, 2003.

[161] M. S. Pometun, E. Y. Chekmenev, and R. J. Wittebort, "Quantitative observation of backbone disorder in native elastin," Journal of Biological Chemistry, vol. 279, no. 9, pp. 7982–7987, 2004.

[162] R. P. Mecham, T. J. Broekelmann, C. J. Fliszar, S. D. Shapiro, H. G. Welgus, and R. M. Senior, "Elastin degradation by matrix metalloproteinases cleavage site specificity and mechanisms of elastolysis," Journal of Biological Chemistry, vol. 272, no. 29, pp. 18071–18076, 1997.

[163] A. Krushelnitsky, D. Reichert, and K. Saalwachter, "Solid-state NMR approaches to internal dynamics of proteins: from picoseconds to microseconds and seconds," Accounts of Chemical Research, vol. 46, no. 9, pp. 2028–2036, 2013.

[164] M. J. Duer, J. Rocha, and J. Klinowski, "Solid-state NMR studies of the molecular motion in the kaolinite: DMSO intercalate," Journal of the American Chemical Society, vol. 114, no. 17, pp. 6867–6874, 1992.

[165] C. Sun and G. S. Boutis, "Investigation of the dynamical properties of water in elastin by deuterium Double Quantum Filtered NMR," Journal of Magnetic Resonance, vol. 205, no. 1, pp. 86–92, 2010.

[166] R. Kleinberg, S. Farooqui, and M. Horsfield, "T_1 /T_2 ratio and frequency dependence of NMR relaxation in porous sedimentary rocks," Journal of Colloid and Interface Science, vol. 158, no. 1, pp. 195–198, 1993.

[167] B. Dhital, P. Durlik, P. Rathod, F. Gul-E-Noor, Z. Wang, C. Sun, E. J. Chang, B. Itin, and G. S. Boutis, "Ultraviolet radiation reduces desmosine cross-links in elastin," Biochemistry and Biophysics Reports, vol. 10, pp. 172–177, 2017.

[168] Y. Feng, Y. Wang, B. Yan, L. Li, and Y. Deng, "Matrix metalloproteinase-1 expression in women with and without pelvic organ prolapse: A systematic review and meta-analysis," Clinical and Translational Science, vol. 9, no. 5, pp. 267–273, 2016.

[169] H. Zhang, S. Neal, and D. S. Wishart, "Refdb: a database of uniformly referenced protein chemical shifts," Journal of Biomolecular NMR, vol. 25, no. 3, pp. 173–195, 2003.

[170] Y. Wang and O. Jardetzky, "Probability-based protein secondary structure identification using combined NMR chemical-shift data," Protein Science, vol. 11, no. 4, pp. 852–861, 2002.

[171] T. Asakura, M. Iwadate, M. Demura, and M. P. Williamson, "Structural analysis of silk with ^{13}C NMR chemical shift contour plots," International Journal of Biological Macromolecules, vol. 24, no. 2-3, pp. 167–171, 1999.

[172] J. E. Jenkins, M. S. Creager, R. V. Lewis, G. P. Holland, and J. L. Yarger, "Quantitative correlation between the protein primary sequences and secondary structures in spider dragline silks," Biomacromolecules, vol. 11, no. 1, pp. 192–200, 2009.

[173] A. Rundgren, "Physical properties of connective tissue as influenced by single and repeated pregnancies in the rat.," Acta Physiologica Scandinavica. Supplementum, vol. 417, pp. 1–138, 1973.

[174] A. Feola, P. Moalli, M. Alperin, R. Duerr, R. E. Gandley, and S. Abramowitch, "Impact of pregnancy and vaginal delivery on the passive and active mechanics of the rat vagina," Annals of Biomedical Engineering, vol. 39, no. 1, pp. 549–558, 2011.

[175] K. Yoshida, C. Reeves, J. Vink, J. Kitajewski, R. Wapner, H. Jiang, S. Cremers, and K. Myers, "Cervical collagen network remodeling in normal pregnancy and disrupted parturition in antxr2 deficient mice," Journal of Biomechanical Engineering, vol. 136, no. 2, p. 021017, 2014.

[176] R. C. Bump and P. A. Norton, "Epidemiology and natural history of pelvic floor dysfunction," Obstetrics and Gynecology Clinics of North America, vol. 25, no. 4, pp. 723–746, 1998.

[177] E. S. Lukacz, J. M. Lawrence, R. Contreras, C. W. Nager, and K. M. Luber, "Parity, mode of delivery, and pelvic floor disorders," Obstetrics and Gynecology, vol. 107, no. 6, pp. 1253–1260, 2006.

[178] R. A. Word, S. Pathi, and J. I. Schaffer, "Pathophysiology of pelvic organ prolapse," Obstetrics and Gynecology Clinics of North America, vol. 36, no. 3, pp. 521–539, 2009.

[179] J. Bella, M. Eaton, B. Brodsky, and H. M. Berman, "Crystal and molecular structure of a collagen-like peptide at 1.9 a resolution," Science, vol. 266, no. 5182, pp. 75–81, 1994.

[180] D. Huster, J. Schiller, and K. Arnold, "Comparison of collagen dynamics in articular cartilage and isolated fibrils by solid-state NMR spectroscopy," Magnetic Resonance in Medicine, vol. 48, no. 4, pp. 624–632, 2002.

[181] H. Saitô, I. Ando, and A. Ramamoorthy, "Chemical shift tensor–the heart of NMR: Insights into biological aspects of proteins," Progress in Nuclear Magnetic Resonance Spectroscopy, vol. 57, no. 2, p. 181, 2010.

[182] R. O. Hynes and A. Naba, "Overview of the matrisomeŮan inventory of extracellular matrix constituents and functions," Cold Spring Harbor Perspectives in Biology, vol. 4, no. 1, p. a004903, 2012.

[183] D. Birk, "Type v collagen: heterotypic type i/v collagen interactions in the regulation of fibril assembly," Micron, vol. 32, no. 3, pp. 223–237, 2001.

[184] M. Alperin, A. Feola, L. Meyn, R. Duerr, S. Abramowitch, and P. Moalli, "Collagen scaffold: a treatment for simulated maternal birth injury in the rat model," American Journal of Obstetrics and Gynecology, vol. 202, no. 6, pp. 589.e1–589.e8, 2010.

[185] H. Saitô, R. Tabeta, A. Shoji, T. Ozaki, I. Ando, and T. Miyata, "A high-resolution ^{13}C-NMR study of collagen like polypeptides and collagen fibrils in solid state studied by the cross-polarization–magic angle-spinning method. manifestation of conformation-dependent ^{13}C chemical shifts and application to conformational characterization," Biopolymers, vol. 23, no. 11, pp. 2279–2297, 1984.

[186] H. Saitô and M. Yokoi, "A ^{13}C NMR study on collagens in the solid state: hydration/dehydration-induced conformational change of collagen and detection of internal motions," Journal of Biochemistry, vol. 111, no. 3, pp. 376–382, 1992.

[187] H. Saitô, "Conformation-dependent ^{13}C chemical shifts: A new means of conformational characterization as obtained by high-resolution solid-state ^{13}C NMR," Magnetic Resonance in Chemistry, vol. 24, no. 10, pp. 835–852, 1986.

[188] W. Y. Chow, A. M. Taylor, D. G. Reid, J. A. Gallagher, and M. J. Duer, "Collagen atomic scale molecular disorder in ochronotic cartilage from an alkaptonuria patient, observed by solid state NMR," Journal of Inherited Metabolic Disease, vol. 34, no. 6, pp. 1137–1140, 2011.

[189] M. J. Dawson and S. Wray, "The effects of pregnancy and parturition on phosphorus metabolites in rat uterus studied by ^{31}P nuclear magnetic resonance.," The Journal of physiology, vol. 368, no. 1, pp. 19–31, 1985.

[190] C. R. Kliment, J. M. Englert, L. P. Crum, and T. D. Oury, "A novel method for accurate collagen and biochemical assessment of pulmonary tissue utilizing one animal," International Journal of Clinical and Experimental Pathology, vol. 4, no. 4, p. 349, 2011.

[191] W. Y. Chow, R. Rajan, K. H. Muller, D. G. Reid, J. N. Skepper, W. C. Wong, R. A. Brooks, M. Green, D. Bihan, R. W. Farndale, et al., "NMR spectroscopy of native and in vitro tissues implicates polyADP ribose in biomineralization," Science, vol. 344, no. 6185, pp. 742–746, 2014.

[192] P. Zhu, J. Xu, N. Sahar, M. D. Morris, D. H. Kohn, and A. Ramamoorthy, "Time-resolved dehydration-induced structural changes in an intact bovine cortical bone revealed by solid-state NMR spectroscopy," Journal of the American Chemical Society, vol. 131, no. 47, pp. 17064–17065, 2009.

[193] J. Xu, P. Zhu, M. D. Morris, and A. Ramamoorthy, "Solid-state NMR spectroscopy provides atomic-level insights into the dehydration of cartilage," The Journal of Physical Chemistry B, vol. 115, no. 33, pp. 9948–9954, 2011.

[194] K. H. Mroue, N. MacKinnon, J. Xu, P. Zhu, E. McNerny, D. H. Kohn, M. D. Morris, and A. Ramamoorthy, "High-resolution structural insights into bone: a solid-state NMR relaxation study utilizing paramagnetic doping," The Journal of Physical Chemistry B, vol. 116, no. 38, pp. 11656–11661, 2012.

[195] C. Singh, R. K. Rai, and N. Sinha, "Experimental aspect of solid-state nuclear magnetic resonance studies of biomaterials such as bones," Solid State Nuclear Magnetic Resonance, vol. 54, pp. 18–25, 2013.

[196] R. K. Rai and N. Sinha, "Dehydration-induced structural changes in the collagen–hydroxyapatite interface in bone by high-resolution solid-state NMR spectroscopy," The Journal of Physical Chemistry C, vol. 115, no. 29, pp. 14219–14227, 2011.

[197] J. M. Haus, J. A. Carrithers, S. W. Trappe, and T. A. Trappe, "Collagen, cross-linking, and advanced glycation end products in aging human skeletal muscle," Journal of Applied Physiology, vol. 103, no. 6, pp. 2068–2076, 2007.

[198] O. W. Smith and N. B. Kaltreider, "Collagen content of the nonpregnant rat uterus as related to the functional responses to estrogen and progesterone," Endocrinology, vol. 73, no. 5, pp. 619–628, 1963.

[199] J. Weiss, "The collagens: biochemistry and pathophysiology," 1993.

[200] S. Y. Yu, C. A. Tozzi, J. Babiarz, and P. C. Leppert, "Collagen changes in rat cervix in pregnancy–polarized light microscopic and electron microscopic studies," Experimental Biology and Medicine, vol. 209, no. 4, pp. 360–368, 1995.

[201] J. L. Lowder, K. M. Debes, D. K. Moon, N. Howden, S. D. Abramowitch, and P. A. Moalli, "Biomechanical adaptations of the rat vagina and supportive tissues in pregnancy to accommodate delivery," Obstetrics & Gynecology, vol. 109, no. 1, pp. 136–143, 2007.

[202] C. Sun, O. Mitchell, J. Huang, and G. S. Boutis, "NMR studies of localized water and protein backbone dynamics in mechanically strained elastin," Journal of Physical Chemistry B, vol. 115, no. 47, pp. 13935–13942, 2011.

[203] J. F. Almine, D. V. Bax, S. M. Mithieux, L. Nivison-Smith, J. Rnjak, A. Waterhouse, S. G. Wise, and A. S. Weiss, "Elastin-based materials," Chemical Society Reviews, vol. 39, no. 9, pp. 3371–3379, 2010.

[204] G. S. Montes, "Structural biology of the fibers of the collagenous and elastic systems," Cell Biology International, vol. 20, no. 1, pp. 15–27, 1996.

[205] Z. Wirtschafter, E. Cleary, D. Jackson, and L. Sandberg, "Histological changes during the development of the bovine nuchal ligament," Journal of Cell Biology, vol. 33, no. 3, pp. 481–488, 1967.

[206] S. Shapiro, S. Endicott, M. Province, J. Pierce, and E. Campbell, "Marked longevity of human lung parenchymal elastic fibers deduced from prevalence of D-aspartate and nuclear weapons-related radiocarbon.," Journal of Clinical Investigation, vol. 87, no. 5, pp. 1828–1834, 1991.

[207] K. G. Bergstrom, "Beyond tretinoin: cosmeceuticals for aging skin," Journal of Drugs in Dermatology, vol. 8, no. 7, pp. 674–677, 2009.

[208] S. Tajima, A. Hayashi, and T. Suzuki, "Elastin expression is up-regulated by retinoic acid but not by retinol in chick embryonic skin fibroblasts," Journal of Dermatological Science, vol. 15, no. 3, pp. 166–172, 1997.

[209] I. M. Braverman and E. Fonferko, "Studies in cutaneous aging: I. The elastic fiber network," Journal of Investigative Dermatology, vol. 78, no. 5, pp. 434–443, 1982.

[210] S. Imayama, K. Nakamura, M. Takeuchi, Y. Hori, Y. Takema, Y. Sakaino, and G. Imokawa, "Ultraviolet-B irradiation deforms the configuration of elastic fibers during the induction of actinic elastosis in rats," Journal of Dermatological Science, vol. 7, no. 1, pp. 32–38, 1994.

[211] G. Imokawa, Y. Takema, Y. Yorimoto, K. Tsukahara, M. Kawai, and S. Imayama, "Degree of ultraviolet-induced tortuosity of elastic fibers in rat skin is age dependent," Journal of Investigative Dermatology, vol. 105, no. 2, pp. 254–258, 1995.

[212] R. M. Lavker, P. Zheng, and G. Dong, "Aged skin: a study by light, transmission electron, and scanning electron microscopy.," Journal of Investigative Dermatology, vol. 88, pp. 44s–51s, 1987.

[213] B. L. Diffey, "Ultraviolet radiation and human health," Clinics in Dermatology, vol. 16, no. 1, pp. 83–89, 1998.

[214] R. Chatterjee, M. J. Benzinger, J. L. Ritter, and D. L. Bissett, "Chronic ultraviolet B radiation-induced biochemical changes in the skin of hairless mice," Photochemistry and Photobiology, vol. 51, no. 1, pp. 91–97, 1990.

[215] M. Guay, G. Lagace, and F. Lamy, "Photolysis and ozonolysis of desmosine and elastolytic peptides," Connective Tissue Research, vol. 14, no. 2, pp. 89–107, 1985.

[216] K. Tsukahara, Y. Takema, T. Fujimura, S. Moriwaki, T. Kitahara, S. Imayama, and G. Imokawa, "All-trans retinoic acid promotes the repair of tortuosity of elastic fibres in rat skin," British Journal of Dermatology, vol. 140, pp. 1048–1053, 1999.

[217] K. J. Johnston, A. I. Oikarinen, N. J. Lowe, J. G. Clark, and J. Uitto, "Ultraviolet radiation-induced connective tissue changes in the skin of hairless mice," Journal of Investigative Dermatology, vol. 82, no. 6, pp. 587–590, 1984.

[218] Q. Fu, "Radiation (solar)," Encyclopedia of Atmospheric Sciences, vol. 5, pp. 1859–1863, 2003.

[219] R. Baurain, J.-F. LAROCHELLE, and F. LAMY, "Photolysis of desmosine and isodesmosine by ultraviolet light," European Journal of Biochemistry, vol. 67, no. 1, pp. 155–164, 1976.

[220] G. C. Sephel, P. H. Byers, K. A. Holbrook, and J. M. Davidson, "Heterogeneity of elastin expression in cutis laxa fibroblast strains," Journal of Investigative Dermatology, vol. 93, no. 1, pp. 147–153, 1981.

[221] Z. Urban, J. Gao, F. M. Pope, and E. C. Davis, "Autosomal dominant cutis laxa with severe lung disease: synthesis and matrix deposition of mutant tropoelastin," Journal of Investigative Dermatology, vol. 124, no. 6, pp. 1193–1199, 2005.

[222] M. Tassabehji, K. Metcalfe, J. Hurst, G. S. Ashcroft, C. Kielty, C. Wilmot, D. Donnai, A. P. Read, and C. J. Jones, "An elastin gene mutation producing abnormal tropoelastin and abnormal elastic fibres in a patient with autosomal dominant cutis laxa," Human Molecular Genetics, vol. 7, no. 6, pp. 1021–1028, 1998.

[223] K. A. Holbrook and P. H. Byers, "Structural abnormalities in the dermal collagen and elastic matrix from the skin of patients with inherited connective tissue disorders.," Journal of Investigative Dermatology, vol. 79, pp. 7s–16s, 1982.

[224] B. A. Kozel, C.-T. Su, J. R. Danback, R. L. Minster, S. Madan-Khetarpal, J. McConnell, M. K. Mac Neal, K. L. Levine, R. C. Wilson, F. C. Sciurba, and Z. Ur-

ban, "Biomechanical properties of the skin in cutis laxa," The Journal of Investigative Dermatology, vol. 134, no. 11, pp. 2836–2838, 2014.

[225] P. Agache, C. Monneur, J. Leveque, and J. De Rigal, "Mechanical properties and young's modulus of human skin in vivo," Archives of Dermatological Research, vol. 269, no. 3, pp. 221–232, 1980.

[226] A. Oba and C. Edwards, "Relationships between changes in mechanical properties of the skin, wrinkling, and destruction of dermal collagen fiber bundles caused by photoaging," Skin Research and Technology, vol. 12, no. 4, pp. 283–288, 2006.

[227] H. Vogel, "Influence of maturation and age on mechanical and biochemical parameters of connective tissue of various organs in the rat," Connective Tissue Research, vol. 6, no. 3, pp. 161–166, 1978.

[228] M. Matsuda, T. Nosaka, M. Sato, and N. Ohshima, "Effects of physical exercise on the elasticity and elastic components of the rat aorta," European Journal of Applied Physiology and Occupational Physiology, vol. 66, no. 2, pp. 122–126, 1993.

[229] A. Brüel and H. Oxlund, "Changes in biomechanical properties, composition of collagen and elastin, and advanced glycation end products of the rat aorta in relation to age," Atherosclerosis, vol. 127, no. 2, pp. 155–165, 1996.

[230] M. Spina, S. Garbisa, J. Hinnie, J. C. Hunter, and A. Serafini-Fracassini, "Age-related changes in composition and mechanical properties of the tunica media of the upper

thoracic human aorta.," Arteriosclerosis, Thrombosis, and Vascular Biology, vol. 3, no. 1, pp. 64–76, 1983.